Steady and Unsteady Visco-Resistive Reconnection in the Presence of the Hall Effect

A thesis

submitted in partial fulfilment

of the requirements for the Degree

of

Doctor of Philosophy in Mathematics

at

The University of Waikato

by

Liam C. McMahon

THE UNIVERSITY OF
WAIKATO
Te Whare Wānanga o Waikato

2021

Preface

Some of the work presented in this thesis has been published in peer-reviewed journals.

Chapter 3 was published as a paper (McMahon, 2017). In this thesis, we have added Section 3.4 and 3.5 that describe the Craig-Henton reconnective annihilation model and its extension into three dimensions respectively. These chapters are necessary for understanding Section 3.8, in which we search for a visco-resistive length scale in flux pile-up models, but are not original derivations and hence were not part of the published article.

Chapter 4 was first published as a letter (Litvinenko and McMahon, 2015a) then in more depth as a paper (Litvinenko and McMahon, 2015b). The letter (Litvinenko and McMahon, 2015a) comprises Sections 4.1-4.4, while the paper (Litvinenko and McMahon, 2015b) comprises Sections 4.1-4.6. The extra sections in the latter are an alternative formulation and an extension into electron inertia effects. While we used asympotic solutions to approximate a singularity time, Janda (2018, 2019) and Brizard (2019) extended our work to derive exact solutions in terms of the Weierstrass Elliptic Function and the Jacobi Elliptic Function respectively. These solutions are described in Section 4.7.

Chapter 6 was published as a paper (McMahon, 2019). The only addition to this thesis is Subsection 6.3.3 which describes an approximation using a Hypergeometric function.

Abstract

In this thesis we investigate the effects of viscosity and the Hall effect on magnetic reconnection. Magnetic reconnection is a process of releasing large amounts of magnetic energy as observed in solar flares. In the first two chapters, we describe the basic mathematics and early models of reconnection.

In Chapter 3, we search for a visco-resistive length scale in reconnection solutions. This is demonstrated in reconnective annihilation and a quasi-one-dimensional series expansion. We find that the visco-resistive length scale appears organically unless a specific geometry is chosen. Upon adding small scale perturbations, the visco-resistive length scale always appears.

In Chapter 4, we build on Litvinenko's (2007) self-similar solution that showed singularities appear with a Hall MHD X-point geometry for a certain set of initial conditions. These singularities signal current sheet formation. We consider a general set of initial conditions and find that the singularities will form in this self-similar solution unless the axial field is many orders of magnitude larger than the planar field.

In Chapter 5, we review the Craig and McClymont (1991) linear, oscillatory model of reconnection. In Chapter 6, we attempt to quantify a general model that includes viscosity, pressure and axial effects, the Hall effect and electron inertia. We perform a dimensional analysis to find order-of-magnitude estimates for how the aforementioned effects perturb the Craig and McClymont (1991) solution. We verify these estimates with numerical simulations.

In Chapter 7, we give an overview of the thesis and make suggestions for future work.

Acknowledgements

Firstly, I am indebted to my Chief Supervisor Yuri Litvinenko for fostering my interest in Vector Calculus and Magnetohydrodynamics in the first place, and for providing ongoing expertise and feedback. I would also like to thank Ian Craig for his constant and infectious enthusiasm for mathematics. Similarly, I have appreciated the insight and advice of my second supervisor Sean Oughton, especially on the numerical side of the thesis. My thanks as well go to Jacob Heerikhuisen for taking the time to proof-read the entire thesis despite his busy schedule.

In addition, I would like to acknowledge the support of The University of Waikato for awarding me a Doctoral Scholarship, thereby making my studies possible. Moreover, I could not have produced this thesis without the help of the Department of Mathematics and Statistics. I was provided with software, a computer and travel grants to several conferences and workshops within New Zealand which allowed me to share my ideas with colleagues and learn from experts in my field. Furthermore, I thank Glenys Williams and Rachael Foote for keeping me organised. I would also like to thank my undergraduate lecturers for inspiring me to pursue a mathematics degree.

Finally, I would like to acknowledge my parents and my brother for their support.

Contents

Chapter 1

Introduction

1.1 Solar Flares

In 1859, Carrington and Hodgson observed a white flare of light emanating from the sun, followed by a critical failure of telegraph systems all over North America and Europe. What they saw we now know to be a solar flare (along with a Coronal Mass Ejection), which if it ever were to occur again on the same scale could have a devastating impact on 21st century technology. Of course, not all flare events are potential doomsday scenarios, but smaller flares could have an important effect on satellites or could pose a potential hazard to astronauts.

Solar flares are huge eruptions of energy that can release up to 10^{25} J in a time period of the order 100 seconds. While large-scale flare events could pose a significant danger for Earth, accurate flare forecasting remains elusive. In fact, the mechanism behind solar flares - magnetic reconnection - has many fundamental aspects which remain unresolved. As its main purpose, this thesis seeks to examine and illuminate the mysterious mechanisms behind magnetic reconnection.

To understand the context within which solar flares manifest, the physical environment of the sun needs to be considered. The four outer regions of the sun comprise the photosphere, chromosphere, transition region and the

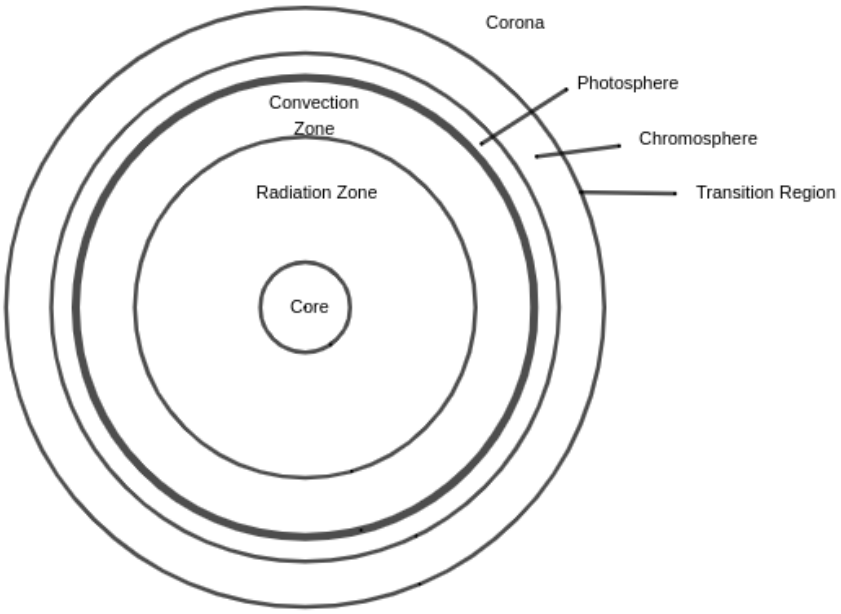

Figure 1.1: A cross-sectional representation of the layers of the Sun

corona, whereas the inner regions are composed of the core, the radiative zone and the convection zone (displayed in Fig. 1.1). The solar corona is the outermost region and it is here that most solar flares occur. Fig. 1.2 shows how reconnection can occur in the corona. Surprisingly, the corona is actually hotter than the other outer regions even though they are closer to the core. In this thesis, we will focus almost exclusively on events which occur within coronal plasmas.

Region	**Density (g cm^{-3})**	**Temperature (K)**	**Thickness (km)**
Photosphere	10^{-9}	4000-6500	300
Chromosphere	10^{-12}	4000-8500	2000
Transition Region	$10^{-13} - 10^{-15}$	8000-500,000	100
Surface of the Earth	10^{-3}	300	30

We model the plasma in the solar corona using the Magnetohydrodynamic (MHD) equations (see e.g. Priest and Forbes, 2000; Biskamp, 2000). The

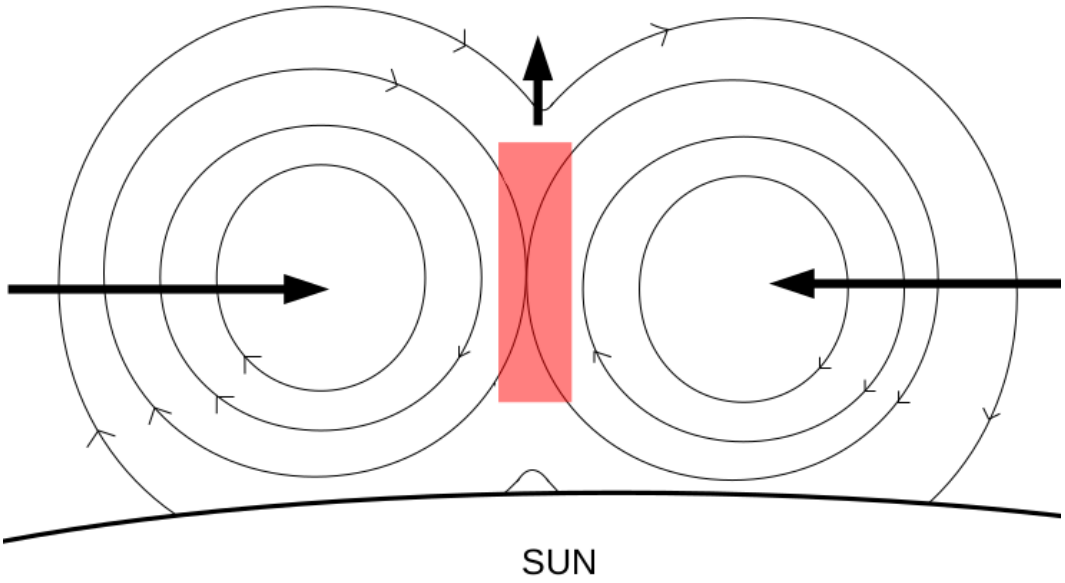

Figure 1.2: Schematic drawing of magnetic reconnection occurring in the Solar Corona. Oppositely directed coronal loops are forced together in the (red) reconnection region.

MHD model unites Maxwell's equations for magnetism and the fluid dynamic equations for conservation of momentum and mass. The MHD equations are highly non-linear and intractable to solve without some simplifying assumptions. Thus, we are always going to be limited in the applicability of our results in some capacity.

1.2 Magnetic Reconnection

In the ideal MHD model resistivity is zero, and magnetic field lines are frozen into the plasma and are not allowed to break. As magnetic field lines move and are twisted into complex topological arrangements, we obtain a build up of magnetic energy. If the magnetic gradient between the field lines becomes sufficiently large, the ideal MHD properties no longer apply, and the field lines are said to break and reconnect into simpler, lower energy topological arrangements (see Fig. 1.3). During this process the magnetic energy stored

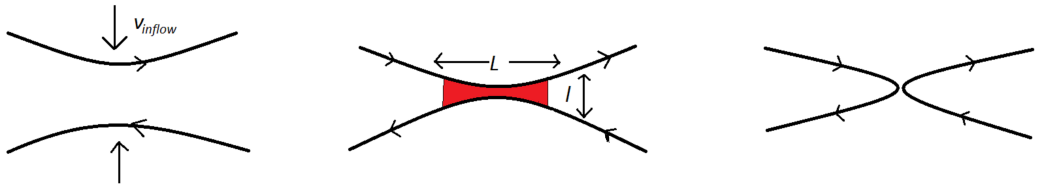

Figure 1.3: Breaking and reconnecting of field lines. The red area represents a current sheet where the local current is sufficiently large that ideal MHD properties no longer apply.

in the field lines is released as kinetic energy.

The reconnection model is necessarily dependent on non-ideal terms in Ohm's law, namely the resistivity η. In dimensionless units $\eta \sim 10^{-14.5}$ in the corona; this is small enough to allow sufficient magnetic energy to build up in field lines before reconnection, but also results in a dissipation rate that is far too small to match with physical observations. Resistive diffusion would take the order of a million years to dissipate the amount of energy observed in a typical flare. In reality, flares erupt on a time scale of the order 100 seconds (e.g. Priest and Forbes, 2000). The need to account for this discrepancy between the predicted rate and the observed rapid energy release is the driving force of this thesis.

Owing to the small magnitude of resistive effects, we turn to other non-ideal terms in the MHD equations. For instance, the Hall effect was shown, in numerical simulations, to improve reconnection rates (e.g. Birn et al., 2001, 2005; Shay et al., 2001; Drake et al., 2008). However, more recent studies have found that it is instead viscous diffusion that could be responsible for the rapid release of energy solar flares (Craig et al., 2005; Armstrong et al., 2011). Even if this were not the case, viscosity still plays a vital role in reconnection due to the overwhelming magnitude of viscous terms in the solar corona in comparison to resistive terms (Hollweg, 1985). Finally, while 2D reconnection has been well studied, perhaps the most exciting new area for research is generalising

2D results into a full 3D geometry. Due to the mathematical complexity of a full 3D model, we stay within the realms of what is known as "2.5D". In 2.5D, we consider all three dimensions but there is no dependence on the third, taken to be z, dimension. That is to say, all partial derivatives with respect to z vanish or $\partial_z = 0$. We leave full 3D effects for further research.

In order to break the flux frozen-in condition we require currents of the order η^{-1} in a length scale of $\sqrt{\eta}$, which naturally leads us to the notion of a current sheet being the site for reconnection. Outside the current sheet, the plasma is governed by large-scale ideal MHD dynamics. Thus, magnetic reconnection problems naturally lend themselves to asymptotic analysis.

Magnetic reconnection has been observed in the solar corona (see e.g. Aschwanden, 2006; Shibata and Magara, 2011, for a review). Magnetic reconnection also has other applications outside the sun. For example, reconnection in the Earth's magnetosphere enhances aurorae (e.g. Case et al., 2017).

1.3 Thesis Outline

In the following chapter, we outline the mathematical framework required to understand magnetic reconnection. We introduce the MHD equations, including the non-ideal effects of resistivity, viscosity, the Hall effect and electron inertia. We detail the motivation for reconnection, the flux frozen-in condition and show how it is able to be broken at a current sheet.

To establish the necessary conceptual framework for the original research presented later in the thesis, we explore three reconnection models: the Sweet-Parker (Parker, 1957) model for steady reconnection; the Imshennik and Syrovatskiĭ (1967) solution for current sheet formation, and the Forbes (1982) unsteady reconnection approach. Sweet-Parker establishes an archetypal model of reconnection at a current sheet formed by a magnetic X-point, while the Imshennik and Syrovatskiĭ (1967) model demonstrates current sheet formation by means of a singularity. Finally, the Forbes (1982) model of one-dimensional

unsteady reconnection resolves the singularity via resistive or gas pressure effects

In Chapter 3, we search for a visco-resistive length scale in magnetic flux pile-up solutions and for steady reconnecting current sheets. We review the viscous modifications to the fundamental (Sonnerup and Priest, 1975) pile-up solution, namely the Gratton et al. (1990); Besser et al. (1990); Phan and Sonnerup (1990); Jardine et al. (1992) solutions. Flux-pile up solutions were later shown to be able to incorporate reconnective effects (Craig and Henton, 1995), which lead to viscous reconnective annihilation (e.g. Fabling and Craig, 1996; Craig and Litvinenko, 2012) in which a visco-resistive length scale was nowhere to be found. By extending a generalised Craig-Henton type solution (Priest et al., 2000; Craig and Watson, 2005) we were able to demonstrate that a visco-resistive length scale would be inevitable for even an infinitely small non-linear perturbation of any steady reconnective model. Furthermore, we perform a series expansion (e.g. Cowley, 1975; Priest and Cowley, 1975; Biskamp, 1986; Jamitzky and Scholer, 1995) of a steady reconnecting current sheet and demonstrate that, apart from one very specific choice of initial current profile, **a visco-resistive length scale will appear**.

In Chapter 4, we observe the temporal evolution of current at an X-point. Chapman and Kendall (1963) showed that current will evolve exponentially in an incompressible, ideal plasma. This solution was extended to include resistive effects (Uberoi, 1963) and compressibility (Imshennik and Syrovatskiĭ, 1967). Litvinenko (2007) demonstrated that including the Hall effect leads to a finite-time singularity in a self-similar solution for the evolution of the magnetic and velocity fields. Here, we expand upon Litvinenko's solution by considering a general set of initial conditions in 2.5D and **find that the finite time-singularity will occur unless the axial magnetic field is d_i^{-1} times larger than the planar field**. We note that near the singularity, our self-similar approximation is no longer valid and the current does not actually become singular, we simply end up with very high currents in very short length

scales, or in other words we have current sheet formation.

In Chapter 5, we review the Craig and McClymont (1991) model for purely resistive linear reconnection. Linearising the resistive MHD equations around a static X-point produces oscillatory reconnection. Energy is released in three phases: an initial implosive phase described by advective waves, the important oscillatory phase and finally a long-time tail of slow energy release. We review the modifications of azimuthal effects, pressure effects (Craig and McClymont, 1993) and higher order equilibrium X-points (Craig, 1994).

In Chapter 6, we generalise the linear reconnection model to include viscosity (Craig et al., 2005), the Hall effect (Senanayake and Craig, 2006a; Craig and Litvinenko, 2008) and axial effects (Craig and McClymont, 1993). Our investigation is threefold. First, we formulate a generalised 2.5D linearised MHD system in the presence of viscous, pressure, collisionless and axial magnetic effects. Second, we find, in accordance with previous studies, **that viscous effects, while reducing the rate of reconnection, boost the rate of total energy release**. Moreover, viscous dissipation, as opposed to resistive dissipation, is unlikely to be impeded by pressure forces. Third, we compare two different equilibrium axial magnetic field profiles. One profile emulates a quasi-separatrix layer (QSL) and the other profile emulates a 3D null point. In 2.5D these profiles actually correspond to a hyperbolic field threaded by an axial field and a null line respectively. **We show evidence that fast reconnection is only attainable in the presence of a null.**

Finally, in Chapter 7 we present our conclusions and possibilities for further research.

Chapter 2

MHD Equations and Early Models of Reconnection

This thesis seeks to cast light on three central topics, namely: current sheet formation, steady reconnection and unsteady reconnection. The next four chapters will focus on a number of problems related to these three topics. In this chapter, we will introduce the necessary mathematical framework to deal with coronal plasmas and we will provide an illustrative example of each of our three topics: the Imshennik and Syrovatskiĭ (1967) solution for current sheet formation, Forbes (1982)'s unsteady reconnection approach and the Sweet-Parker (1957) model for steady reconnection.

First, we introduce the magnetohydrodynamic (MHD) equations, and show how the flux frozen-in theorem follows naturally from the ideal MHD approximation. The phenomenon of flux being tied to the plasma in ideal MHD provides the mechanism for astronomically large amounts of magnetic energy to build up and be stored in the field line topology, but also requires the energy release rate to be dependent on the extremely small non-ideal parameter $\eta \sim 10^{-14.5}$. Accordingly, we move on to introduce the traditional Sweet-Parker model of steady reconnection, which has a flux transfer rate $\sim \sqrt{\eta}$.

Due to the low resistivity, reconnection requires regions of extremely large currents $\sim \eta^{-1}$ called current sheets. This motivates the need for a model to

explain how current sheets can naturally form in the solar corona. We explore the X-point collapse model proposed by Dungey (1953) and later described mathematically by Imshennik and Syrovatskiĭ (1967). The X-point collapse model utilises naturally forming finite-time singularities in the current function, which can be arrested by resistive or gas pressure effects (Forbes, 1982) followed by unsteady reconnection (McClymont and Craig, 1996).

2.1 The MHD Equations

The MHD equations describe the evolution of the plasma velocity $\mathbf{v}$ and the magnetic field $\mathbf{B}$. In cgs units they consist of the conservation of mass equation

$$\partial_t \rho + \nabla \cdot (\rho \mathbf{v}) = 0, \tag{2.1}$$

the momentum equation

$$\rho \left[\partial_t \mathbf{v} + (\mathbf{v} \cdot \nabla)\mathbf{v}\right] = -\nabla p + \frac{1}{c}\mathbf{J} \times \mathbf{B} + \rho\nu\nabla^2\mathbf{v}, \tag{2.2}$$

Ohm's law (Rossi and Olbert, 1970)

$$\begin{aligned}\mathbf{E} + \frac{1}{c}\mathbf{v} \times \mathbf{B} =& \eta\mathbf{J} + \frac{1}{nec}(\mathbf{J} \times \mathbf{B} - \nabla p_e) \\ &+ \frac{m_e}{ne^2}[\partial_t \mathbf{J} + (\mathbf{v} \cdot \nabla)\mathbf{J} + (\mathbf{J} \cdot \nabla)\mathbf{v}],\end{aligned} \tag{2.3}$$

Gauss' law

$$\nabla \cdot \mathbf{B} = 0, \tag{2.4}$$

Faraday's law

$$\nabla \times \mathbf{E} = -\frac{1}{c}\partial_t \mathbf{B}, \tag{2.5}$$

and Ampere's law

$$\nabla \times \mathbf{B} = \frac{4\pi}{c}\mathbf{J}. \tag{2.6}$$

For both the sake of elegance and for the more practical reason of needing dimensionless parameters, such as the Reynold's and Magnetic Reynold's numbers, to use for asymptotic analysis and limiting cases we non-dimensionalise the MHD equations.

Our primary variables and parameters and their dimensions are summarised in the following table (for values see e.g. Priest and Forbes, 2000; Craig and Watson, 2005; Craig et al., 2005)

Symbol	**Meaning**	**Dimensions**	**Typical Coronal Value**
$\mathbf{v}$	plasma velocity	$v_A = B_0/\sqrt{4\pi\rho_0}$	$10^{8.5}$ cm s^{-1}
$\mathbf{B}$	magnetic field	B_0	10^2G
ρ	plasma density	ρ_0	10^{-14} g cm^{-3}
l	length	L	$10^{9.5}$ cm
t	time	$t_A = L/v_A$	10 s
η	resistivity	$4\pi L v_A/c^2$	10^{-12} to $10^{-14.5}$
ν	plasma viscosity	Lv_A	$10^{-4.5}$

and our secondary variables are

Symbol	**Meaning**	**Dimensions**
$\mathbf{J}$	current density	$cB_0/(4\pi L)$
$\mathbf{E}$	electric field	$v_A B_0/c$
p	gas pressure	$\rho_0 v_A^2$
p_e	electron pressure	$\rho_0 v_A^2$

The resistivity η and viscosity ν are assumed to be constant. The pressures p and p_e are assumed to be scalar (e.g., Wang et al., 2000), v_A and t_A are the Alfvén velocity and time respectively, and we have assumed a temperature of the order $10^6 K$.

The dimensionless equations are

$$\mathbf{E} + \mathbf{v} \times \mathbf{B} = \eta \mathbf{J} + d_i(\mathbf{J} \times \mathbf{B} - \nabla p_e) + d_e^2[\partial_t \mathbf{J} + (\mathbf{v} \cdot \nabla)\mathbf{J} + (\mathbf{J} \cdot \nabla)\mathbf{v}], \tag{2.7}$$

$$\rho\left[\partial_t \mathbf{v} + (\mathbf{v} \cdot \nabla)\mathbf{v}\right] = -\nabla p + \mathbf{J} \times \mathbf{B} + \nu \nabla^2 \mathbf{v}, \tag{2.8}$$

$$\partial_t \rho + \nabla \cdot (\rho \mathbf{v}) = 0, \tag{2.9}$$

$$\nabla \cdot \mathbf{B} = 0, \tag{2.10}$$

$$\mathbf{J} = \nabla \times \mathbf{B}, \tag{2.11}$$

$$\nabla \times \mathbf{E} = -\partial_t \mathbf{B}. \tag{2.12}$$

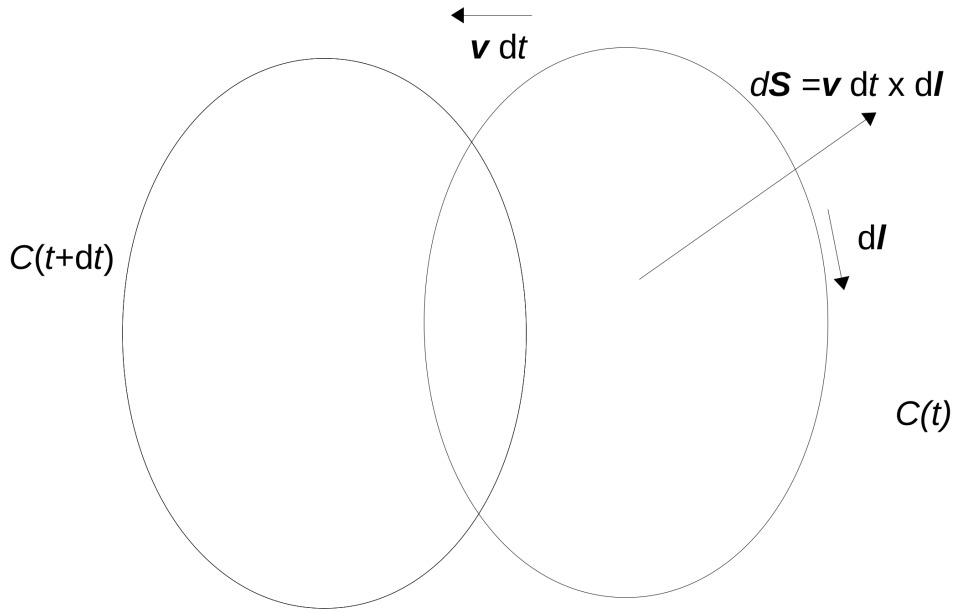

Figure 2.1: Flux frozen-in theorem: $C(t)$ is a curve with in the surface $S(t)$. The infinitesimal line segment $d\mathbf{l}$ is an element of C.

The dimensionless parameters that quantify the role of collisionless effects are displayed in the table below.

Symbol	**Meaning**	**Typical Coronal Value**
d_i	ion skin depth	$c/(L\omega_{pi}) \sim 10^{-6.5}$
d_e	electron skin depth	$c/(L\omega_{pe}) \sim 10^{-8}$
ω_{pi}	ion plasma frequency	$(4\pi ne^2/m_i)^{1/2}$
ω_{pe}	electron plasma frequency	$(4\pi ne^2/m_e)^{1/2}$
c	speed of light	3×10^{10} cm s^{-1}
e	electron charge	1.602×10^{-19} C
m_i	ion mass	1.673×10^{-24} g
m_e	electron mass	9.109×10^{-28} g
n	number density	10^9 cm^{-3}

2.2 Flux Frozen-In Theorem

In order to study how magnetic reconnection is able to liberate such vast quantities of energy, we first need to understand how magnetic energy is able to build up in the solar corona. Consider an ideal plasma with $\eta \equiv 0$. Then Ohm's law (2.7) reduces to

$$\mathbf{E} + \mathbf{v} \times \mathbf{B} = \mathbf{0}, \tag{2.13}$$

which we take the curl of to derive the ideal induction equation using (2.12)

$$\frac{\partial \mathbf{B}}{\partial t} = \nabla \times (\mathbf{v} \times \mathbf{B}) \,. \tag{2.14}$$

We define the magnetic flux as

$$\Phi(t) = \int_S \mathbf{B} \cdot \mathrm{d}\mathbf{S}, \tag{2.15}$$

through a surface $S(t)$. Consider a curve $C(t)$ within S (Fig. 2.1). If $\mathrm{d}\mathbf{l}$ is an element of C, then it carves out an area

$$\mathbf{v} \times \mathrm{d}\mathbf{l} \tag{2.16}$$

per unit time. Hence differentiating (2.15) with respect to time, we obtain the rate of change of flux

$$\frac{\mathrm{d}\Phi}{\mathrm{d}t} = \int_S \frac{\partial \mathbf{B}}{\partial t} \cdot \mathrm{d}\mathbf{S} + \int_C \mathbf{B} \cdot (\mathbf{v} \times \mathrm{d}\mathbf{l}) \,. \tag{2.17}$$

Rewriting the final term as

$$\int_C \mathbf{B} \cdot (\mathbf{v} \times \mathrm{d}\mathbf{l}) = -\int_C (\mathbf{v} \times \mathbf{B}) \cdot \mathrm{d}\mathbf{l} \tag{2.18}$$

and applying Stokes' theorem yields

$$\frac{\mathrm{d}\Phi}{\mathrm{d}t} = \int_S \left[\frac{\partial \mathbf{B}}{\partial t} - \nabla \times (\mathbf{v} \times \mathbf{B}) \right] \cdot \mathrm{d}\mathbf{S}, \tag{2.19}$$

which vanishes by (2.14).

This result gives rise to the notion of flux tubes- surfaces that contain magnetic field such that the cylindrical sides of the tube are everywhere parallel

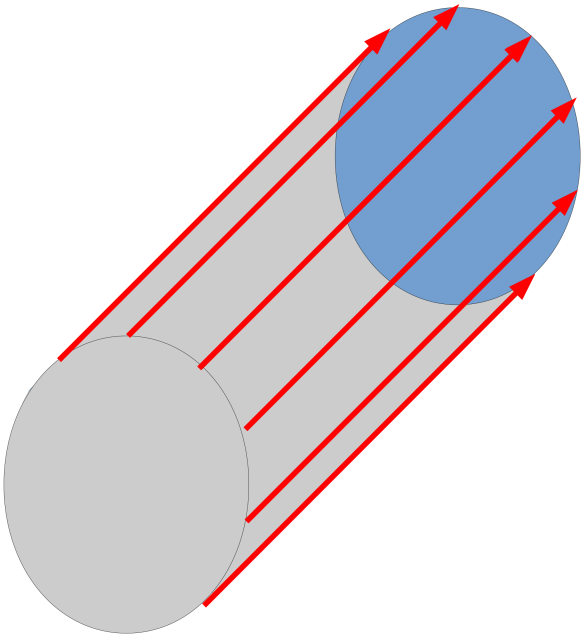

Figure 2.2: A flux tube: A surface that contains magnetic field such that the cylindrical sides of the tube are parallel to the magnetic field lines (red) along its whole length.

to the magnetic field lines (see Fig. 2.2). Hence, the total magnetic flux of the tube must remain constant. Thus ideal MHD restricts field lines from touching and forbids any change in topology of field lines, though tubes are allowed to be squeezed and stretched. This is the flux frozen-in theorem.

The ideal MHD approximation holds as the term $\eta\mathbf{J}$ is small, that is regions of low current. Hence, current sheets represent excellent sites for magnetic reconnection as they comprise long, thin regions of high current. Outside current sheets, we still apply the flux frozen-in theorem.

2.3 Steady Reconnection: The Sweet-Parker model

When two oppositely directed magnetic field lines are carried towards each other they are, under certain circumstances able to break off and rearrange

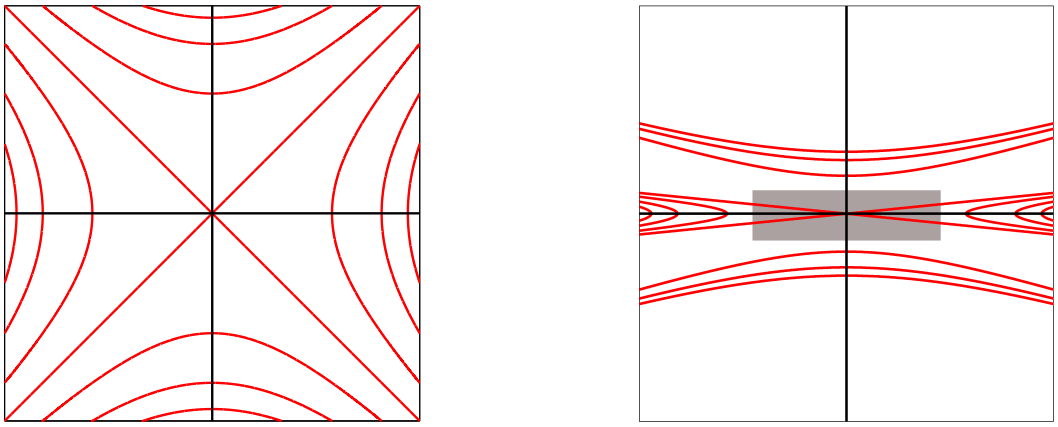

Figure 2.3: A magnetic X-point that collapses to form a current sheet (grey), which can then reconnect. At the centre of the X-point lies a magnetic null point surrounded by hyperbolic, oppositely directed magnetic field lines (red).

into new field lines. This process, known as reconnection, was first proposed by Sweet (1958) and Parker (1957) in order to account for the energy released in solar flares. The Sweet-Parker model, based largely on dimensional arguments, predicted a release of energy that is large enough to explain solar flares, however it could not account for the rapid release of energy in solar flares.

Magnetic reconnection takes place at current sheets, which comprise long thin regions of extremely high current density. In 2D these often arise from the collapse of **magnetic X-points** (see Fig. 2.3). At the centre of the X-point lies a magnetic null point surrounded by hyperbolic magnetic field lines. A **magnetic null point** is defined to be a point where the magnetic field vanishes. A null point is required in order for reconnection to occur in two dimensions. In three dimensions, however, a null point is no longer necessary for reconnection.

This breaking and rearranging of magnetic field lines is not possible in ideal MHD. Hence we need to consider non-ideal terms in Ohm's law. The most obvious choice is to include the resistive term $\eta\mathbf{J}$. Later we will also consider terms that are even smaller (in the solar corona): the Hall and electron inertia terms. By including the resistive term we limit ourselves to the region in which it becomes significant. That is, in a region with a length scale of order

$\sqrt{\eta}$. Given the tiny size of η this means that the current $\mathbf{J}$ must be locally for very high reconnection to work. As the field lines are fairly straight, that means reconnection takes place in a small rectangular region, often called the diffusion region due to the resistive term's ability to diffuse magnetic energy.

For the rest of this thesis we define **purely resistive** to refer to plasma that is in every way, other than the resistive diffusion term $\eta\mathbf{J}$ in Ohm's law, ideal.

In purely resistive, steady, incompressible 2D MHD we have:

$$\mathbf{E} + \mathbf{v} \times \mathbf{B} = \eta\mathbf{J}, \tag{2.20}$$

$$(\mathbf{v} \cdot \nabla)\,\mathbf{v} = \nabla p + \mathbf{J} \times \mathbf{B}. \tag{2.21}$$

In addition the incompressibility assumption means that

$$\nabla \cdot \mathbf{v} = 0, \tag{2.22}$$

and Gauss's law tells us

$$\nabla \cdot \mathbf{B} = 0. \tag{2.23}$$

We have non dimensionalised equations (2.20)-(2.23) in terms of the Alfvén velocity v_A, a typical magnetic field value $B_0 \sim 100G$ and a typical length scale L. We consider a diffusion region along the x-axis with length L, which is taken to be 1 in our units, and width l (displayed in Fig. 2.4). The inflow magnetic field component B_x is also taken to be 1 in units of B_0. Our remaining variables are the inflow velocity v_y, outflow velocity v_x, and outflow magnetic field B_y. Differentiating with respect to x is of the order $1/L = 1$ and differentiating with respect to y is taken as $\sim 1/l$. From equation (2.22)

$$\frac{v_x}{1} \sim \frac{v_y}{l}. \tag{2.24}$$

Similarly, for equation (2.23)

$$\frac{1}{1} \sim \frac{B_y}{l}. \tag{2.25}$$

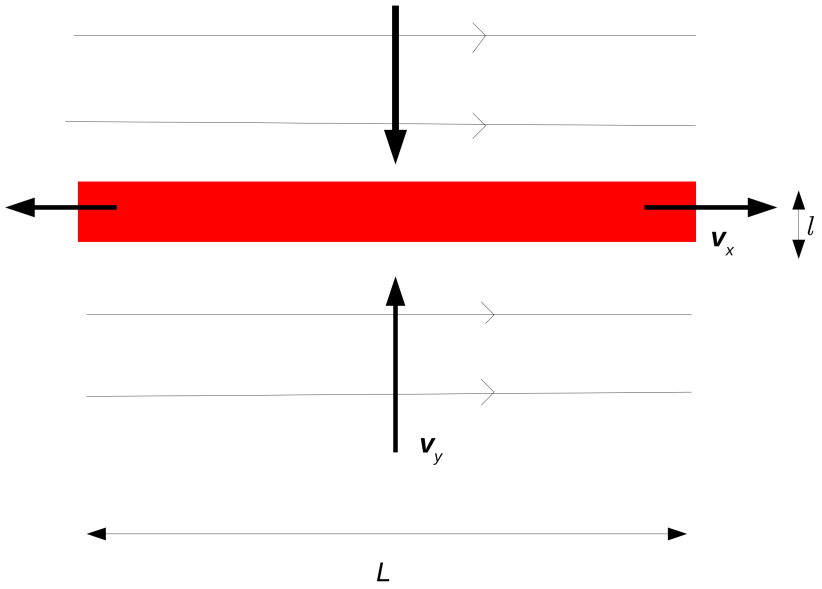

Figure 2.4: Schematic representation of the Sweet-Parker model. Magnetic field reconnects at the current sheet (red).

At the origin we can take $\mathbf{B} = 0$ and taking $\mathbf{E} = E\hat{\mathbf{z}}$ and $\mathbf{J} = J\hat{\mathbf{z}}$

$$E \sim \eta J. \tag{2.26}$$

Outside the diffusion region we can neglect $\eta\mathbf{J}$. Hence E is proportional to the inflow speed and magnetic field:

$$E \sim v_y \tag{2.27}$$

Following Ampere's law

$$\mathbf{J} = \nabla \times \mathbf{B}, \tag{2.28}$$

we can take the current at the origin to be

$$J \sim \frac{B_x}{l} = \frac{1}{l}. \tag{2.29}$$

Substituting equation (2.29) into (2.26) and equating to equation (2.27), we have

$$v_y \sim \frac{\eta}{l}. \tag{2.30}$$

From equation (2.24), $l \sim v_y/v_x$. Hence

$$v_y^2 \sim \eta v_x. \tag{2.31}$$

Taking the x-component of the momentum equation and using equation (2.24)

$$(\mathbf{v} \cdot \nabla)\, \mathbf{v} \cdot \hat{\mathbf{x}} \sim v_x^2, \tag{2.32}$$

and using equation (2.29)

$$(\mathbf{J} \times \mathbf{B}) \cdot \hat{\mathbf{x}} \sim \frac{B_y}{l}. \tag{2.33}$$

Combining equations (2.25), (2.32) and (2.33) yields

$$v_x^2 \sim \frac{B_y}{l} \sim 1. \tag{2.34}$$

Unsurprisingly, the outflow velocity then is taken to be of the order of its typical reference value - the Alfvén velocity - so that $v_x = v_A \equiv 1$. Combining equations (2.24) and (2.30) we find

$$v_y \sim l \sim \sqrt{\eta}. \tag{2.35}$$

The dimensionless inflow velocity v_y is the reconnection rate, often called the inflow Alfvén Mach number M_i. In the solar corona, fields reconnect at between 10^{-3} and 10^{-6} of the Alvén speed (Priest and Forbes, 1986). However, typical values of the solar corona give a dimensionless resistivity of $\eta \sim 10^{-14.5}$ (see e.g. Craig and Watson, 2005).

2.4 The Petschek model

The first and most popular solution to this problem for a long period of time was the Petschek (1964) model. Petschek considered a diffusion region with a length λ and width l much smaller than the global length scale L. Furthermore, he considered a wide X-point angle with slow mode shocks along the separatrices. Consequently, the inflow speed v_{inflow} into the region (for an incompressible plasma) is of the order

$$v_{\text{inflow}} \sim v_{\text{outflow}}\, \frac{l}{\lambda}, \tag{2.36}$$

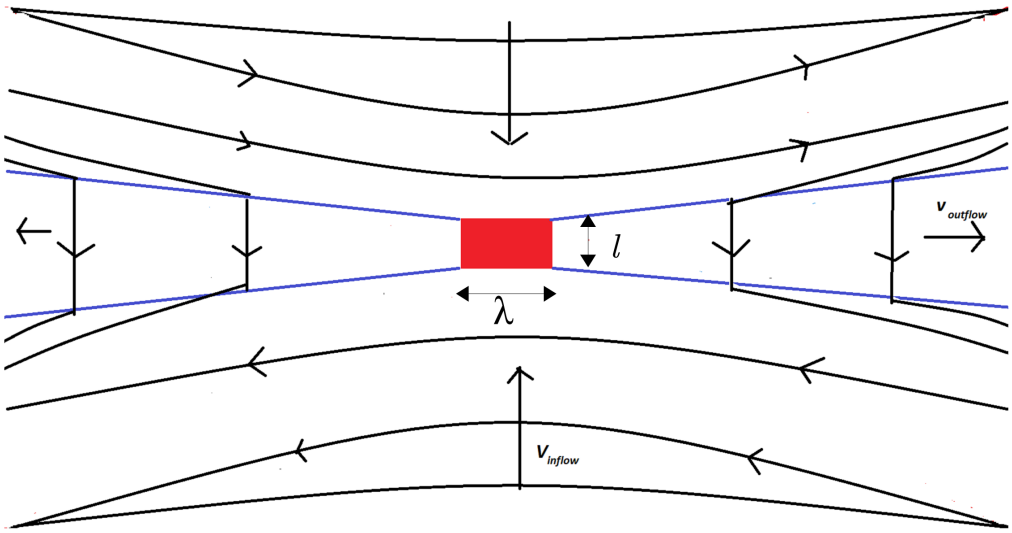

Figure 2.5: Schematic representation of the Petschek model. Magnetic field reconnects at the current sheet (red). The blue lines represent slow mode shocks.

where the outflow speed v_{outflow} has magnitude $v_A \sim 1$. Thus the inflow speed depends on the aspect ratio l/λ of the diffusion region. If $l \sim \lambda$ we have rapid reconnection.

Consequently, for two decades, the reconnection problem was thought to have been solved. However, while physically valid, numerical simulations of driven reconnection were unable to produce a Petschek configuration for small η. On the other hand, a Petschek-like configuration was found in simulations with an anomalous (i.e. locally enhanced) resistivity (e.g Heyn and Semenov, 1996). For a full discussion, we refer the reader to the monographs by Priest and Forbes (2000) or Biskamp (2000).

2.5 Current Sheet Formation in Compressible MHD

As proposed by Dungey (1953), a small perturbation of a current-free X-point can lead to an explosive growth of current. In certain cases, the current can

become singular in a finite-time, which we call *current sheet formation*. Of course, an infinite amount of current density cannot actually exist. From a mathematical perspective, near the singularity our model must break down and no longer be a suitable approximation for a reconnecting plasma. Physically, this means that effects such as pressure and resistive effects are able to limit the growth of the current and quench the singularity.

Taking into account Gauss' law:

$$\nabla \cdot \mathbf{B} = 0, \tag{2.37}$$

we can set

$$\mathbf{B} = \nabla \times \psi \hat{\mathbf{z}}. \tag{2.38}$$

in 2.5D. Thus the compressible MHD equations can be written as:

$$\frac{\partial \rho}{\partial t} + \mathbf{v} \cdot \nabla \rho = -\rho \nabla \cdot \mathbf{v}, \tag{2.39}$$

$$\frac{\partial \psi}{\partial t} + \mathbf{v} \cdot \nabla \psi = \eta \nabla^2 \psi, \tag{2.40}$$

$$\rho \left(\frac{\partial \mathbf{v}}{\partial t} + (\mathbf{v} \cdot \nabla) \mathbf{v} \right) = -\nabla p - \nabla^2 \psi \nabla \psi. \tag{2.41}$$

We adopt the polytropic form for gas pressure

$$p = \bar{\beta} \rho^r, \tag{2.42}$$

where $\bar{\beta}$ and r are constants. Imshennik and Syrovatskiĭ (1967) found the following self-similar solution

$$\psi = \alpha(t) x^2 - \beta(t) y^2 + 2\eta \int (\alpha - \beta) \, \mathrm{d}t, \tag{2.43}$$

$$\rho = \rho(t), \tag{2.44}$$

$$\mathbf{v} = (\gamma(t) x, \delta(t) y) \, . \tag{2.45}$$

This leads to the set of ODEs:

$$\dot{\alpha} + 2\alpha\gamma = 0, \tag{2.46}$$

$$\dot{\beta} + 2\beta\delta = 0, \tag{2.47}$$

$$\rho\left(\dot{\gamma}+\gamma^2\right)=4\alpha\left(\beta-\alpha\right), \tag{2.48}$$

$$\rho\left(\dot{\delta}+\delta^2\right)=-4\beta\left(\beta-\alpha\right), \tag{2.49}$$

$$\dot{\rho}+\rho\left(\gamma+\delta\right)=0. \tag{2.50}$$

We assume here that $\alpha(t)$ and $\beta(t)$ are always positive in order to preserve the geometry of our X-point. Making the transformation

$$\alpha=\frac{1}{a^2}, \tag{2.51}$$

$$\beta=\frac{1}{b^2}, \tag{2.52}$$

yields

$$\gamma=\frac{\dot{a}}{a}, \tag{2.53}$$

$$\delta=\frac{\dot{b}}{b}, \tag{2.54}$$

$$\rho=\frac{4}{ab}, \tag{2.55}$$

$$\ddot{a}=-b\left(\frac{1}{a^2}-\frac{1}{b^2}\right), \tag{2.56}$$

$$\ddot{b}=a\left(\frac{1}{a^2}-\frac{1}{b^2}\right). \tag{2.57}$$

In order to illustrate the singularity, we choose the initial conditions

$$\alpha(0)=a(0)=1, \tag{2.58}$$

$$\beta(0)=b(0)=1, \tag{2.59}$$

$$\gamma(0)=\gamma_0, \tag{2.60}$$

$$\delta(0)=\delta_0. \tag{2.61}$$

Here we let γ_0 and δ_0 be non-zero in order to avoid trivial static plasma solutions. Furthermore, due to the symmetry of the X-point, that is by asserting that the x coordinate is not inherently preferable to the y coordinate, we find that the replacement

$$\alpha\to-\beta,\qquad\beta\to-\alpha,\qquad\gamma\to\delta,\qquad\delta\to\gamma, \tag{2.62}$$

corresponds to swapping the x and y axis. Hence, we only need to consider the case $\gamma_0\geq\delta_0$. The case $\gamma_0=\delta_0$ is a special class of current-free solutions

that we do not consider here (see Imshennik and Syrovatskiĭ, 1967). Thus we assert that $a > b$ and $\dot{a} > \dot{b}$ for early times. Equations (2.56) and (2.57) tell us that $\ddot{a} > 0$ and $\ddot{b} < 0$ for early time. Hence, $a > b$ for all time and since $\ddot{b} < 0$, we will reach a singular point $b = 0$ at some finite time t_s. Near the singularity, equations (2.56) and (2.57) can be approximated by

$$\ddot{a} = \frac{1}{b}, \tag{2.63}$$

$$\ddot{b} = -\frac{a}{b^2}. \tag{2.64}$$

Near the singularity we approximate the solution as

$$b = ct^p, \tag{2.65}$$

and solve for the constants c and p. This yields the asymptotic solutions

$$b = \frac{9}{2} a\left(t_s\right)\left(t - t_s\right)^{2/3}, \tag{2.66}$$

$$a = a(t_s). \tag{2.67}$$

An interesting special case, that we explore in Chapter 4, is the incompressible case $\gamma_0 = -\delta_0$. As discussed in Chapter 4, the incompressible case does not lead to a finite time singularity (Chapman and Kendall, 1963; Uberoi, 1963; Sulem et al., 1985).

2.6 Unsteady Reconnection in One Dimension

Forbes (1982) uses a one-dimensional magnetic configuration to describe an evolving current sheet. While the one-dimensional model is a severe assumption, it allows for analytical solutions which describe non-linear behaviour. In Chapters 5 and 6 we will consider analytical solutions for 2D and 2.5D, that is 3D models with no dependence on the z co-ordinate, but our drawback will be that we can only describe linear behaviour. By employing numerical simulations, McClymont and Craig (1996) were able to describe non-linear 2.5D reconnection and show the limiting cases where the Forbes (1982) model is necessary and where a linear model is sufficient.

In one dimension the purely resistive MHD equations with a magnetic field $\mathbf{B} = B(x,t)\,\hat{\mathbf{y}}$ and velocity field $\mathbf{v} = v(x,t)\,\hat{\mathbf{x}}$ reduce to

$$\dot{B} + (vB)' = \eta B'' \tag{2.68}$$

$$\rho\left[\dot{v} + vv'\right] = -p' - BB', \tag{2.69}$$

$$\dot{\rho} + (\rho v)' = 0, \tag{2.70}$$

where the overdot refers to differentiation with respect to time and a dash refers to differentiation with respect to x. As with the Imshennik and Syrovatskiĭ (1967) model we adopt the polytropic gas pressure (2.42) and let

$$B = \alpha(t)x, \tag{2.71}$$

$$v = q(t)x, \tag{2.72}$$

$$\rho = \rho(t), \tag{2.73}$$

which reduces equations (2.68)-(2.70) to

$$\dot{\alpha} + 2\alpha q = 0, \tag{2.74}$$

$$\rho\left(\dot{q} + q^2\right) = -\alpha^2, \tag{2.75}$$

$$\dot{\rho} + \rho q = 0. \tag{2.76}$$

Substituting $q = -\dot{\rho}/\rho$ into (2.74) and applying the initial conditions (Forbes and Speiser, 1979)

$$\alpha(0) = 1, \quad \rho(0) = 1, \quad q(0) = 0, \tag{2.77}$$

yields the solution

$$\alpha = \rho^2. \tag{2.78}$$

Substituting (2.78) into (2.75) produces the equation

$$\dot{q} + q^2 = -\rho^3, \tag{2.79}$$

which we solve by letting

$$q(t) = f(t)\rho(t), \tag{2.80}$$

where $f = -\dot{\rho}/\rho^2$ by (2.76). Thus equation (2.79) simplifies to

$$\dot{f} = -\rho^2. \tag{2.81}$$

Hence, substituting $\rho^2 = -\dot{\rho}/f$:

$$f\dot{f} = \dot{\rho}, \tag{2.82}$$

and integrating with respect to time yields

$$\tfrac{1}{2}f^2 = \rho - 1, \tag{2.83}$$

after solving for the integration constant since $f(0) = 0$. Observing that (2.83) has two solutions, we take the negative root (since $\rho > 0$ in (2.80)) to ensure that at $x = \pm 1$, the plasma is flowing towards the origin (i.e. ensuring that $q < 0$ in (2.72)) . Hence putting

$$q = -\sqrt{2}\rho\left(\rho - 1\right)^{1/2}, \tag{2.84}$$

into (2.76) yields

$$\frac{\dot{\rho}}{\rho^2\left(\rho - 1\right)^{1/2}} = \sqrt{2}, \tag{2.85}$$

which integrates to (Forbes and Speiser, 1979)

$$\frac{(\rho - 1)^{1/2}}{\rho} + \tan^{-1}\left[(\rho - 1)^{1/2}\right] = \sqrt{2}t. \tag{2.86}$$

We calculate the singularity time t_s by letting $\rho \to \infty$. The first term approaches zero and the second term on the left hand side approaches $\pi/2$ as the density approaches infinity. Hence

$$t_s = \frac{\pi}{2\sqrt{2}}. \tag{2.87}$$

To calculate the length scale we impose some boundary at $x = \pm 1$. Since far from the origin the plasma is approximately ideal, we say that information from the boundary travels in the form of waves with speed $v_A = B/\sqrt{\rho}$. The speed of such a wave is given by (Priest and Forbes, 2000)

$$\frac{\mathrm{d}x}{\mathrm{d}t} = u - v_A. \tag{2.88}$$

Substituting our values for B and u into (2.88) yields

$$\dot{x} = -\frac{\dot{\rho}}{\rho}x - \rho^{3/2}x. \tag{2.89}$$

Covering up the last term on the right-hand side motivates the substitution

$$x(t) = \frac{g(t)}{\rho(t)}, \tag{2.90}$$

which reduces (2.89) to

$$\dot{g} = -\rho^{3/2}g. \tag{2.91}$$

Finally letting $\rho = -\dot{\rho}/q$, we end up with the relation

$$\frac{\dot{g}}{g} = \frac{\dot{\rho}}{\sqrt{2\rho(\rho-1)}}, \tag{2.92}$$

which upon integration and substitution into (2.90), we obtain the length scale (Forbes, 1982)

$$x = \rho^{-1}\left(\sqrt{\rho} + \sqrt{\rho-1}\right)^{-\sqrt{2}}. \tag{2.93}$$

2.6.1 After the Singularity

In order to arrest the singularity, we assume that the current build up is stalled by the resistivity or gas pressure (Forbes, 1982). For resistive diffusion, we balance the terms

$$(vB)' \sim \eta B'', \tag{2.94}$$

in equation (2.68), which requires dimensionally that

$$v \sim \frac{\eta}{x}. \tag{2.95}$$

Recalling that near the singularity $\rho \gg 1$, the length scale (2.93) and velocity function (2.84) become

$$x \sim \rho^{-1.707}, \quad u \sim \rho^{3/2}x. \tag{2.96}$$

Substituting (2.96) into (2.95) and (2.78) we obtain the scalings required to halt the collapse of a current sheet (Forbes, 1982; McClymont and Craig, 1996)

$$\rho \sim \eta^{-0.522}, \quad x \sim \eta^{0.892}, \quad B \sim \eta^{-0.153}, \quad J \sim \eta^{-1.045}. \tag{2.97}$$

These scalings are especially significant, as pointed out by Priest and Forbes (2000), since they imply a maximum reconnection rate of

$$E \sim \eta J \sim \eta^{-0.045}, \tag{2.98}$$

which would be very fast compared to the Sweet-Parker model. We often use the maximum reconnection rate in unsteady models as a comparison with the steady Sweet-Parker rate since if the maximum reconnection rate is slow, we can immediately dismiss the model. In this case, since our maximum reconnection rate is fast, we can dig deeper and search for the average reconnection rate given by

$$E_{\text{ave}} = \frac{1}{\tau}\int_0^{\tau} \eta J \,\mathrm{d}t \tag{2.99}$$

over a collapse time τ. Letting $J = \rho^2$ from (2.78), we obtain

$$E_{\text{ave}} = \frac{\eta}{\tau}\int_1^{\rho_\tau} \frac{\rho^2}{\dot{\rho}} \,\mathrm{d}\rho, \tag{2.100}$$

which, after recalling that $\dot{\rho}/\rho^2 = -f(\rho)$, integrates to

$$E_{\text{ave}} = \frac{\eta}{\tau}\sqrt{2}\left(\rho_\tau - 1\right)^{1/2}. \tag{2.101}$$

Taking τ to be the singularity time t_s and employing equations (2.87) and (2.97) yields

$$E_{\text{ave}} \sim \eta^{0.739}, \tag{2.102}$$

which we deem slow since it scales as a positive power of η.

Alternatively, if gas pressure effects arrest the singularity then we balance the terms

$$BB' \sim \bar{\beta}\left(\rho^r\right)' \tag{2.103}$$

in equation (2.69), where we have used the polytropic gas pressure (2.42). For a sufficiently high temperature, we assume a monatomic gas with $r = 5/3$. Substituting the magnetic field scaling (2.78) and the length scale (2.93), with $\rho \gg 1$, into (2.103), we find (Forbes, 1982)

$$\rho \sim \beta^{-0.925}, \quad x \sim \beta^{1.579}, \quad B \sim \bar{\beta}^{-0.271}, \quad J \sim \beta^{-1.850}. \tag{2.104}$$

Finally, we use the scaling $J \sim \bar{\beta}^{-1.850}$ as a condition on when pressure effects will overwhelm resistive effects. A quick comparison to the resistive scaling $J \sim \eta^{-1.045}$ yields

$$\bar{\beta} \lesssim \eta^{0.565}, \tag{2.105}$$

as a limitation on when we can safely ignore pressure. Considering that $\eta \ll 1$, we require a very small $\bar{\beta} \sim T/B^2$ in order for gas pressure effects to be negligible, or in other words a very high temperature or a very small magnetic pressure.

2.7 Summary

We have first introduced then, for the sake of easier mathematical manipulation, non-dimensionalised Magnetohydrodynamic equations. In ideal MHD, the rate of change of flux through a surface is zero, leading to the idea that flux is frozen in to the plasma. However, when resistive effects become significant, the flux frozen-in condition is broken and topology may change. Resistive effects only become large enough in the presence of very high current over a very small length scale - in other words at a current sheet.

The Sweet-Parker mechanism requires a current sheet. At the current sheet, resistive effects are significant and field lines are allowed to break and reconnect. Far from the current sheet ideal MHD applies. Hence, the Sweet-Parker model naturally lends itself well to asymptotic analysis. Such an analysis predicts the release of a large amount of magnetic energy at the rate of $\sqrt{\eta}$. This is a rate many orders of magnitude smaller than observations. A "fast" magnetic reconnection rate we define to have a logarithmic dependence on η or be dependent on η to a zero or negative power. This slow reconnection rate is the central problem that motivates the original research in this thesis.

Furthermore, we have introduced a model for current sheet formation. In a compressible, purely resistive framework Imshennik and Syrovatskiĭ (1967) found a self-similar solution that leads to a finite time singularity in the current.

Notably, the same singularity does not occur in a finite time in incompressible MHD (Chapman and Kendall, 1963). Clearly, a singular current is not physically possible. In this case, the singularity is ultimately arrested by pressure effects and is described (in one dimension) by the Forbes (1982) model.

Chapter 3

Visco-Resistive Length Scale in Flux Pile-Up and Series Solutions for Steady Magnetic Reconnection

3.1 Introduction

Flux pile-up is a regime in which oppositely directed magnetic field lines are swept towards each other and as they approach the origin they are pushed together and the flux becomes high at the edge of the diffusion region (Priest and Forbes, 1986). A particular case of flux pile-up is magnetic annihilation, in which straight magnetic field lines are directed at each other in a stagnation point plasma flow. The magnetic field is said to be annihilated at the origin. This differs from magnetic reconnection, in which there is a topological rearrangement of field lines at the origin. However, by introducing a shear flow, Craig and Henton (1995) were able to construct an annihilation model that can be turned into a reconnection model by allowing for topological rearrangement.

3.2 Governing Equations

We consider 2D steady, incompressible ($\rho = 1$) MHD and ignore the Hall effect and electron inertia ($d_i = d_e = 0$). The dimensionless MHD system (2.7)-(2.12) reduces to

$$\mathbf{E} + \mathbf{v} \times \mathbf{B} = \eta \mathbf{J} \tag{3.1}$$

$$(\mathbf{v} \cdot \nabla)\mathbf{v} = -\nabla p + \mathbf{J} \times \mathbf{B} + \nu \nabla^2 \mathbf{v}, \tag{3.2}$$

$$\nabla \cdot \mathbf{v} = 0, \tag{3.3}$$

$$\nabla \cdot \mathbf{B} = 0, \tag{3.4}$$

$$\mathbf{J} = \nabla \times \mathbf{B}, \tag{3.5}$$

$$\nabla \times \mathbf{E} = \mathbf{0}. \tag{3.6}$$

We use the flux function $\psi(x, y)$ and stream function $\phi(x, y)$ to satisfy equations (3.3) and (3.4):

$$\mathbf{B} = \nabla \times \psi \hat{\mathbf{z}} = (\partial_y \psi, -\partial_x \psi, 0), \tag{3.7}$$

$$\mathbf{v} = \nabla \times \phi \hat{\mathbf{z}} = (\partial_y \phi, -\partial_x \phi, 0), \tag{3.8}$$

Assuming $\mathbf{E}$ only has a $\hat{\mathbf{z}}$ component, the solution to (3.6) is

$$\mathbf{E} = E \hat{\mathbf{z}}, \tag{3.9}$$

where E is a constant. After taking the curl of (3.1) and (3.2), The MHD equations simplify as follows:

$$-E + [\psi, \phi] = \eta \nabla^2 \psi, \tag{3.10}$$

$$[\nabla^2 \phi, \phi] - \nu \nabla^2 \left(\nabla^2 \phi\right) = [\nabla^2 \psi, \psi], \tag{3.11}$$

where Poisson bracket notation is defined as

$$[\psi, \phi] = (\partial_x \psi)\partial_y \phi - (\partial_y \psi)\partial_x \phi.$$

3.3 Flux Pile-Up Models

The flux pile-up regime is of interest to us because it provides one of the few avenues for finding exact analytical solutions to the MHD equations from which we can describe a current sheet. The simplest non-trivial flux pile-up solution (Sonnerup and Priest, 1975) comes from considering straight vertical magnetic field lines and sending them towards the origin, that is to say we let

$$\mathbf{B} = B\,(x)\,\hat{\mathbf{y}}. \tag{3.12}$$

and assume a hyperbolic plasma flow

$$\phi = -xy \tag{3.13}$$

and neglecting viscosity ($\nu = 0$). Substituting (3.13) into (3.10) yields

$$E - xB = \eta \frac{\partial B}{\partial x}, \tag{3.14}$$

which has the solution

$$B = \frac{2E}{\sqrt{2\eta}}\,\mathrm{daw}\left(\frac{x}{\sqrt{2\eta}}\right), \tag{3.15}$$

in terms of the Dawson function

$$\mathrm{daw}(u) = \mathrm{e}^{-u^2}\int_0^u e^{\mu^2}\mathrm{d}\mu. \tag{3.16}$$

Later models generalised the flux pile-up model to include viscosity and vorticity. Gratton et al. (1988, 1990) considered a viscous stagnation point flow, however their solution did not represent any realistic flow for magnetic annihilation. The problem is that their velocity field exhibited cusplike behaviour which implied a viscous drag force directed towards the origin (Sonnerup and Phan, 1990). Besser et al. (1990) modified Gratton et al.'s solution to represent a perturbed Sonnerup and Priest (1975) flow, rather than a cusplike flow. Hence, Besser et al. (1990) assume that the magnetic field takes the form (3.12). However for a more general plasma flow, equation (3.14) can be generalised to

$$E + \frac{\partial \phi}{\partial y}B = \eta \frac{\partial B}{\partial x}. \tag{3.17}$$

For simplicity, we follow Besser et al. (1990) and consider

$$v_x = \frac{\partial \phi}{\partial y} = f(x), \tag{3.18}$$

so that equation (3.17) has the solution

$$B = \frac{E}{\eta} \exp\left(\frac{K(x)}{\eta}\right) \int_1^x \exp\left(-\frac{K(\lambda)}{\eta}\right) \mathrm{d}\lambda, \tag{3.19}$$

where

$$K(x) = \int_1^x f(\xi) \mathrm{d}\xi. \tag{3.20}$$

Integrating equation (3.18) yields

$$\phi = y f(x) + g(x). \tag{3.21}$$

Using a steady viscous flow requires that the momentum equation takes the form

$$(\mathbf{v} \cdot \nabla)\, \mathbf{v} = -\nabla p - \nabla \left(\tfrac{1}{2} B^2\right) + \nu \nabla^2 \mathbf{v}. \tag{3.22}$$

Taking the curl and noting that $\nabla \times \mathbf{v} = -\partial_{xx}\phi\, \hat{\mathbf{z}}$ gives

$$y \left[\nu f^{(4)} + f f''' - f' f''\right] + \left[\nu g^{(4)} + f g''' - f'' g'\right] = 0. \tag{3.23}$$

Equating each bracket to zero and integrating yields

$$\nu f''' + f f'' - f'^2 = \text{const}, \tag{3.24}$$

$$\nu g''' + f g'' - f' g' = \text{const}. \tag{3.25}$$

For our purposes here we are not interested in finding a general solution but rather a particular solution. Hence we assume integration constants to be zero. Following Besser et al. (1990) we let

$$f(x) = -x \tag{3.26}$$

as in the Sonnerup-Priest model. Substituting into equation (3.25) we are left with

$$\nu g''' - x g'' + g' = 0. \tag{3.27}$$

Integration yields

$$\nu g'' - x g' + 2g = 0. \tag{3.28}$$

which we can write as a Sturm-Liouville equation

$$\frac{\mathrm{d}}{\mathrm{d}x}\left(e^{-\frac{x^2}{2\nu}}\, g'(x)\right) + \frac{2}{\nu} e^{-\frac{x^2}{2\nu}}\, g(x) = 0. \tag{3.29}$$

Eventually we end up with the solution

$$\begin{aligned} g(x) =& c_1 \left[\left(\nu - x^2\right) \int \exp\left(\frac{x^2}{2\nu}\right) \mathrm{d}x + \sqrt{\nu}\, x \exp\left(\frac{x^2}{2\nu}\right)\right] \\ &+ c_2(\nu - x^2). \end{aligned} \tag{3.30}$$

Finally, we substitute equations (3.26) and (3.30) into (3.21) to describe $\phi(x, y)$. Hence, we have generalised the exact, irrotational Sonnerup and Priest (1975) solution to add a rotational component, provided a finite c_2 in equation (3.30).

3.4 Craig-Henton solution

The Craig-Henton (1995) solution is not strictly a magnetic annihilation solution since it throws away the condition (3.12) and hence the magnetic field lines are not straight. However, it shares enough similarities with magnetic annihilation that it should be considered with them. It is however an example of a flux pile-up solution. If we ignore (3.12) then the MHD equations become:

$$\left[\nabla^2\phi, \phi\right] = \left[\nabla^2\psi, \psi\right], \tag{3.31}$$

$$E + [\psi, \phi] = \eta \nabla^2 \psi. \tag{3.32}$$

Their approach was to first solve equation (3.31) in such a way that the advection term $[\psi, \phi]$ does not disappear in equation (3.32). Which means we cannot let $\psi = f(\phi)$. They used a harmonic function $H(x, y)$, where

$$\nabla^2 H(x, y) = 0. \tag{3.33}$$

Let

$$\phi = \alpha H(x, y) + u(x), \tag{3.34}$$

$$\psi = \beta H(x, y) + b(x). \tag{3.35}$$

Substituting (3.34) and (3.35) into (3.31) yields

$$\left(\alpha u''' - \beta b'''\right) \partial_y H = 0. \tag{3.36}$$

We solve (3.36) by simply letting

$$u(x) = \frac{\beta}{\alpha} b(x), \tag{3.37}$$

and ignoring any integration constants. Equation (3.32) then becomes

$$E + \left(\frac{\alpha^2 - \beta^2}{\alpha}\right) u'(x) \partial_y H = \eta u''(x). \tag{3.38}$$

From here, we can infer that $\partial_y H$ is a function of x only. Hence, by equation (3.33), $H(x, y)$ must take the form $H = xy$. Solving for u in equation (3.38) yields the solution

$$u(x) = \frac{E}{\eta\mu} \mathrm{daw}\left(\mu x\right), \tag{3.39}$$

where

$$\mu^2 = \frac{(\beta^2 - \alpha^2)}{2\alpha\eta}. \tag{3.40}$$

Much like the Besser et al. (1990) solution, the Craig-Henton solution takes a stagnation point flow and distorts it by adding a shear flow. The difference is that the Craig-Henton solution has non-straight magnetic field lines.

3.5 Three Dimensional Reconnective Annihilation

While, in this thesis, we restrict ourselves to a 2.5D regime, one of the reasons the Craig-Henton model is important is that it scales up easily into three dimensions. Craig and Fabling (1996) split the magnetic field and plasma velocity functions into a background field $\mathbf{P}(\mathbf{x}, \mathbf{y}, \mathbf{z})$ and a shear field $\mathbf{Q}(x, y, z)$ where

$$\mathbf{B} = \lambda \mathbf{P} + \mathbf{Q} \tag{3.41}$$

and

$$\mathbf{v} = \mathbf{P} + \lambda\mathbf{Q}. \tag{3.42}$$

We take the simplest possible (non-trivial) 3D background field that satisfies $\nabla \cdot \mathbf{P} = 0$:

$$\mathbf{P} = (-x, \kappa y, (1-\kappa)z). \tag{3.43}$$

Taking the field line equations (Fabling, 1997)

$$-\frac{\mathrm{d}x}{x} = \frac{\mathrm{d}y}{\kappa y} = \frac{\mathrm{d}z}{(1-\kappa)z}, \tag{3.44}$$

produces the characteristic equations

$$\psi = - yx^{\kappa}, \tag{3.45}$$

$$\chi = zx^{1-\kappa}, \tag{3.46}$$

$$\xi = yz^{(1-\kappa)/\kappa}, \tag{3.47}$$

where ψ, χ and ξ are constant along field lines. Letting $\kappa = 0$ reduces us to the 2D xz plane and letting $\kappa = 1$ reduces us to the xy plane. Thus we take

$$0 \leq \kappa \leq 1. \tag{3.48}$$

Much as in the 2D case we add a shearing field that satisfies $\nabla \cdot \mathbf{Q} = 0$:

$$\mathbf{Q} = X(y,z)\hat{\mathbf{x}} + Y(x,z)\hat{\mathbf{y}} + Z(x,y)\hat{\mathbf{z}}. \tag{3.49}$$

Letting

$$\mathbf{Q} = Y(x)\hat{\mathbf{y}} + Z(x)\hat{\mathbf{z}} \tag{3.50}$$

corresponds to what is known as a fan current geometry and

$$\mathbf{Q} = X(y,z)\hat{\mathbf{x}} \tag{3.51}$$

corresponds to what is known as a spine current geometry (see Lau and Finn, 1990, for a definition). Fully three dimensional magnetic reconnection is beyond the scope of this thesis (see e.g. Pontin, 2011, for a review) but it is worth noting here how easily the Craig-Henton model translates into 3D.

3.6 Visco-Resistive Length Scale in Magnetic Flux Pile-Up

Different models of visco-resistive (VR) reconnection have produced different length scales for a VR current sheet. Significantly, a VR scale does not appear in a certain class of reconnection solutions called flux pile-up solutions (Besser et al., 1990; Phan and Sonnerup, 1990; Craig and Litvinenko, 2012). Thus, any VR length scale is not necessarily a universal scaling for reconnection, a surprising result considering the simple VR dimensional argument used by Park et al. (1984) should be widely applicable. Furthermore, the VR scale does feature in many classes of solutions, such as linear reconnection (Craig et al., 2005; Titov and Priest, 1997; Hassam and Lambert, 1996), reconnective annihilation solutions (Fabling and Craig, 1996; Litvinenko, 2006; Craig and Litvinenko, 2012), more general scaling arguments (Simakov et al., 2010) and plasmoid instability models (e.g. Comisso and Bhattacharjee, 2016, and references therein). This discrepancy in length scales for seemingly similar models motivates our investigation to find a more detailed description of a VR current sheet.

3.7 Dimensional Argument

Before we search for the visco-resistive length scale in flux pile-up models, we first review the Park et al. (1984) scaling argument and the flux pile-up solutions that incorporate viscosity. The first step to determine some unknown scaling is to use a rough estimation. Here, we review a dimensional argument (Park et al., 1984) to demonstrate where the VR length scale originates. We use our own notation and units in order to provide context for arguments we present later in the paper. From equation (3.1) we estimate

$$-E \sim [\psi, \phi] \sim \eta \partial_x^2 \psi \tag{3.52}$$

for the outflow flux ψ_0 and inflow stream function magnitude ϕ_0. We normalise units and choose $\partial_y \sim 1/L \sim 1$. The outflow velocity and magnetic field are also order unity. Approximating $\partial_x \sim 1/l$ gives

$$\frac{\psi_0 \phi_0}{l} = \frac{\eta \psi_0}{l^2}. \tag{3.53}$$

Hence

$$\eta = l\phi_0. \tag{3.54}$$

Similarly, for equation (3.2) we obtain

$$-\frac{\phi_0^2}{Ll^3} - \nu\frac{\phi_0}{l^4} = -\frac{\psi_0^2}{Ll^3}, \tag{3.55}$$

where the negative sign in the first term comes from $\partial_x^2 v_y < 0$ for $v_y = -\partial_x \phi > 0$ (Biskamp, 2000, 1993) since we assume that the velocity field localises around the origin so if v_y is positive at the origin we can also say that it is concave down and hence $\partial_x^2 v_y$ is negative. The same argument applies for ψ_0 term on the right hand side. Rearranging yields

$$\phi_0 = \psi_0 \left(1 + \frac{\nu L}{\phi_0 l}\right)^{-1/2}. \tag{3.56}$$

Substituting equation (3.54) into (3.56) gives

$$\phi_0 = \psi_0 \left(1 + \frac{\nu}{\eta}\right)^{-1/2}. \tag{3.57}$$

Normalising the magnetic field so that $B_y = \partial_x \psi \sim 1$ requires that

$$\psi_0 \sim l, \tag{3.58}$$

and hence the visco-resistive scale

$$l \sim \sqrt{\eta}\left(1 + \frac{\nu}{\eta}\right)^{1/4}. \tag{3.59}$$

For the limiting case $\nu \gg \eta$, we obtain the scaling

$$l \sim (\eta\nu)^{1/4}, \tag{3.60}$$

which is the length scale that appears in previous solutions (e.g. Titov and Priest, 1997; Craig et al., 2005).

3.8 Presence of the VR Scale in Flux Pile-Up Models

A peculiarity of the flux pile-up solutions in Sections 3.3 and 3.4 is the absence of a VR length scale. In Besser et al.'s solution we can see the emergence of a length scale $\sqrt{\eta}$ in equation (3.19) but a length scale $\sqrt{\nu}$ in equation (3.30). Which suggests that unlike traditional reconnection models (Park et al., 1984), we have separate viscous and resistive current layers. This also appears to be a feature of the reconnective Craig-Henton solution (Craig and Henton, 1995; Fabling and Craig, 1996; Craig and Litvinenko, 2012).

The reason for a lack of a VR length scale in Besser et al.'s solution is clear. The magnetic field is solved in terms of the function $f(x) = v_x$. Since the function $f(x)$ is chosen so that viscous terms will vanish, the magnetic field is independent of viscosity. The viscosity does however feature in equation (3.30) for g, which is solved independently of the magnetic field and hence the resistivity. Thus $\mathbf{B}$ depends on η and $v_y = -yf'(x) - g'(x)$ depends on ν.

However, in other more general solutions for magnetic annihilation (Sonnerup and Phan, 1990; Jardine et al., 1992), the function $f(x)$ has to be solved from equation (3.24). We can make equation (3.24) dimensionless by making the transformation

$$\bar{x} = \frac{x}{\nu}. \tag{3.61}$$

Equation (3.24) becomes

$$f'''(\bar{x}) + f(\bar{x})f''(\bar{x}) - f'^2(\bar{x}) = 0. \tag{3.62}$$

While we have to resort to numerical methods to find any physically meaningful solutions to (3.62) (see Jardine et al., 1992), we argue that if the velocity function $v_x = f(x)$ has a viscous dependence then the magnetic field (3.19) will also have a viscous dependence, hence a VR length scale will appear naturally. More generally, as long as the third derivative of $f(x)$ does not

vanish we should expect a viscous scale in the velocity and a VR scale in the magnetic field.

We expect that the same sort of dimensional argument should also apply for the reconnective flux pile-up Craig-Henton solution. In order to force a VR scale we adopt a more general solution described by Priest et al. (2000) and Craig and Watson (2005):

$$\psi = \psi_0(x) + \psi_1(x)y, \tag{3.63}$$

$$\phi = \phi_0(x) + \phi_1(x)y. \tag{3.64}$$

Substituting into equations (3.10) and (3.11) yields, for the case $\partial_x \gg \partial_y$:

$$-\phi_1\psi_1' + \phi_1'\psi_1 - \eta\psi_1'' = 0, \tag{3.65}$$

$$\nu\phi_1''' - \phi_1'^2 + \phi_1''\phi_1 + \psi_1'^2 - \psi_1''\psi_1 = \text{constant}, \tag{3.66}$$

$$E - \phi_1\psi_0' + \phi_0'\psi_1 - \eta\psi_0'' = 0, \tag{3.67}$$

$$\nu\phi_0''' - \phi_0'\phi_1' + \phi_0''\phi_1 + \psi_1'\psi_0 - \psi_0''\psi_1 = \text{constant} \tag{3.68}$$

Assuming none of the above terms vanish we can put forward a simple dimensional argument to find a length scale.

Letting $x \sim l$ and substituting into equation (3.65) yields

$$\frac{\phi_1\psi_1}{l} \sim \frac{\eta\psi_1}{l^2}, \tag{3.69}$$

and substituting into equation (3.66) yields

$$\left(\frac{\nu\phi_1}{l^3} + \frac{\phi_1^2}{l^2}\right) \sim \frac{\psi_1^2}{l^2} \sim 1. \tag{3.70}$$

Rearranging we find

$$\psi_1 \sim l \sim \sqrt{\eta}\left(1 + \frac{\nu}{\eta}\right)^{1/4}, \tag{3.71}$$

$$\phi_1 \sim \sqrt{\eta}\left(1 + \frac{\nu}{\eta}\right)^{-1/4}. \tag{3.72}$$

Continuing for ϕ_0 and ψ_0, we find

$$\psi_0 \sim \psi_1, \tag{3.73}$$

$$E \sim \phi_0 \sim \phi_1. \tag{3.74}$$

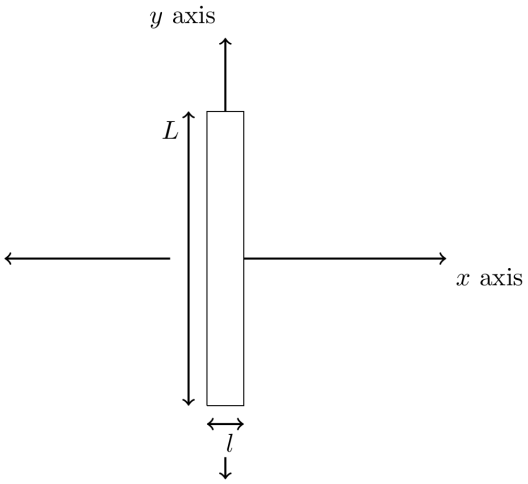

Figure 3.1: Alignment of current sheet

Hence we recover the scalings described by Park et al. (1984).

We compare this scaling argument to the solution given by Craig and Litvinenko (2012). They write the velocity and magnetic fields in the form

$$\mathbf{v} = \alpha \mathbf{P}(x, y) + u(x)\hat{\mathbf{y}}, \tag{3.75}$$

$$\mathbf{B} = \beta \mathbf{P}(x, y) + b(x)\hat{\mathbf{y}}, \tag{3.76}$$

where $\mathbf{P}(x, y) = \nabla \times (\psi_1 y)\hat{\mathbf{z}}$ is a large scale background field and $u(x) = -\phi_0'$ and $b(x) = -\psi_0'$ are reconnection fields. In this case $\phi_1 = \psi_1$. We argue that if the Laplacian of the background field vanishes there will be no VR scale, regardless of the form of the reconnection fields. Thus, the presence of a VR scale is independent of any fields other than the background velocity field or in other words the inflow velocity profile.

It is worth mentioning here that the system (3.63) and (3.64) naturally closes even when accounting for the Hall effect (Craig and Watson, 2005).

3.9 Description of a Purely Resistive Current Sheet in Steady Magnetic Reconnection

Before we describe a visco-resistive current sheet, we should briefly review a description of a purely resistive current sheet. Considering a long, thin current sheet aligned on the y-axis (see Fig. 3.1) with width l, Biskamp (1986) used a series expansion to describe the sheet near the origin. Approximating the sheet as quasi-one-dimensional, Biskamp (1986) let $\partial_x^2 \sim l^{-2} \gg \partial_y^2$. Hence, we approximate $\nabla^2 \approx \partial_x^2$. Equations (3.10) and (3.11), with viscosity ν set to zero, become

$$-E + [\psi, \phi] = \eta \partial_x^2 \psi, \tag{3.77}$$

$$[\partial_x^2 \phi, \phi] = [\partial_x^2 \psi, \psi]. \tag{3.78}$$

Near the origin, we let the flux and stream functions can be represented by a power series expansion of odd and even functions

$$\psi(x,y) = \psi_0(x) + \psi_2(x)\, y^2/2! + \psi_4(x)\, y^4/4! \ldots, \tag{3.79}$$

$$\phi(x,y) = \phi_1(x)\, y + \phi_3(x)\, y^3/3! + \ldots, \tag{3.80}$$

and chose the zeroth order current profile

$$J_0(x) \equiv -\partial_{xx}\psi_0 = \frac{E}{\eta} \mathrm{sech}^2\left(\frac{x}{l}\right), \tag{3.81}$$

which describes a Harris sheet. Note we use factorial denominators which Biskamp (2000) did not use. Hence, for instance, our ψ_2 is $1/(2!)$ the size of Biskamp's ψ_2. Substituting the expansions (3.79)-(3.80) into (3.1)-(3.5) and collecting the coefficients of like powers of y terms yields

$$-E + \psi_0' \phi_1 = \eta \psi_0'', \tag{3.82}$$

$$\phi_1 \phi_1''' - \phi_1' \phi_1'' = \psi_0''' \psi_2 - \psi_0' \psi_2'', \tag{3.83}$$

$$\psi_2' \phi_1 + \psi_0' \phi_3 - 2\psi_2 \phi_1' = \eta \psi_2'', \tag{3.84}$$

where the dash refers to differentiation with respect to x. From here Biskamp (1986) calculated

$$\psi_0 = -\frac{El^2}{\eta} \ln\left(\cosh\left(\frac{x}{l}\right)\right) \tag{3.85}$$

$$\phi_1 = -\frac{\eta}{l} \tanh\left(\frac{x}{l}\right), \tag{3.86}$$

$$\psi_2 = \frac{\eta^3}{El^4} \tanh\left(\frac{x}{l}\right)\left[\frac{x}{l} - \tanh\left(\frac{x}{l}\right)\right]. \tag{3.87}$$

$$\phi_3 = \frac{\eta^4}{E^2 l^7}\left[6\eta \tanh^3\left(\frac{x}{l}\right) - 7\eta \tanh\left(\frac{x}{l}\right) + \frac{3\eta x}{l}\mathrm{sech}^2\left(\frac{x}{l}\right)\right]. \tag{3.88}$$

Note there was a factor of two error in Biskamp's expression for ψ_2. From here Jamitzky and Scholer (1995) found the fourth order flux term

$$\psi_4 = \frac{\eta^7}{l^{10}E^3}\left[8 - \frac{3x^2}{l^2}\mathrm{sech}^2\left(\frac{x}{l}\right) - 4\tanh^2\left(\frac{x}{l}\right) + 2\tanh^4\left(\frac{x}{l}\right) + \frac{23x}{l}\tanh\left(\frac{x}{l}\right) - \frac{12x}{l}\tanh^3\left(\frac{x}{l}\right)\right]. \tag{3.89}$$

3.10 Visco-Resistive Length Scale in Steady Magnetic Reconnection

Now we extend Biskamp (1986)'s description of a purely resistive current sheet near the origin to include viscous effects. This could be useful in terms of numerical simulations or laboratory experiments that incorporate viscosity. The calculation has one degree of freedom that manifests in the choice of a zeroth order current profile. Hence, we perform this calculation for three different zeroth order current profiles as prescribed by Biskamp (2000) and find that two contain a VR length scale while the other does not, despite the three zeroth order current profiles being qualitatively similar and having the same limit near the origin. Finally, we compare flux pile-up models with our series expansion solution and discuss the physical implications of our results.

Following Biskamp (1986), we assume a long, thin current sheet with thickness l aligned along the y axis as pictured in Figure 3.1. This implies that, near the y axis, $\partial_x^2 \sim l^{-2} \gg \partial_y^2$. Hence, we approximate $\nabla^2 \approx \partial_x^2$. Equations

(3.10) and (3.11) become

$$-E+[\psi,\phi]=\eta\partial_x^2\psi, \tag{3.90}$$

$$[\partial_x^2\phi,\phi]-\nu\partial_x^2\left(\partial_x^2\phi\right)=[\partial_x^2\psi,\psi]. \tag{3.91}$$

Finding an exact solution for a reconnecting current sheet, and hence an exact VR length scale, that is valid everywhere is infeasible. However, if we only consider a small length scale then we can use a series expansion technique which, to a sufficient order, is valid in the vicinity of the current sheet. The series expansion method was first used to describe a 2D purely resistive current sheet (Priest and Cowley, 1975). This was then refined to a quasi-one dimensional series expansion by taking $\partial_x \gg \partial_y$ and expanding only in the y direction for a resistive current sheet (Biskamp, 1986; Sonnerup, 1988; Jamitzky and Scholer, 1995) and a Hall current sheet (Litvinenko, 2009).

Near the origin, we again assume that the flux and stream functions can be represented by the series expansion of odd and even functions (3.79)-(3.80), and substitute into (3.1)-(3.5). Collecting the coefficients of like powers of y terms yields

$$-E+\psi_0'\phi_1=\eta\psi_0'', \tag{3.92}$$

$$\phi_1\phi_1'''-\phi_1'\phi_1''-\nu\phi_1^{(4)}=\left(\psi_0'''\psi_2-\psi_0'\psi_2''\right), \tag{3.93}$$

$$\psi_2'\phi_1+\psi_0'\phi_3-2\psi_2\phi_1'=\eta\psi_2'', \tag{3.94}$$

$$\begin{aligned}&3\left(\phi_1'''\phi_3-\phi_3''\phi_1'\right)+\left(\phi_3'''\phi_1-\phi_1''\phi_3'\right)-\nu\phi_3^{(4)}=\\&\left(\psi_0'''\psi_4-\psi_4''\psi_0'\right)+3\left(\psi_2'''\psi_2-\psi_2''\psi_2'\right),\end{aligned} \tag{3.95}$$

$$\phi_1\psi_4'+6\psi_2'\phi_3+\psi_0'\phi_5-4\psi_2\phi_3'-4\phi_1'\psi_4=\eta\psi_4'', \tag{3.96}$$

where again the dash refers to differentiation with respect to x.

We must assume a profile for $\psi_0'=-B_y(x,0)$, the magnetic field profile near the y axis, in order to start the expansion. First we consider a zeroth order flux function that replicates flux-pile up solutions of the form (3.15):

$$\psi_0'=-\frac{El}{\eta}\mathrm{daw}\left(\frac{x}{l}\right). \tag{3.97}$$

This profile yields the higher order solutions

$$\psi_2 = k_2\psi_0 \tag{3.98}$$

$$\psi_4 = k_4\psi_0 \tag{3.99}$$

$$\psi_6 = k_6\psi_0 \tag{3.100}$$

$$\vdots \tag{3.101}$$

and

$$\phi_3 = k_3\phi_1 \tag{3.102}$$

$$\phi_5 = k_5\phi_1 \tag{3.103}$$

$$\phi_7 = k_7\phi_1 \tag{3.104}$$

$$\vdots \tag{3.105}$$

for arbitrary constants k_i. Setting all higher order terms to zero recovers the Sonnerup-Priest solution and thus kills our VR scale.

Alternatively, we follow previous studies (Biskamp, 1986; Jamitzky and Scholer, 1995; Litvinenko, 2009) and choose the zeroth order function

$$\psi_0 = -\frac{El^2}{\eta}\ln\left(\cosh\left(\frac{x}{l}\right)\right). \tag{3.106}$$

This particular current sheet profile, which describes a Harris sheet, is used here since it is one of the only functions for which it is possible to perform the expansion in terms of elementary functions. Furthermore, it is similar to a Gaussian function which was postulated to be a more accurate profile (Biskamp, 2000), and which we use in Section VIII. Substituting equation (3.106) into equation (3.92) yields

$$\phi_1 = -\frac{\eta}{l}\tanh\tilde{x}, \tag{3.107}$$

where we let $\tilde{x} = x/l$. Integrating equation (3.93) twice gives

$$\psi_2 = -\frac{\phi_1\phi_1'}{\psi_0'} + \nu\psi_0'\int\frac{\phi_1'''}{\psi_0'^2}\,\mathrm{d}x + c_2\psi_0'\int\frac{1}{\psi_0'^2}\,\mathrm{d}x, \tag{3.108}$$

which yields

$$\psi_2 = \frac{\eta^2}{El^4}\left[(6\nu-\eta)\tanh^2\tilde{x} + c_2\tilde{x}\tanh\tilde{x} + 2\nu + \eta - c_2\right]. \tag{3.109}$$

Here, the arbitrary constant c_2 has been redefined after integration and we have used the boundary condition $\psi_2'(0) = 0$ to specify another integration constant since $B_y(0) = 0$ at an X-point. Equation (3.94) shows that $\phi_3 \to \infty$ as $x \to 0$ unless

$$c_2 = \eta - 2\nu. \tag{3.110}$$

Substituting this result into (3.109), we find

$$\psi_2 = \frac{\eta^2}{El^4}\left[(\eta - 2\nu)\,\tilde{x}\tanh\tilde{x} + (6\nu - \eta)\tanh^2\tilde{x} + 4\nu\right]. \tag{3.111}$$

Setting $\nu = 0$ recovers equation (3.87). To find ϕ_3 we use equation (3.94). The result is

$$\begin{aligned}\phi_3 =& \frac{\eta^4}{E^2l^7}\left[6\,(\eta - 6\nu)\tanh^3\tilde{x}\right. && (3.112)\\ &\left. - (7\eta - 38\nu)\tanh\tilde{x} + 3\,(\eta - 2\nu)\,\tilde{x}\mathrm{sech}^2\tilde{x}\right]. && (3.113)\end{aligned}$$

Setting $\nu = 0$ recovers equation (3.88). Next, to find ψ_4, we integrate equation (3.95). The result is

$$\begin{aligned}\psi_4 =& \frac{\eta^5}{l^{10}E^3}\left[\,8\left(\eta^2 + \eta\nu - 58\nu^2\right) - 3\,(\eta - 2\nu)^2\,\tilde{x}^2\mathrm{sech}^2\tilde{x}\right.\\ &- 4\left(\eta^2 - 62\eta\nu + 408\nu^2\right)\tanh^2\tilde{x}\\ &+ 2\,(\eta - 6\nu)\,(7\eta - 66\nu)\tanh^4\tilde{x}\\ &+ \left(23\eta^2 - 212\eta\nu + 460\nu^2\right)\tilde{x}\tanh\tilde{x}\\ &\left. - 12\,(\eta - 2\nu)\,(\eta - 6\nu)\,\tilde{x}\tanh^3\tilde{x}\,\right]. \end{aligned}\tag{3.114}$$

Note that setting $\nu = 0$ recovers equation (3.89). Substituting equations (3.106), (3.111) and (3.114) into (3.79), and substituting (3.112) and (3.107) into (3.80) yields the flux and stream functions up to fourth order. We use these flux and stream functions to find the length scale of our current sheet.

3.11 Description of a Visco-Resistive Current Sheet

We want to find the length scale of a VR current sheet and quantify the role of viscosity in magnetic reconnection. We obtain predictions for the reconnection rate, the outflow speed and the thickness of the current sheet. We approximate $\psi(x,y)$ near the X-point by substituting the leading order terms of ψ_0, ψ_2 and ψ_4 into (3.79):

$$\psi \approx -\frac{E}{2\eta}x^2 + \frac{2\nu\eta^2}{El^4}y^2 + \frac{E}{12\eta l^2}x^4 + \frac{2\nu\eta^2}{El^6}x^2y^2 + \frac{\eta^5}{3l^{10}E^3}\left(\eta^2+\eta\nu-58\nu^2\right)y^4. \tag{3.115}$$

To find the thickness l from equation (3.92), we note that in our units we have set the magnetic field to be measured in terms of some known inflow magnetic field B_0. Hence we can set $\max|B_y(x,0)| = B_0 \equiv 1$ and hence we obtain the scale

$$l = \frac{\eta}{E}. \tag{3.116}$$

We substitute (3.116) into (3.115)

$$\psi \approx -\frac{E}{2\eta}\left(x^2 - \frac{4\nu E^2}{\eta}y^2 - \frac{E^2}{6\eta^2}x^4 - \frac{4E^4\nu}{\eta^3}x^2y^2 - \frac{2E^6}{3\eta^4}\left(\eta^2+\eta\nu-58\nu^2\right)y^4\right). \tag{3.117}$$

This flux function describes an X-point at the origin and is plotted in Fig. 3.2. In the limit $\nu \to 0$ the magnetic separatrix angle approaches zero, which describes an osculatory solution.

In order to find the length scale and reconnection rate, we need to calculate the current function

$$J_z(x,y) = -\psi_0''(x) - \frac{1}{2!}\psi_2''(x)\,y^2 - \frac{1}{4!}\psi_4''(x)\,y^4 + \ldots \tag{3.118}$$

We could insist that at the boundary of the current sheet the current drops off to zero. Hence

$$J_z(0,L) = 0, \tag{3.119}$$

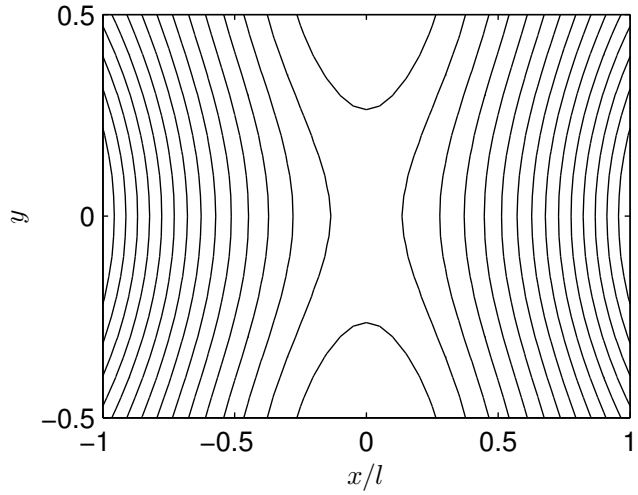

Figure 3.2: Magnetic field lines plotted for a visco-resistive current sheet: equation (3.117) is plotted for $\eta = 10^{-8}$, $\nu = 10^{-4}$. E is calculated from equation (3.127) with L set to 1 without loss of generality. Note: $l \ll 1$ so the actual aspect ratio is much greater than it appears in the figure.

for some known current sheet length $L \sim 1$. Substituting our values for $\psi_0''(0)$, $\psi_2''(0)$ and $\psi_4''(0)$ we get

$$J_z(0, L) = \frac{E}{\eta}\left(1 - \frac{4E^4\nu}{\eta^3}L^2 \; - \frac{4E^8\left(\eta^2 + 3\eta\nu - 74\nu^2\right)}{3\eta^6}L^4\right). \tag{3.120}$$

However, if $\nu \gg \eta$ the current will always be positive and never drop off to zero. Hence, the definition (3.119) would give us a complex length. Instead we introduce the current density and compare our solution to a Syrovatskiĭ current sheet. It should be noted that Syrovatskiĭ (1971)'s solution is for ideal MHD, but nevertheless the definition that the current density becomes negative beyond the boundary of the current sheet is particularly useful here. The electric current per unit length is defined as

$$\frac{\mathrm{d}I}{\mathrm{d}y} = \int_{-\infty}^{\infty} J_z(x, y)\mathrm{d}x, \tag{3.121}$$

where

$$I = \int_{-L}^{L} \frac{\mathrm{d}I}{\mathrm{d}y}\,\mathrm{d}y \tag{3.122}$$

is the total current and J_z is given by (3.118). Integrating J_z yields

$$\frac{\mathrm{d}I}{\mathrm{d}y} = 2\left[1 - \frac{E^4}{2\eta^3}\left(\eta - 2\nu\right)y^2 - \frac{E^8}{24\eta^6}\left(11\eta^2 - 116\eta\nu + 316\nu^2\right)y^4\right], \tag{3.123}$$

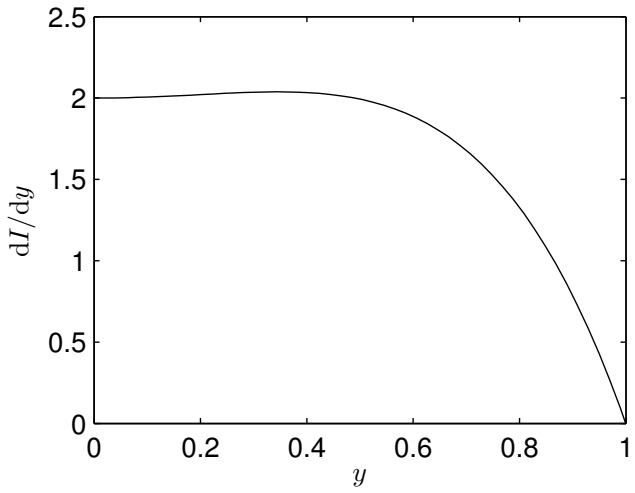

Figure 3.3: Electric current per unit length: equation (3.123) is plotted for $\eta = 10^{-8}$, $\nu = 10^{-4}$. E is calculated from equation (3.127) with L set to 1 without loss of generality.

which is plotted in Figure 3.3. We observe that the current density is relatively even across the sheet and quickly drops off at the boundary of the current sheet as expected. Imposing the boundary condition

$$I'(L) = 0 \tag{3.124}$$

produces the result

$$L^2 = \frac{4\eta^3}{E^4\left(\eta - 2\nu + \kappa\right)}, \tag{3.125}$$

where

$$\kappa = \left[\frac{1}{3}\left(25\eta^2 - 244\eta\nu + 644\nu^2\right)\right]^{(1/2)}. \tag{3.126}$$

Defining the current sheet length as $L \equiv 1$ in our units, we rearrange equation (3.125) to obtain the reconnection rate

$$E = \sqrt{\eta}\left(\frac{(\eta - 2\nu + \kappa)}{4\eta}\right)^{-1/4}. \tag{3.127}$$

We obtain the outflow speed v_y by evaluating $v_y = -\partial_x\phi(x, y)$ at the point $(x, y) = (0, L)$ and using the leading order term of equation (3.107) along with (3.116) (Litvinenko, 2009):

$$v_{\text{out}} = \frac{L}{l}E. \tag{3.128}$$

Substituting our values for L and E yields

$$v_{\text{out}} = \left(\frac{4\eta}{\eta - 2\nu + \kappa} \right)^{1/2}. \tag{3.129}$$

Finally, we can substitute equation (3.127) into (3.116) to find

$$l = \sqrt{\eta} \left(\frac{(\eta - 2\nu + \kappa)}{4\eta} \right)^{1/4}. \tag{3.130}$$

Equations (3.127), (3.129) and (3.130) are plotted in Figs. 3.4-3.6 respectively. The curves in Figs. 3.4-3.6 closely resemble their asymptotic approximations (3.188)-(3.193) for large ν/η. We would expect, based on the (Park et al., 1984) scalings, the Sweet-Parker normalised reconnection rate $E/\sqrt{\eta}$ and the outflow velocity v_{out} to be unity when $\nu = 0$ and then monotonically decrease as we increase the viscosity. Similarly, we would expect the Sweet-Parker normalised length scale $l/\sqrt{\eta}$ to monotonically increase as we increase ν/η. However, for the scalings we have obtained, which are valid for all values of ν, we observe an initial increase in $E/\sqrt{\eta}$ and v_{out} and an initial decrease in $l/\sqrt{\eta}$ as we increase the viscosity. Mathematically, the increasing $l/\sqrt{\eta}$ can be explained by the fourth order correction term κ (3.126) which reaches a minimum at $\nu/\eta = 244/(2 \times 644) \approx 0.189$.

3.12 Gaussian current profile

We have adopted two different zeroth order current profiles, equations (3.97) and (3.106) (pictured in Fig. 3.7), and have attained two different length scales for a VR current sheet. The fascinating aspect of Fig. 3.7 is that even though there is a small difference in boundary conditions between the two current profiles we obtain two completely different length scales. Additionally, we remark that Fig. 3.7 depicts back currents at the boundary of the diffusion region for the Dawson profile (3.97), however this is not the cause of the varying length scales, in fact it is the boundary conditions of the inflow velocity that determine the presence of a VR length scale.

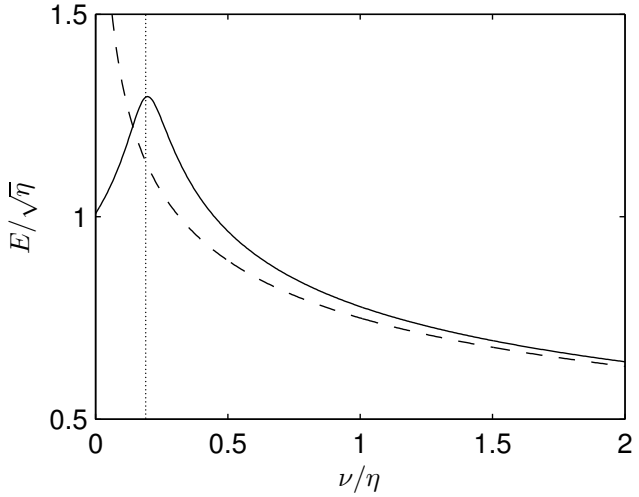

Figure 3.4: The reconnection rate E, normalised by the Sweet-Parker reconnection rate $\sqrt{\eta}$, plotted against ν/η. The dashed line is the $\nu \to \infty$ limit given by equation (3.193). Without loss of generality L is set as 1. The dotted line depicts the maximum at $\nu \approx 0.189\eta$.

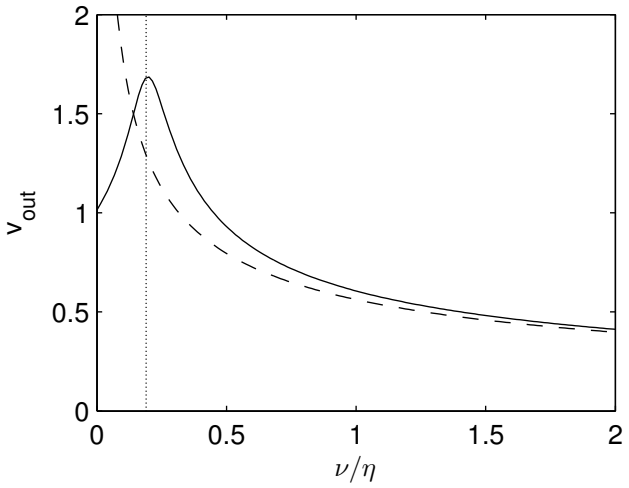

Figure 3.5: The outflow velocity v_{out} plotted against ν/η. The dashed line is the $\nu \to \infty$ limit given by equation (3.192). The dotted line depicts the maximum at $\nu \approx 0.189\eta$.

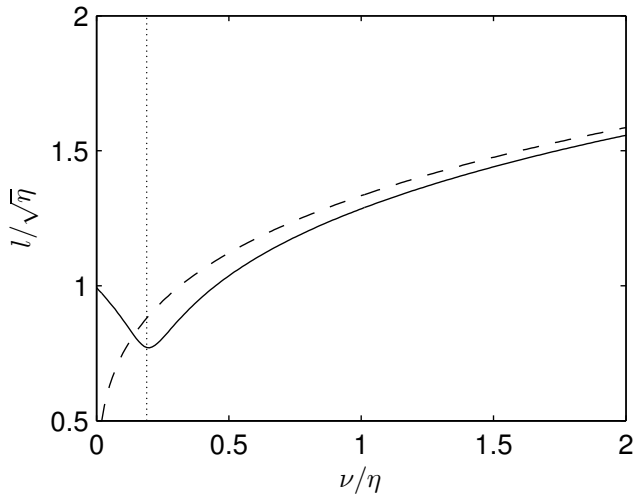

Figure 3.6: The current sheet thickness l, normalised by the Sweet-Parker current sheet thickness $\sqrt{\eta}$, plotted against ν/η. The dashed line is the $\nu \to \infty$ limit given by equation (3.191). The dotted line depicts the maximum at $\nu \approx 0.189\eta$.

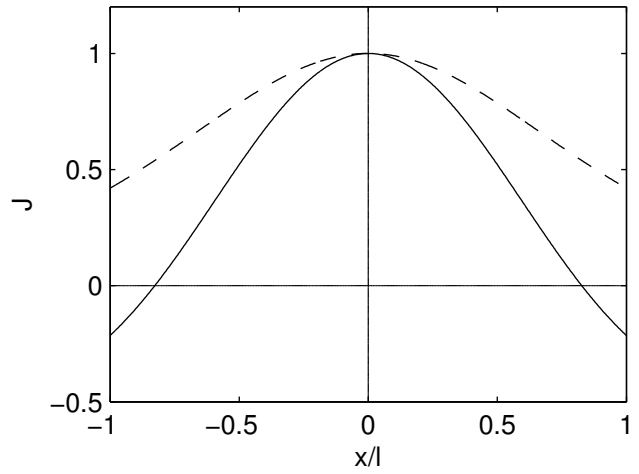

Figure 3.7: Zeroth order current profile as described by Biskamp (2000). The solid line is the current profile that corresponds the flux function (3.97) and the dashed line is the current profile associated with the flux function (3.106).

This begs the need for a more general formulation for substituting zeroth order current profiles and producing length scales. In particular, we want to use a Gaussian function

$$J(x,0) = \psi_0''(x) = -\frac{E}{\eta}\exp\left[-\left(\frac{x}{l}\right)^2\right], \tag{3.131}$$

since it can be justified in terms of statistical thermodynamics (Biskamp, 2000). However, calculating a fourth-order series expansion in terms of a Gaussian function would prove intractable.

In place of the exact Gaussian profile (3.131), we approximate it by a 14th order Taylor series

$$\psi_0 = -\frac{El}{\eta}\left(\frac{\tilde{x}^2}{2} - \frac{\tilde{x}^4}{12} + \frac{\tilde{x}^6}{60} + \cdots + \frac{\tilde{x}^{14}}{131040}\right). \tag{3.132}$$

Furthermore, we approximate the functions ψ_n or ϕ_n by employing the following scheme (Cowley, 1975; Priest and Cowley, 1975):

$$\psi_0 = \psi_{00} + \psi_{02}x^2 + \psi_{04}x^4 + \ldots, \tag{3.133}$$

$$\phi_1 = \phi_{11}x + \phi_{13}x^3 + \ldots \tag{3.134}$$

$$\psi_2 = \psi_{20} + \psi_{22}x^2 + \psi_{24}x^4 + \ldots, \tag{3.135}$$

$$\phi_3 = \phi_{31}x + \phi_{33}x^3 + \ldots \tag{3.136}$$

$$\psi_4 = \psi_{40} + \psi_{42}x^2 + \psi_{44}x^4 + \ldots. \tag{3.137}$$

Substitution of equations (3.133)-(3.137) into equation (3.92) and collecting the coefficients of like powers of x yields

$$\psi_{02} = -\frac{E}{2\eta}, \tag{3.138}$$

$$\psi_{02}\phi_{11} = 6\eta\psi_{04}, \tag{3.139}$$

$$\psi_{02}\phi_{13} = 15\eta\,\psi_{06} - 2\psi_{04}\phi_{11}, \tag{3.140}$$

$$\psi_{02}\phi_{15} = 28\eta\,\psi_{08} - 3\psi_{06}\phi_{11} - 2\psi_{04}\phi_{13}, \tag{3.141}$$

$$\psi_{02}\phi_{17} = 45\eta\psi_{010} - 4\psi_{08}\phi_{11} - 3\psi_{06}\phi_{13} - 2\psi_{04}\phi_{15}, \tag{3.142}$$

$$\psi_{02}\phi_{19} = 66\eta\psi_{012} - 5\psi_{010}\phi_{11} - 4\psi_{08}\phi_{13} - 3\psi_{06}\phi_{15} - 2\psi_{04}\phi_{17}, \tag{3.143}$$

$$\psi_{02}\phi_{111} = 91\eta\psi_{014} - 6\psi_{012}\phi_{11} - 5\psi_{010}\phi_{13} - 4\psi_{08}\phi_{15} - 3\psi_{06}\phi_{17} - 2\psi_{04}\phi_{19}. \tag{3.144}$$

Substituting into equation (3.93) produces

$$\psi_{02}\psi_{22} = 30\nu\,\phi_{15} + 6\psi_{04}\psi_{20}, \tag{3.145}$$

$$6\psi_{02}\psi_{24} = -10\phi_{15}\phi_{11} + \phi_{13}^2 + 210\nu\,\phi_{17} + 30\psi_{06}\psi_{20} + 4\psi_{04}\psi_{22}, \tag{3.146}$$

$$\begin{aligned} 10\psi_{02}\psi_{26} =& 4\phi_{13}\phi_{15} - 28\phi_{11}\phi_{17} + 504\nu\,\phi_{19} \\ & 56\psi_{08}\psi_{20} + 18\psi_{06}\psi_{22} - 4\psi_{04}\psi_{24}, \end{aligned} \tag{3.147}$$

$$\begin{aligned} 14\psi_{02}\psi_{28} =& -54\phi_{11}\phi_{19} - 6\phi_{13}\phi_{17} + 5\phi_{15}^2 + 990\nu\phi_{111} \\ & + 90\psi_{010}\psi_{20} + 40\psi_{08}\psi_{22} + 6\psi_{06}\psi_{24} - 12\psi_{04}\psi_{26}. \end{aligned} \tag{3.148}$$

Similarly for (3.94):

$$-\phi_{11}\psi_{20} = \eta\,\psi_{22}, \tag{3.149}$$

$$\psi_{02}\phi_{31} = 6\eta\,\psi_{24} + 3\phi_{13}\psi_{20}, \tag{3.150}$$

$$\psi_{02}\phi_{33} = 15\eta\,\psi_{26} - \psi_{24}\phi_{11} + 2\psi_{22}\phi_{13} - 2\psi_{04}\phi_{31} + 5\psi_{20}\phi_{15}, \tag{3.151}$$

$$\begin{aligned} \psi_{02}\phi_{35} =& 28\eta\,\psi_{28} - 2\psi_{26}\phi_{11} + \psi_{24}\phi_{13} + 4\psi_{22}\phi_{15} \\ & - 3\psi_{06}\phi_{31} - 2\psi_{04}\phi_{33} + 7\psi_{20}\phi_{17}. \end{aligned} \tag{3.152}$$

And finally, substituting into (3.95) and (3.96) gives

$$\begin{aligned} 6\psi_{04}\psi_{40} - \psi_{02}\psi_{42} =& -3\left(\phi_{13}\phi_{31} - \phi_{33}\phi_{11}\right) + 30\nu\phi_{35} \\ & + 3\left(6\psi_{24}\psi_{20} - \psi_{22}^2\right), \end{aligned} \tag{3.153}$$

$$-2\psi_{20}\phi_{31} - 2\psi_{40}\phi_{11} = \eta\psi_{42}. \tag{3.154}$$

From here we compute the current along the y axis as

$$J_z(0,y) = -2\left(\psi_{02} + \frac{1}{2!}\psi_{22}y^2 + \frac{1}{4!}\psi_{42}y^4 + \dots\right). \tag{3.155}$$

Solving equations (3.138)- (3.155) for the zeroth order profile (3.132) yields

$$J_z(0,y) = \frac{E}{\eta}\left(1 - \frac{E^4\nu}{3\eta^3}y^2 + \frac{E^8 k}{9\eta^6}y^4\right), \tag{3.156}$$

where

$$k = \frac{15855\eta^2 - 6071\eta\nu + 93069\nu^2}{9450}. \tag{3.157}$$

We cannot use the definition (3.124) here since our series does not converge for large y. Instead, we use Jamitzky and Scholer (1995)'s definition that the region of validity is our system size. That is to say the point where our series no longer converges is defined as the current sheet length L. This is the point where

$$\frac{1}{4!}|\psi_{42}| \geq \frac{1}{2!}|\psi_{22}|. \tag{3.158}$$

Adopting this definition, we find

$$E^4 = \frac{3\eta^3\nu}{k}, \tag{3.159}$$

and finally

$$E = \sqrt{\eta}\left(\frac{k}{3\eta\nu}\right)^{-1/4}, \tag{3.160}$$

and hence

$$l = \sqrt{\eta}\left(\frac{k}{3\eta\nu}\right)^{1/4}. \tag{3.161}$$

The flux function near the origin is computed as

$$\begin{aligned}\psi = -\frac{E}{2\eta}\Bigg(x^2 - \frac{\nu E^2}{3\eta}y^2 - \frac{E^2}{6\eta^2}x^4 - \frac{\nu E^4}{3\eta^3}x^2y^2 \\ + \frac{E^6}{170100\eta^4}\left(155855\eta^2 - 5546\eta\nu + 1056669\nu^2\right)y^4\Bigg)\end{aligned} \tag{3.162}$$

as plotted in Fig. 3.8.

In the previous section we used two different zeroth order current profiles- equations (3.97) and (3.106)- and found two different length scales- one with a VR scale and the other not containing a VR scale. Our third zeroth order current profile- the Gaussian profile (3.132)- does contain a VR scale. Hence, we might suspect a VR scale to be present more generally. To this end, we formulate a general method for finding whether or not a VR scale is present, based on a zeroth order profile, in the next section.

3.13 Inflow velocity profile

The series expansion described in Section 3.9 has one degree of freedom which we took to be the zeroth order current profile. This is primarily owing to

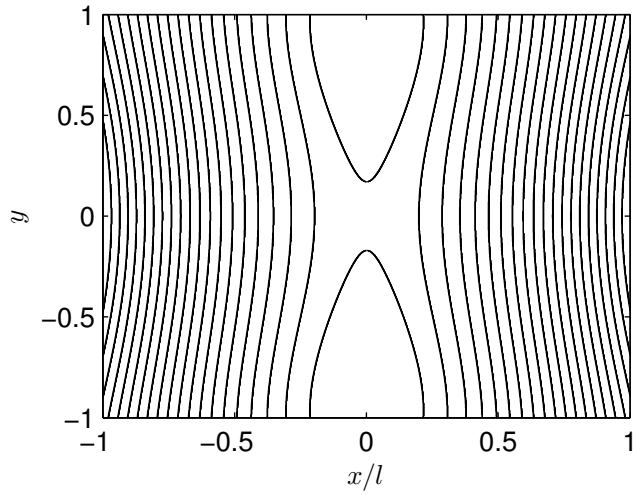

Figure 3.8: Current sheet using the zeroth order current profile (3.131). We have taken $\nu = 10^{-4}$, $\eta = 10^{-8}$.

reasons of convenience as assuming a velocity profile in equation (3.92) necessitates solving a first order differential equation in order to find the leading order flux function ψ_0. However, in equations (3.138)-(3.144) neither the flux nor the stream function is more convenient than the other.

Profiles (3.97) and (3.106) are difficult to unify into a more general function. Alternatively, we could use the inflow velocity $v_x(x, 0) = \phi_1$ as our degree of freedom. Consider the function

$$\phi_1(x) = -\frac{\eta}{\mu l} \tanh\left(\frac{\mu x}{l}\right). \tag{3.163}$$

If we let $\mu = 1$ then we get the profile (3.106) and the limit $\mu \to 0$ produces the profile (3.97) as plotted in Fig. 3.9. Here we observe that μ acts as a parameter that represents a boundary condition for the inflow velocity at the edge of the diffusion region. Then

$$\psi_{22} = \frac{4\eta^2\mu^4\nu}{El^6}, \tag{3.164}$$

$$\psi_{42} = \frac{\eta^5\mu^4 m}{E^3 l^{12}}, \tag{3.165}$$

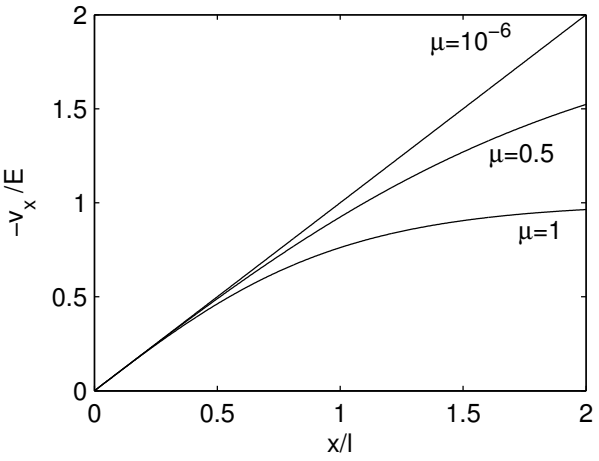

Figure 3.9: The inflow velocity profile (3.163) normalised by E plotted for different values of μ. Note the negative sign appears due to the velocity at $x = l$ pointing toward the origin.

where

$$\begin{aligned} m =& \frac{16}{105}(175\eta^2\mu^2 - 70\eta^2 + 1148\eta\mu^4\nu \\ & - 1029\eta\mu^2\nu + 196\eta\nu - 15640\mu^6\nu^2 + 10378\mu^4\nu^2 \\ & - 2804\mu^2\nu^2 + 296\nu^2). \end{aligned} \tag{3.166}$$

Employing equations (3.158) and (3.116) yields

$$E = \sqrt{\eta}\left(\frac{|m|}{48\eta\nu}\right)^{-1/4}. \tag{3.167}$$

For a small but non-zero μ we get

$$m = -\frac{16}{105}(70\eta^2 - 196\eta\nu - 296\nu^2). \tag{3.168}$$

Here μ represents the size of nonlinear terms in the inflow velocity and for any small but finite μ we still get a VR scale. From equation (3.145) we can conclude that if any fifth order terms are present in the leading order stream function ϕ_1 then we will attain a VR length scale. This leaves us with one final particular case- a cubic inflow velocity profile. Hence we try the profile

$$\phi_1 = -\frac{\eta}{l}\left(x + bx^3\right), \tag{3.169}$$

where $b \geq -1$ to ensure that $v_x(1,0) < 0$. Combining equations (3.139), (3.145) and (3.149) produces

$$\psi_{20} = \psi_{22} = 0. \tag{3.170}$$

Substituting (3.170) reduces equations (3.140)-(3.154) to

$$15\eta\,\psi_{06} = \psi_{02}\phi_{13} + 2\psi_{04}\phi_{11}, \tag{3.171}$$

$$28\eta\,\psi_{08} = 2\psi_{04}\phi_{13} + 3\psi_{06}\phi_{11}, \tag{3.172}$$

$$45\eta\psi_{010} = 3\psi_{06}\phi_{13} + 4\psi_{08}\phi_{11}, \tag{3.173}$$

$$66\eta\psi_{012} = 4\psi_{08}\phi_{13} + 5\psi_{010}\phi_{11}, \tag{3.174}$$

$$91\eta\psi_{014} = 5\psi_{010}\phi_{13} + 6\psi_{012}\phi_{11}, \tag{3.175}$$

$$6\psi_{02}\psi_{24} = \phi_{13}^2, \tag{3.176}$$

$$5\psi_{02}\psi_{26} = -2\psi_{04}\psi_{24}, \tag{3.177}$$

$$7\psi_{02}\psi_{28} = 3\psi_{06}\psi_{24} - 6\psi_{04}\psi_{26}, \tag{3.178}$$

$$\psi_{02}\phi_{31} = 6\eta\,\psi_{24}, \tag{3.179}$$

$$\psi_{02}\phi_{33} = 15\eta\,\psi_{26} - \psi_{24}\phi_{11} - 2\psi_{04}\phi_{31}, \tag{3.180}$$

$$\psi_{02}\phi_{35} = 28\eta\,\psi_{28} - 2\psi_{26}\phi_{11} + \psi_{24}\phi_{13} - 3\psi_{06}\phi_{31} - 2\psi_{04}\phi_{33}, \tag{3.181}$$

$$30\nu\phi_{35} = 6\psi_{04}\psi_{40} - \psi_{02}\psi_{42} + 3\left(\phi_{13}\phi_{31} - \phi_{33}\phi_{11}\right) \tag{3.182}$$

$$\eta\psi_{42} = -2\psi_{40}\phi_{11}. \tag{3.183}$$

We calculate the fourth order current profile as

$$J_z(0,y) = 2\left(\frac{E}{2\eta} - \frac{2b^2E^9p}{3\eta^6}y^4\right), \tag{3.184}$$

where

$$p = \left[(2-3b)\eta - (8-3b)\nu\right]. \tag{3.185}$$

Equation (3.158) is trivially satisfied since $\psi_{22} = 0$. Instead we replace equation (3.158) with

$$\frac{1}{4!}|\psi_{42}| \leq |\psi_{02}|, \tag{3.186}$$

which could also be obtained from using the definition (3.119). Hence we attain the reconnection rate

$$E = \sqrt{\eta}\left(\frac{4p}{3\eta}\right)^{-1/4}. \tag{3.187}$$

There exists a particular solution $b = 8/3$ for a cubic inflow velocity profile in which we do not obtain a VR scale when we use a fourth order approximation for the current. However, the lack of a VR scale here is owing to the current only being calculated to fourth order. If we were to include higher order terms the VR scale would inevitably appear. So for any nonlinear inflow velocity we will obtain a VR scale regardless of how weakly nonlinear the inflow velocity profile is. In other words, the Park et al. scale is the fundamental length scale of a VR current sheet but there exist particular solutions in which we get separate viscous and resistive current layers.

3.14 Discussion

In this chapter, we have searched for the length scale of a reconnecting VR current sheet. To this end we have reviewed a dimensional argument and flux-pile up solutions. Furthermore, we have used a series expansion method to describe in detail a VR current sheet near the origin that is valid for any viscosity. We have calculated the series expansion for three different zeroth order current profiles as prescribed by Biskamp (2000) and for a more general inflow velocity profile.

We conclude that the presence of a VR length scale in reconnection is determined by the form of the inflow velocity $v_x(x, 0)$. If nonlinear terms are present in the inflow velocity profile a VR length scale will be present regardless of how small these nonlinear terms are. Thus we postulate that the Park et al. (1984) scale (3.59) is a fundamental length scale that is only invalid for a limited range of particular inflow velocity profiles.

Since our general description of the inflow and outflow speeds and current sheet thickness is applicable for any viscosity, we can compare the limiting

cases of $\nu \to 0$ and $\nu \gg \eta$ to previous studies. In the case $\nu \to 0$ we recover the Sweet-Parker scalings

$$l \sim \eta^{1/2}, \tag{3.188}$$

$$v_{\text{out}} \sim 1, \tag{3.189}$$

$$E \sim \eta^{1/2}. \tag{3.190}$$

In the case $\nu \gg \eta$ we recover the previous scaling arguments for viscosity dominant reconnection (Park et al., 1984; Biskamp, 2000)

$$l \sim (\eta\nu)^{1/4}, \tag{3.191}$$

$$v_{\text{out}} \sim \left(\frac{\nu}{\eta}\right)^{-1/2}, \tag{3.192}$$

$$E \sim \eta^{1/2}\left(\frac{\nu}{\eta}\right)^{-1/4}. \tag{3.193}$$

Some vigilance is required in attempting to generalise our solution, in particular to incorporate Hall or time-dependent effects. We note that the osculation of field lines in the inviscid limit was shown not to be a property of time-dependent magnetic merging (Heerikhuisen et al., 2000).

Additionally, we remark that our series solution only represents the inner region of a current sheet. Painting a full picture requires an asymptotic analysis. The outer region solution is independent of both resistivity and viscosity and accordingly we can refer to Jamitzky and Scholer (1995) for a typical outer region solution.

Finally, we compare our investigation to a previous study. Uzdensky and Kulsrud (1998) use the zeroth order function

$$B_y(0, y) = \sqrt{1 - y^2}, \tag{3.194}$$

and find singularities in the stream function. It is clear to see from equations (3.138)-(3.144) that the choice of either a zeroth order flux function or a zeroth order stream function is arbitrary. In other words, the choice of flux function dictates the form of the stream function. Hence, at least in the way we have set up our calculation, we can avoid the singularities in the stream function

described by Uzdensky and Kulsrud (1998) by simply choosing a non-singular stream function.

Chapter 4

Current Sheet Formation in a Weakly Collisional Plasma

4.1 Introduction

Current sheet formation at a magnetic neutral line has been studied in standard magnetohydrodynamics (MHD) and Hall MHD. Current sheets can be modelled as singularities in the current density. Exact self-similar MHD solutions have been found that exhibit both exponential behaviour (e.g., Chapman and Kendall, 1963; Uberoi, 1963) and finite-time collapse to a singularity (e.g., Shivamoggi, 1986). Numerical simulations (Sulem et al., 1985; Grauer and Marliani, 1998) and analytical arguments (Klapper, 1998) show that ideal incompressible MHD solutions grow exponentially unless a singularity is driven by an imposed pressure. More recently, analytical solutions that include the Hall term in the generalised Ohm's law have been found, yet the role of the Hall term in the singularity formation remains a subject of debate (e.g., Litvinenko, 2007; Shivamoggi, 2011).

Magnetic reconnection rates, predicted by traditional resistive MHD models (Parker, 1957; Sweet, 1958) are too slow to explain reconnection in laboratory and astrophysical plasmas (Bhattacharjee, 2004; Zweibel and Yamada, 2009). The Hall effect is believed to play a key role in fast magnetic reconnec-

tion in weakly collisional plasmas (Shay et al., 1999). Numerical simulations (e.g., Birn et al., 2001, 2005; Shay et al., 2001; Drake et al., 2008) demonstrated that including the Hall terms can speed up reconnection. However, this is only possible by the thinning of the current sheet. Several recent scaling models attempted to quantify the dependence of steady reconnection on the Hall effect (Malyshkin, 2008; Uzdensky, 2009; Simakov and Chacón, 2009). By contrast, the value of the singularity formation models is that they provide one of the few opportunities to describe the current sheet formation using exact analytical solutions in Hall MHD (see also Craig and Watson, 2005).

In this chapter we investigate a self-similar solution for current sheet formation in Hall MHD. We generalise previous studies by considering a general set of initial conditions and we derive a criterion for the formation of a finite-time singularity. The new solution reduces to the exponentially evolving MHD solution upon setting the Hall term to zero. We also discuss an alternative approach to the singularity formation in Hall MHD proposed by Shivamoggi (2011). Finally, we generalise our new solution to incorporate the resistive, viscous and electron inertia terms in Ohm's law and the momentum equation.

4.2 Generalised Ohm's Law and MHD equations

In the incompressible regime, the dimensionless MHD equations (2.7)-(2.12) reduce to

$$\begin{aligned}\mathbf{E}+\mathbf{v}\times\mathbf{B} &= \eta\mathbf{J}+d_i(\mathbf{J}\times\mathbf{B}-\nabla p_e)\\ &\quad + d_e^2[\partial_t\mathbf{J}+(\mathbf{v}\cdot\nabla)\mathbf{J}+(\mathbf{J}\cdot\nabla)\mathbf{v}],\end{aligned} \tag{4.1}$$

$$\partial_t\mathbf{v}+(\mathbf{v}\cdot\nabla)\mathbf{v} = -\nabla p+\mathbf{J}\times\mathbf{B}+\nu\nabla^2\mathbf{v}, \tag{4.2}$$

$$\nabla\cdot\mathbf{v}=0, \tag{4.3}$$

$$\nabla\cdot\mathbf{B}=0, \tag{4.4}$$

$$\mathbf{J}=\nabla\times\mathbf{B}, \tag{4.5}$$

$$\nabla\times\mathbf{E}=-\partial_t\mathbf{B}. \tag{4.6}$$

The resistive term $\eta\mathbf{J}$ is much greater than the Hall term $d_i(\mathbf{J}\times\mathbf{B})$ in the solar corona. However, the Hall term needs to be considered if large magnetic gradients are present. To estimate the value of d_i at which the Hall term becomes significant during reconnection we let $|\eta\mathbf{J}|\sim d_i|\mathbf{J}\times\mathbf{B}|$. We note that reconnection implies a large gradient in the planar magnetic field, whereas the out-of-plane $\hat{\mathbf{z}}$-component of the magnetic field changes relatively slowly. Using (4.5), we estimate that $J_{planar}\sim 1$ and so $|\mathbf{J}_{planar}\times\mathbf{B}_{planar}|\simeq B_{planar}$. We have $J_z\sim B_{planar}/l$ where l is the current sheet thickness and so $E_z\sim \eta B_{planar}/l\sim d_i B_{planar}$. A typical Sweet-Parker length scale is $l\sim\eta^{1/2}$, which implies that the Hall effect becomes significant roughly when $d_i^2\gtrsim\eta$ (e.g., Craig and Litvinenko, 2008, and references therein).

In ideal Hall MHD, we set $d_e=\nu=\eta=0$. So Ohm's law (4.1) and the momentum equation (4.2) are approximated by

$$\mathbf{E}+\mathbf{v}\times\mathbf{B}=d_i(\mathbf{J}\times\mathbf{B}-\nabla p_e), \tag{4.7}$$

$$\partial_t\mathbf{v}+(\mathbf{v}\cdot\nabla)\mathbf{v}=-\nabla p+\mathbf{J}\times\mathbf{B}. \tag{4.8}$$

We assume a 2.5D model, in which all quantities are considered in three dimensions but there is no dependence on the z co-ordinate ($\partial_z=0$). The

incompressibility equation (4.3) then dictates that

$$\mathbf{v}(x, y, t) = \nabla\phi \times \hat{\mathbf{z}} + W\,\hat{\mathbf{z}}. \tag{4.9}$$

Similarly, to satisfy (4.4), we use the flux function ψ to represent the magnetic field:

$$\mathbf{B}(x, y, t) = \nabla\psi \times \hat{\mathbf{z}} + Z\,\hat{\mathbf{z}}. \tag{4.10}$$

Furthermore, we take the curl of (4.7) and (4.8). Taking the $\hat{\mathbf{z}}$ components of (4.7) and (4.8) and their curls, yields the following system (see also Craig and Watson, 2005):

$$\partial_t\psi + [\psi, \phi] = d_i[\psi, Z], \tag{4.11}$$

$$\partial_t Z + [Z, \phi] = [W, \psi] + d_i[\nabla^2\psi, \psi], \tag{4.12}$$

$$\partial_t W + [W, \phi] = [Z, \psi], \tag{4.13}$$

$$\partial_t(\nabla^2\phi) + [\nabla^2\phi, \phi] = [\nabla^2\psi, \psi], \tag{4.14}$$

where the Poisson bracket notation is typified by

$$[\psi, \phi] = \partial_x\psi\partial_y\phi - \partial_y\psi\partial_x\phi.$$

4.3 Self-Similar Solutions

We solve the ideal Hall MHD equations (4.11)-(4.14) via similarity reduction. The self-similar solutions we derive generalise those of standard MHD. Originally, Chapman and Kendall (1963, 1966) obtained a solution for the collapse of a magnetic X-point to a current sheet in an incompressible, infinitely conducting plasma in 2D (see also Sulem et al., 1985). A key feature of the solution is an exponential growth of the X-point magnetic field. Uberoi (1963, 1966) noted the validity of the solution for finite conductivity, whereas Imshennik and Syrovatskiĭ (1967) obtained a solution for a compressible plasma. For an incompressible plasma, Shivamoggi (1986) presented a solution that predicts a finite-time collapse to the current sheet. However, numerical simulations by

Sulem et al. (1985) and Grauer and Marliani (1998) have shown an exponential flattening of the 2D X-point in ideal incompressible MHD. Klapper (1998) proved a general result that a finite-time collapse to a current sheet cannot occur in planar incompressible MHD flows unless a singularity is pressure-driven (e.g., Shivamoggi, 1986). Hence we derive a solution in Hall MHD which is consistent with exponential evolution in the MHD limit $d_i = 0$.

To reduce the system (4.11)-(4.14) to a system of ordinary differential equations, we seek the flux function ψ and the stream function ϕ as in 2D MHD solutions:

$$\psi = \alpha(t)x^2 - \beta(t)y^2, \tag{4.15}$$

$$\phi = -\gamma(t)xy, \tag{4.16}$$

which describe a hyperbolic planar magnetic field, driven by a stagnation-point flow. Similarly, for the axial velocity field W and the axial magnetic field Z we assume

$$W = f(t)x^2 + g(t)y^2, \tag{4.17}$$

$$Z = h(t)xy, \tag{4.18}$$

where the functional form of the axial magnetic field Z corresponds to a quadrupolar structure in Hall magnetic reconnection (Sonnerup, 1979; Wang et al., 2000). On substituting (4.15)-(4.18) into (4.11)-(4.14) we get

$$\dot{\alpha} - 2\alpha(\gamma + d_i h) = 0, \tag{4.19}$$

$$\dot{\beta} + 2\beta(\gamma + d_i h) = 0, \tag{4.20}$$

$$\dot{f} - 2\gamma f + 2\alpha h = 0, \tag{4.21}$$

$$\dot{g} + 2\gamma g + 2\beta h = 0, \tag{4.22}$$

$$\dot{h} + 4\alpha g + 4\beta f = 0, \tag{4.23}$$

where the overdot notation represents differentiation with respect to dimen-

sionless time. These equations are integrated to yield

$$\alpha\beta = \text{const}, \tag{4.24}$$

$$\alpha + d_i f = \text{const}\exp(2\Gamma), \tag{4.25}$$

$$\beta - d_i g = \text{const}\exp(-2\Gamma), \tag{4.26}$$

$$h^2 - 4fg = \text{const}, \tag{4.27}$$

where $\Gamma = \int_0^t \gamma(t')\,\mathrm{d}t'$. These equations reduce to those derived by Litvinenko (2007) in the case $\gamma = \text{const}$.

Once the solution is determined, we can use the momentum equation to find the pressure. We calculate

$$\partial_t \mathbf{v} = \dot{\gamma}(-x, y, 0),$$

$$(\mathbf{v}\cdot\nabla)\mathbf{v} = \gamma^2(x, y, 0),$$

$$\mathbf{J}\times\mathbf{B} = [-h^2xy^2 - 4\alpha x(\alpha-\beta)]\hat{\mathbf{x}} + [-h^2x^2y + 4\beta y(\alpha-\beta)]\hat{\mathbf{y}},$$

and substitute into the momentum equation (2.21) to get

$$\partial_x p = -h^2xy^2 - 4\alpha x(\alpha-\beta) + \gamma^2 x - \dot{\gamma}x,$$

$$\partial_y p = -h^2x^2y + 4\beta y(\alpha-\beta) - \gamma^2 y - \dot{\gamma}y.$$

Integration yields the pressure profile

$$p(x,y,t) = -\frac{1}{2}h^2x^2y^2 + \frac{1}{2}\left[\gamma^2 - \dot{\gamma} - 4\alpha(\alpha-\beta)\right]x^2 + \frac{1}{2}\left[-\gamma^2 - \dot{\gamma} + 4\beta(\alpha-\beta)\right]y^2. \tag{4.28}$$

The 2D MHD result is recovered by setting $h(t) = 0$.

4.4 Collapse to a Current Sheet in Hall MHD

For a general set of initial conditions,

$$\alpha(0) = \alpha_0, \qquad \beta(0) = \beta_0, \qquad \gamma(0) = \gamma_0,$$

$$f(0) = f_0, \qquad g(0) = g_0, \qquad h(0) = h_0,$$

we specify the integration constants in the system (4.24)-(4.27):

$$\alpha\beta = \alpha_0\beta_0, \tag{4.29}$$

$$\alpha + d_i f = (\alpha_0 + d_i f_0)\exp(2\Gamma), \tag{4.30}$$

$$\beta - d_i g = (\beta_0 - d_i g_0)\exp(-2\Gamma), \tag{4.31}$$

$$h^2 - 4fg = h_0^2 - 4f_0 g_0. \tag{4.32}$$

Now we obtain an equation for $h(t)$ by differentiating (4.23):

$$\ddot{h} + 4(\dot{\alpha}g + \alpha\dot{g} + \dot{\beta}f + \beta\dot{f}) = 0.$$

On using (4.19)-(4.23), after some algebra, this simplifies to

$$\ddot{h} + 8h[d_i(\alpha g - \beta f) - 2\alpha_0\beta_0] = 0.$$

To express $(\alpha g - \beta f)$ in terms of h, we note that (4.30) and (4.31) yield

$$(\alpha + d_i f)(\beta - d_i g) = (\alpha_0 + d_i f_0)(\beta_0 - d_i g_0).$$

On expanding the left-hand side and using (4.29), we get

$$d_i(\alpha g - \beta f) = \alpha_0\beta_0 - d_i^2 fg - (\alpha_0 + d_i f_0)(\beta_0 - d_i g_0).$$

Next we use (4.32) to eliminate fg. The result is

$$\ddot{h} - 2d_i^2 h(h^2 - h_0^2 + 4f_0 g_0) + 8h[d_i(\alpha_0 g_0 - \beta_0 f_0) + d_i^2 f_0 g_0 - 2\alpha_0\beta_0] = 0,$$

or

$$\ddot{h} - 2d_i^2 h^3 - a^2 h = 0, \tag{4.33}$$

where a^2 is defined as

$$a^2 = -2[4d_i(\alpha_0 g_0 - \beta_0 f_0) - 8\alpha_0\beta_0 + d_i^2 h_0^2]. \tag{4.34}$$

Note that the equation is valid for any $\gamma(t)$.

A finite-time collapse to a current sheet occurs if a finite-time singularity is present in the solution, that is if $h(t) \to \infty$ as $t \to t_s$. We note, if $h(t) \to \infty$ then either $f(t)$ or $g(t)$ must be singular as $t \to t_s$ by (4.32). Accordingly, either

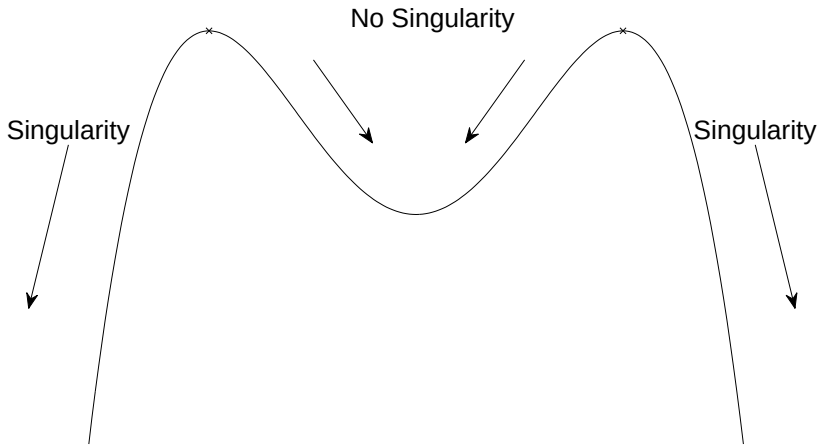

Figure 4.1: $U(h)$ vs h.

$\alpha(t)$ or $\beta(t)$ must also be singular as $t \to t_s$ by (4.30) and (4.31). Finally, $\alpha(t)$ and $\beta(t)$, and consequently $f(t)$ and $g(t)$, cannot both be singular by (4.29).

We obtain a singularity criterion by using a mechanical analogy. We rewrite (4.33) as

$$\ddot{h} + U'(h) = 0, \tag{4.35}$$

where $U(h)$ is analogous to potential energy in mechanics (Figure 4.1). Hence we can view the solution to (4.33) as particle motion in this potential. Integration of (4.35) yields an analogue of energy conservation:

$$\frac{1}{2}\dot{h}^2 = -U(h), \tag{4.36}$$

where

$$U(h) = -\frac{1}{2}(d_i^2 h^4 + a^2 h^2) + \frac{1}{2}(d_i^2 h_0^4 + a^2 h_0^2) - 8(\alpha_0 g_0 + \beta_0 f_0)^2. \tag{4.37}$$

The quartic function $U(h)$ tends to $-\infty$ for large h. By setting $U'(h_{max}) = 0$, we find

$$h_{max}^2 = -\frac{a^2}{2d_i^2}. \tag{4.38}$$

The solution $h(t)$ is stable if the following three conditions are satisfied. First, $U(h)$ has a local minimum. Second, $h(t)$ stays between the local maxima

$\pm h_{max}$ of $U(h)$. In other words, $h(t)$ does not escape the local potential well. Third, at $t = 0$, $h(t) = h_0$ lies between the maxima.

Near the origin $U(h) \approx -a^2h^2/2$. To satisfy the first condition we must have

$$a^2 < 0. \tag{4.39}$$

To satisfy the second condition we require that $\dot{h} \leq 0$ at the maxima, or equivalently that $U(h_{max}) \geq 0$. Consequently

$$-\frac{1}{2}(d_i^2 h_{max}^4 + a^2 h_{max}^2) + \frac{1}{2}(d_i^2 h_0^4 + a^2 h_0^2) - 8(\alpha_0 g_0 + \beta_0 f_0)^2 \geq 0.$$

On substituting h_{max} from (4.38), we get

$$\frac{a^4}{8d_i^2} + \frac{1}{2}(d_i^2 h_0^4 + a^2 h_0^2) - 8(\alpha_0 g_0 + \beta_0 f_0)^2 \geq 0.$$

On substituting a^2 from (4.34) and simplifying, we have

$$\alpha_0\beta_0(\alpha_0 + d_i f_0)(\beta_0 - d_i g_0) \geq 0. \tag{4.40}$$

The third condition means that

$$h_0^2 \leq h_{max}^2,$$

and so

$$d_i(\alpha_0 g_0 - \beta_0 f_0) - 2\alpha_0\beta_0 \geq 0. \tag{4.41}$$

Equation (4.41) is in fact a stronger condition than (4.39). So we only have the last two conditions on the initial values of α, β, f and g for the solution $h(t)$ to be stable. Therefore, our self-similar solution will not contain a finite-time singularity if the initial conditions α_0, β_0, f_0 and g_0 are such that equations (4.40) and (4.41) are satisfied. Significantly, these conditions do not contain $\gamma(t)$ and h_0. If either (4.40) or (4.41) are not satisfied, the solution develops a singularity, and so, in sharp contrast to the exponential collapse in MHD, the collapse to a current sheet can occur in a finite time in Hall MHD. For

example, equation (4.41) is not satisfied for the particular case considered by Litvinenko (2007) ($\alpha_0 = \beta_0, \gamma_0 = 0.5, f_0 = g_0 = 0$).

Equation (4.33) can be solved in terms of Jacobi elliptic functions. However, these solutions are difficult to work with, so we approximate the collapse solution in terms of elementary functions, assuming $a^2 > 0$. Near the singularity, we let each variable be dependent on a power of $\tau = (t_s - t)$, where t_s is the singularity time, then let $\tau \to 0$. This requires that $\Gamma(t) \to \Gamma_s = \int_0^{t_s} \gamma(t')\,\mathrm{d}t'$, where we assume that the integral converges. It is reasonable to assume that $\gamma(t)$ is non-singular because $\gamma(t)$ represents the driving flow. Due to the hyperbolic shape of the flow, either $\alpha \to \infty$, $\beta \to 0$ or $\alpha \to 0$, $\beta \to \infty$. For large h, $\ddot{h} \approx 2d_i^2 h^3$, so h is proportional to $\pm\tau^{-1}$. We substitute $d_i h = \tau^{-1}$ into (4.19), (4.20), (4.31) and (4.32) with $\tau \to 0$ and $\Gamma \to \Gamma_s$ and balance the leading-order terms. The resulting scalings are

$$\alpha \approx \frac{1}{4(\beta_0 - d_i g_0)} \exp(2\Gamma_s)\,\tau^{-2}, \tag{4.42}$$

$$\beta \approx 4\alpha_0\beta_0(\beta_0 - d_i g_0) \exp(-2\Gamma_s)\,\tau^2, \tag{4.43}$$

$$d_i f \approx \frac{-1}{4(\beta_0 - d_i g_0)} \exp(2\Gamma_s)\,\tau^{-2}, \tag{4.44}$$

$$d_i g \approx -(\beta_0 - d_i g_0) \exp(-2\Gamma_s), \tag{4.45}$$

$$d_i h \approx \tau^{-1}, \tag{4.46}$$

or

$$\alpha \approx 4\alpha_0\beta_0(\alpha_0 + d_i f_0) \exp(2\Gamma_s)\,\tau^2, \tag{4.47}$$

$$\beta \approx \frac{1}{4(\alpha_0 + d_i f_0)} \exp(-2\Gamma_s)\,\tau^{-2}, \tag{4.48}$$

$$d_i f \approx (\alpha_0 + d_i f_0) \exp(2\Gamma_s), \tag{4.49}$$

$$d_i g \approx \frac{1}{4(\alpha_0 + d_i f_0)} \exp(-2\Gamma_s)\,\tau^{-2}, \tag{4.50}$$

$$d_i h \approx -\tau^{-1}. \tag{4.51}$$

Next, we use asymptotic analysis to determine the singularity time t_s. For small h, $h^3 \ll h$, and so

$$\ddot{h} \approx a^2 h.$$

The general solution is

$$h(t) \approx c_1 \cosh(at) + c_0 \sinh(at).$$

Based on initial conditions we choose $c_1 = h_0$ and $c_0 = \dot{h}_0/a$, where $\dot{h}_0 = -4(\alpha_0 g_0 + \beta_0 f_0)$, so that

$$h(t) \approx h_0 \cosh(at) + \frac{\dot{h}_0}{a} \sinh(at) \tag{4.52}$$

for small time. For large t we use equations (4.36) and (4.37):

$$\dot{h}^2 = d_i^2 h^4 + a^2 h^2 + \text{const.}$$

Near the singularity, $h \to \infty$, and so the integration constant can be neglected:

$$\dot{h} \approx h(d_i^2 h^2 + a^2)^{\frac{1}{2}}.$$

Integrating this equation gives

$$h(t) \approx \frac{2a^2 k \exp(at)}{1 - (d_i a k)^2 \exp(2at)}, \tag{4.53}$$

where k is an integration constant.

We use (4.52) and (4.53) to find an intermediate asymptotic solution for all times. Letting $t \to \infty$ in (4.52) and $t \to 0$ in (4.53) and equating them will yield an equation for k. Equation (4.52) becomes

$$h(t) \approx \left(\frac{h_0}{2} + \frac{\dot{h}_0}{2a} \right) \exp(at),$$

and (4.53) becomes

$$h(t) \approx \frac{2a^2 k}{1 - (d_i a k)^2} \exp(at).$$

Consequently, k is defined by

$$\frac{2a^2 k}{1 - (d_i a k)^2} = \frac{h_0}{2} + \frac{\dot{h}_0}{2a}.$$

On solving the resulting quadratic equation

$$\left(h_0 + \frac{\dot{h}_0}{a} \right) (d_i a)^2 + (4a^2) \frac{1}{k} - \left(h_0 + \frac{\dot{h}_0}{a} \right) \frac{1}{k^2} = 0,$$

and assuming $\left(h_0 + \dot{h}_0/a\right)(d_i a)^2 \ll 1$, we obtain

$$k = \frac{1}{4a^2}\left(h_0 + \frac{\dot{h}_0}{a}\right). \tag{4.54}$$

Substituting (4.54) into (4.53), we find

$$h(t) \approx \left(\frac{h_0}{2} + \frac{\dot{h}_0}{2a}\right)\exp(at)\left[1 - \frac{d_i^2}{16a^2}\left(h_0 + \frac{\dot{h}_0}{a}\right)^2 \exp(2at)\right]^{-1}.$$

Comparing this with (4.52) we have the intermediate asymptotic solution

$$\begin{aligned} h(t) \approx &\left(h_0 \cosh(at) + \frac{\dot{h}_0}{a}\sinh(at)\right) \\ &\times \left[1 - \frac{d_i^2}{16a^2}\left(h_0 + \frac{\dot{h}_0}{a}\right)^2 \exp(2at)\right]^{-1}. \end{aligned} \tag{4.55}$$

Therefore the singularity time t_s in terms of the initial values is

$$t_s = \frac{1}{2a}\ln\left[\frac{16a^2}{d_i^2}\left(h_0 + \frac{\dot{h}_0}{a}\right)^{-2}\right]. \tag{4.56}$$

When we substitute $a = 4$ and $\dot{h}_0 = 0$ we recover the case considered by Litvinenko (2007).

We illustrate the criteria (4.40) and (4.41) by plotting the numerical solutions of the system (4.19)-(4.23) with varied initial conditions (see Figs. 4.2-4.6). There are six variables in our system but only five equations, so we have to make an assumption for one of the variables in order to solve the system. We choose $\gamma(t) = \text{const}$ for consistency with previous studies (e.g., Sulem et al., 1985; Grauer and Marliani, 1998; Litvinenko, 2007). Specifically, we choose initial conditions $\alpha_0 = \beta_0 = 1, \gamma_0 = 0.5$ and vary f_0, g_0 and h_0. Equation (4.55) predicts that $h \to \infty$ when $(h_0 + \dot{h}_0/a) > 0$, and $h \to -\infty$ when $(h_0 + \dot{h}_0/a) < 0$. Figure 4.2 shows a nonsingular solution, whereas Figs. 4.3-4.6 show singular solutions when one or both conditions (4.40)-(4.41) are not satisfied. The numerical results also show that the accuracy of the predicted value of t_s increases as a^2 increases.

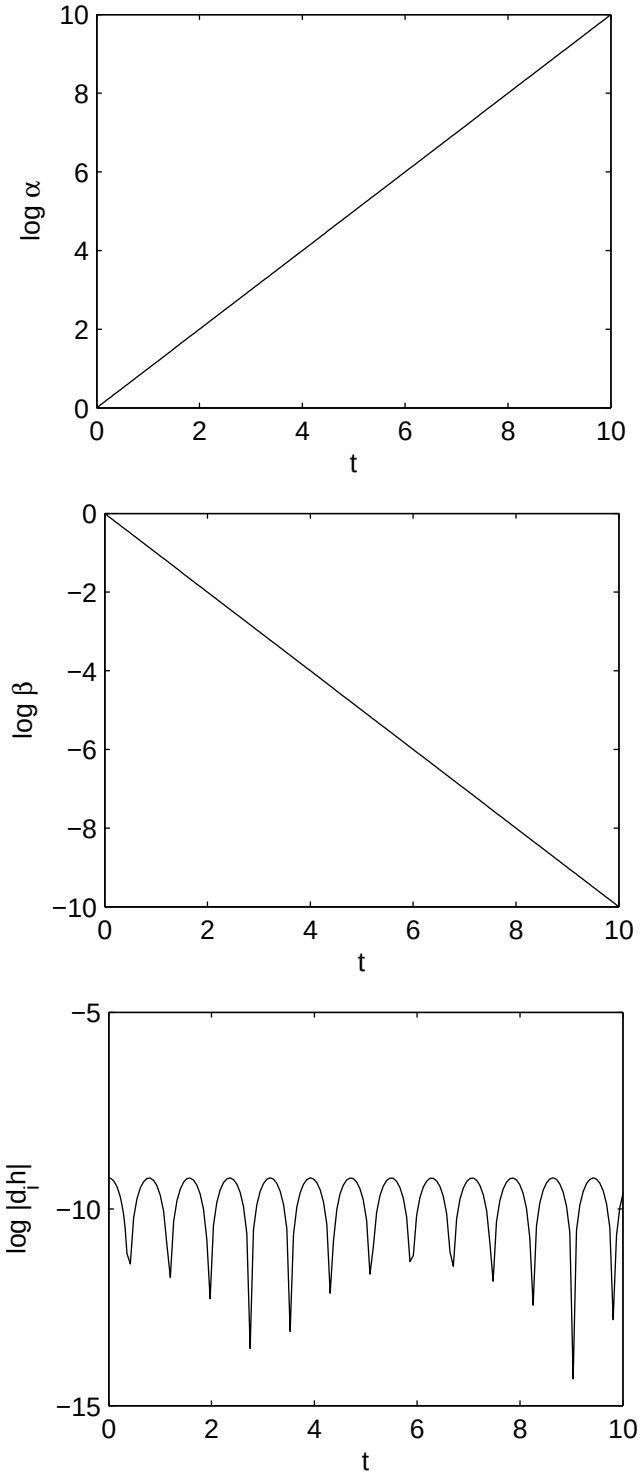

Figure 4.2: Plots of α, β and h for the initial conditions $\alpha_0 = \beta_0 = 1, \gamma_0 = 0.5, d_i f_0 = -2, d_i g_0 = 2$ and $d_i h_0 = 10^{-4}$. These initial conditions satisfy the criteria (4.40) and (4.41), hence no finite-time singularity is present, and $h(t)$ oscillates about $h = 0$.

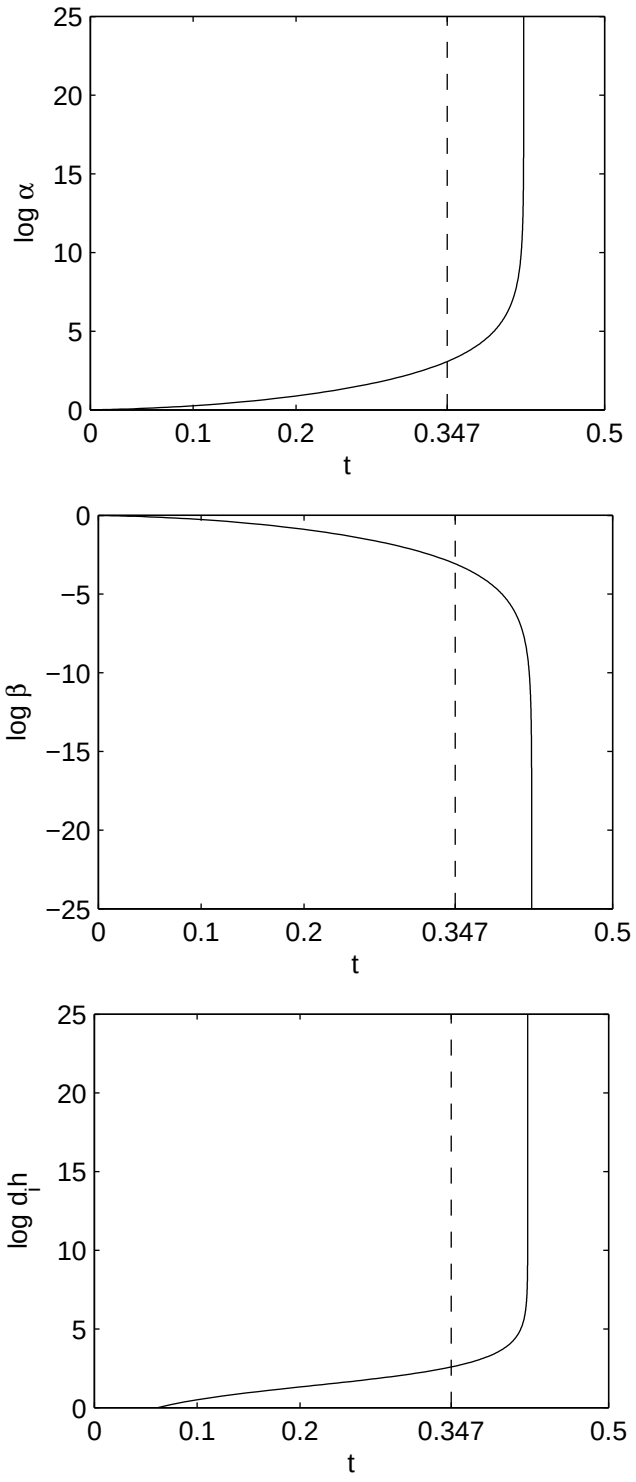

Figure 4.3: Plots of α, β and h for the initial conditions $\alpha_0 = \beta_0 = 1, \gamma_0 = 0.5, d_i f_0 = -2, d_i g_0 = -2$ and $d_i h_0 = 10^{-4}$ so $a = 4$ and $d_i \dot{h}_0 = 16$. Equation (4.55) predicts $h \to \infty$ because $(h_0 + \dot{h}_0/a) > 0$. Equation (4.56) predicts the singularity time $t_s = 0.347$.

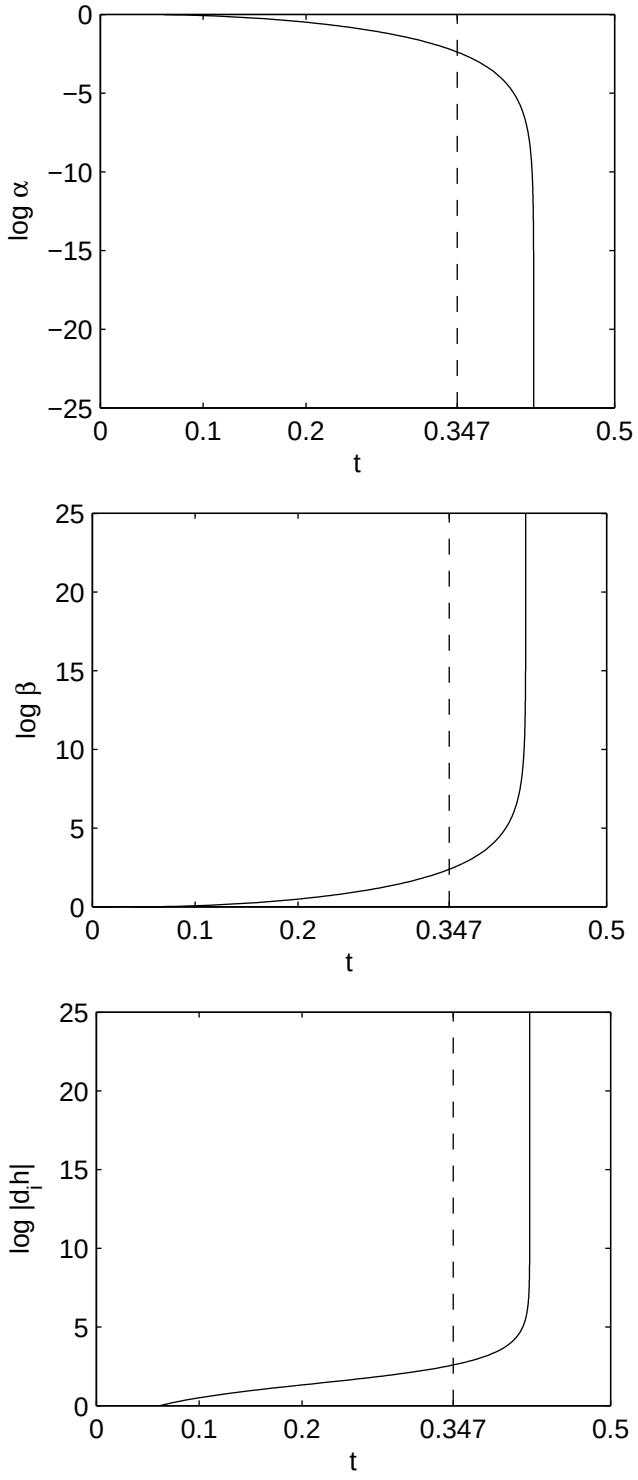

Figure 4.4: Plots of α, β and h for the initial conditions $\alpha_0 = \beta_0 = 1, \gamma_0 = 0.5, d_i f_0 = 2, d_i g_0 = 2$ and $d_i h_0 = 10^{-4}$ so $a = 4$ and $d_i \dot{h}_0 = -16$. Equation (4.55) predicts $h \to -\infty$ because $(h_0 + \dot{h}_0/a) < 0$. Equation (4.56) predicts the singularity time $t_s = 0.347$.

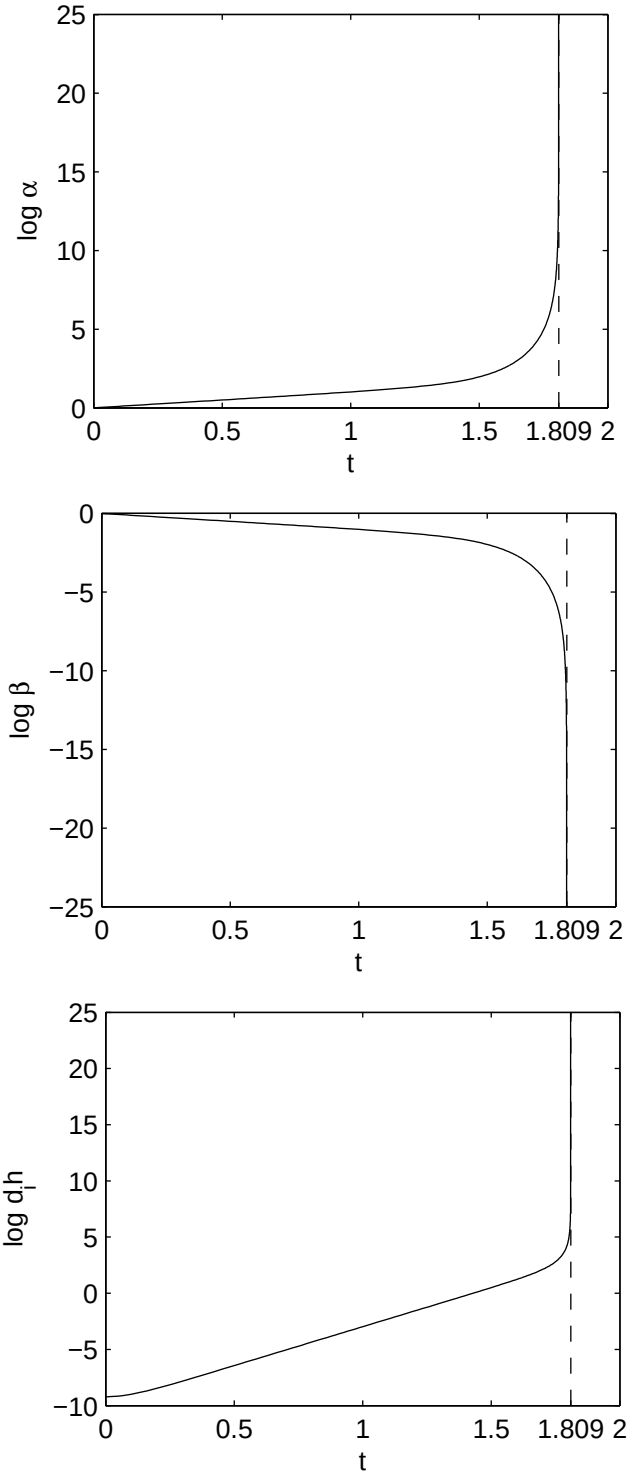

Figure 4.5: Plots of α, β and h for the initial conditions $\alpha_0 = \beta_0 = 1, \gamma_0 = 0.5, d_i f_0 = 2, d_i g_0 = -2$ and $d_i h_0 = 10^{-4}$ so $a = 4\sqrt{3}$ and $d_i \dot{h}_0 = 0$. Equation (4.55) predicts $h \to \infty$ because $(h_0 + \dot{h}_0/a) > 0$. Equation (4.56) predicts the singularity time $t_s = 1.809$.

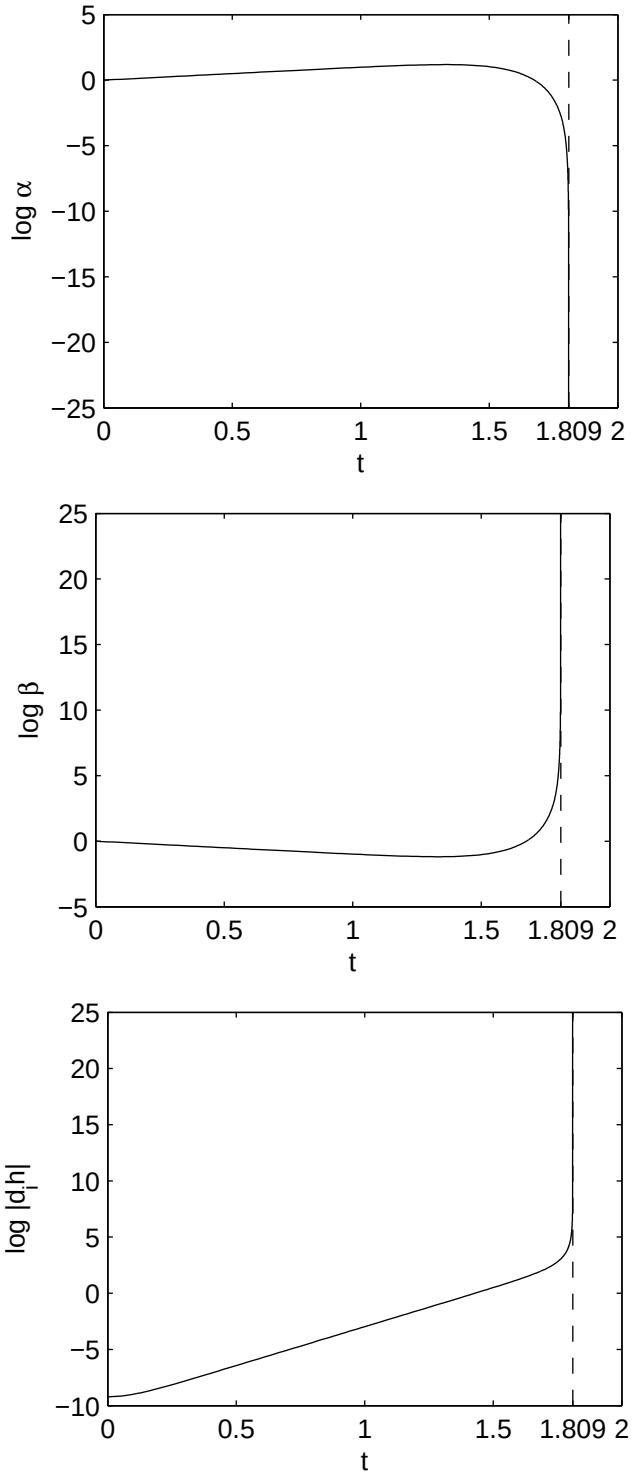

Figure 4.6: Plots of α, β and h for the initial conditions $\alpha_0 = \beta_0 = 1, \gamma_0 = 0.5, d_i f_0 = 2, d_i g_0 = -2$ and $d_i h_0 = -10^{-4}$ so $a = 4\sqrt{3}$ and $d_i \dot{h}_0 = 0$. Equation (4.55) predicts $h \to -\infty$ because $(h_0 + \dot{h}_0/a) < 0$. Equation (4.56) predicts the singularity time $t_s = 1.809$.

4.5 An Alternative Reduction

In the previous section we derived a criterion for $h(t)$ to develop a singularity, and we derived an asymptotic solution to the system (4.19)-(4.23), assuming that $\gamma(t)$ remains non-singular. Now we allow the possibility for $\gamma(t)$ to be singular, which would imply an infinite flow speed. Note that the choice of γ that is singular appears to contradict previous numerical simulations in ideal MHD (e.g., Sulem et al., 1985; Grauer and Marliani, 1998). Since we have six variables and only five equations (4.19)-(4.23), an equation for $\gamma(t)$ is needed. Shivamoggi (2011) assumes that the pressure is defined by

$$p(x,y,t) = -\frac{1}{2}h^2x^2y^2 + \mu(t)(x^2+y^2). \tag{4.57}$$

Matching this pressure profile to our general equation for the pressure (4.28) gives

$$\mu(t) = -4\alpha(\alpha-\beta) + \gamma^2 - \dot{\gamma} = 4\beta(\alpha-\beta) - \gamma^2 - \dot{\gamma}.$$

Rearranging gives an equation for $\gamma(t)$:

$$\dot{\gamma} = 2(\alpha^2 - \beta^2). \tag{4.58}$$

Shivamoggi (2011) further assumes

$$\alpha(t) = -d_i f(t), \qquad \beta(t) = d_i g(t).$$

These assumptions modify the set of equations (4.19)-(4.23) to

$$\dot{\alpha} - 2\alpha(\gamma + d_i h) = 0, \tag{4.59}$$

$$\dot{\beta} + 2\beta(\gamma + d_i h) = 0, \tag{4.60}$$

$$\dot{\gamma} = 2(\alpha^2 - \beta^2), \tag{4.61}$$

$$d_i f = -\alpha, \tag{4.62}$$

$$d_i g = \beta, \tag{4.63}$$

$$h = h_0 = \text{const.} \tag{4.64}$$

This system satisfies the conditions (4.40) and (4.41) for h to be non-singular, however a singularity in $\gamma(t)$ may lead to a singularity in either $\alpha(t)$ or $\beta(t)$. We

find an equation for $\gamma(t)$ in terms of initial conditions, similar to our treatment of $h(t)$. Differentiating (4.61) and substituting (4.59) and (4.60) yields

$$\ddot{\gamma} = 8(\gamma + d_i h_0)(\alpha^2 + \beta^2). \tag{4.65}$$

Differentiating again gives

$$\dddot{\gamma} = 8\dot{\gamma}(\alpha^2 + \beta^2) + 32(\gamma + d_i h_0)^2(\alpha^2 - \beta^2). \tag{4.66}$$

Rearranging (4.61) and (4.65) and substituting into (4.66) yields

$$\dddot{\gamma}(\gamma + d_i h_0) = \dot{\gamma}\ddot{\gamma} + 16\dot{\gamma}(\gamma + d_i h_0)^3. \tag{4.67}$$

Integration yields

$$\ddot{\gamma}(\gamma + d_i h_0) = \dot{\gamma}^2 + 4(\gamma + d_i h_0)^4 - c, \tag{4.68}$$

where we integrated $\dddot{\gamma}\gamma$ by parts. Here the integration constant is

$$\begin{aligned} c = 4(\gamma_0 + d_i h_0 + \alpha_0 + \beta_0)(\gamma_0 + d_i h_0 + \alpha_0 - \beta_0) \\ \times (\gamma_0 + d_i h_0 - \alpha_0 + \beta_0)(\gamma_0 + d_i h_0 - \alpha_0 - \beta_0). \end{aligned} \tag{4.69}$$

This reduction was previously shown to exhibit singularities in ideal MHD (Shivamoggi, 1986), that is when $d_i h(t) = 0$. Shivamoggi (2011) argues that the Hall term will quench the singularity, because the system has a steady solution $\alpha = \alpha_0, \beta = \beta_0, \gamma = -d_i h_0$ if $\alpha_0 = \beta_0$ and $h_0 \neq 0$ (see also Núñez et al., 2008; Shivamoggi, 2009). It is worth noting, however, that other choices of the initial value $\gamma_0 \neq -d_i h_0$ will still lead to a finite-time singularity. We demonstrate this by solving equation (4.68). Near the singularity, we neglect the integration constant and let $\gamma(t)$ be dependent on a power of $(t - t_0)$:

$$\gamma + d_i h_0 = A(t - t_0)^q + \ldots \tag{4.70}$$

Matching the leading-order terms yields the nonsteady solution

$$\gamma \approx \pm \frac{1}{2(t - t_0)} - d_i h_0, \tag{4.71}$$

which implies a singularity at $t = t_0$ unless $\gamma_0 = -d_i h_0$ (which implies $t_0 \to \infty$). This singularity is illustrated by a numerical solution in Figure 4.7.

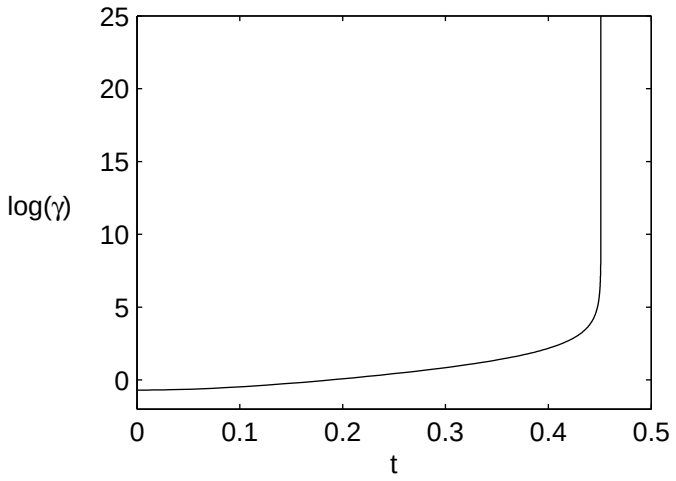

Figure 4.7: $\gamma(t)$ from the numerical solution of the system of equations (4.59)-(4.61). The initial conditions are $\alpha_0 = \beta_0 = 1, \gamma_0 = 0.5$ and $d_i h_0 = 1$.

To sum up, Shivamoggi (2011) argues that the addition of the Hall term quenches the singularity in $\gamma(t)$ because the initial condition $\gamma_0 = -d_i h_0$ leads to a steady solution if the pressure profile is given by (4.57). However, we show that another choice of γ_0 would lead to the same singularity as in ideal MHD. This is why we believe Shivamoggi's argument to be of limited validity.

4.6 Generalisations

We generalise the results of the previous section to include the electron inertia, resistivity and viscosity. The generalised system is given by equations (4.1)-(4.6). We analyse the generalised system as we did the ideal Hall MHD system. Taking the $\hat{\mathbf{z}}$ component of (4.1) and (4.2) and their curls yields the following system:

$$\partial_t \psi + [\psi, \phi] = \eta \nabla^2 \psi + d_i [\psi, Z] + d_e^2 (\partial_t \nabla^2 \psi + [\nabla^2 \psi, \phi] + [Z, W]), \quad (4.72)$$

$$\begin{aligned} \partial_t Z + [Z, \phi] = \eta \nabla^2 Z + [W, \psi] + d_i [\nabla^2 \psi, \psi] \\ + d_e^2 (\partial_t \nabla^2 Z + [\nabla^2 Z, \phi] + [\nabla^2 \phi, Z]), \end{aligned} \quad (4.73)$$

$$\partial_t W + [W, \phi] = [Z, \psi] + \nu \nabla^2 W, \quad (4.74)$$

$$\partial_t (\nabla^2 \phi) + [\nabla^2 \phi, \phi] = [\nabla^2 \psi, \psi] + \nu \nabla^4 \phi. \quad (4.75)$$

We modify our similarity reduction so that the viscous and resistive terms cancel when we perform the substitution. Uberoi (1963) noted that the resistivity can be accounted for by adding a function of time only to ψ. Significantly, this does not change the magnetic field $\mathbf{B}$. Similarly, we also incorporate the viscous and the $\partial_t \nabla^2 \psi$ terms:

$$\psi = \alpha(t)x^2 - \beta(t)y^2 + 2\eta \int (\alpha - \beta)\,\mathrm{d}t + 2d_e^2(\alpha - \beta), \tag{4.76}$$

$$\phi = -\gamma(t)xy, \tag{4.77}$$

$$W = f(t)x^2 + g(t)y^2 + 2\nu \int (f + g)\,\mathrm{d}t, \tag{4.78}$$

$$Z = h(t)xy. \tag{4.79}$$

This yields the generalised system

$$\dot{\alpha} - 2\alpha(\gamma + d_i h) + 2d_e^2 fh = 0, \tag{4.80}$$

$$\dot{\beta} + 2\beta(\gamma + d_i h) + 2d_e^2 gh = 0, \tag{4.81}$$

$$\dot{f} - 2\gamma f + 2\alpha h = 0, \tag{4.82}$$

$$\dot{g} + 2\gamma g + 2\beta h = 0, \tag{4.83}$$

$$\dot{h} + 4\alpha g + 4\beta f = 0. \tag{4.84}$$

The integrals that generalise equations (4.29) and (4.32) are

$$4\alpha\beta = 4\alpha_0\beta_0 + d_e^2(h^2 - h_0^2), \tag{4.85}$$

$$4fg = 4f_0g_0 + (h^2 - h_0^2). \tag{4.86}$$

Equations (4.30) and (4.31) are harder to generalise. We note, however, that

$$(\alpha + d_i f)(\beta - d_i g) = (\alpha_0 + d_i f_0)(\beta_0 - d_i g_0),$$

$$\mathrm{d}_t\left[(\alpha + d_i f)(\beta - d_i g)\right] = 0.$$

in Hall MHD. Now if $d_e \neq 0$, we have

$$\begin{aligned}
\mathrm{d}_t(\alpha + d_i f)(\beta - d_i g) &= (\dot{\alpha} + d_i \dot{f})(\beta - d_i g) + (\alpha + d_i f)(\dot{\beta} - d_i \dot{g}) \\
&= (-2d_e^2 fh)(\beta - d_i g) + (\alpha + d_i f)(-2d_e^2 gh) \\
&= \frac{1}{2} d_e^2 h\dot{h},
\end{aligned}$$

and so the generalised integral is

$$4(\alpha + d_i f)(\beta - d_i g) = 4(\alpha_0 + d_i f_0)(\beta_0 - d_i g_0) + d_e^2(h^2 - h_0^2). \tag{4.87}$$

Again, we derive equation for h in order to investigate the collapse to a current sheet. We have as before

$$\ddot{h} + 4(\dot{\alpha} g + \alpha \dot{g} + \dot{\beta} f + \beta \dot{f}) = 0,$$

which can be written as

$$\ddot{h} + 8h[d_i(\alpha g - \beta f) - 2\alpha\beta - 2d_e^2 fg] = 0. \tag{4.88}$$

To find an expression for $d_i(\alpha g - \beta f)$ we use the property (4.87). Rearranging terms yields

$$-d_i(\alpha g - \beta f) = (\alpha_0 + d_i f_0)(\beta_0 - d_i g_0) - \alpha_0\beta_0 + d_i^2 fg.$$

We also use equations (4.85) and (4.86). Substituting these into (4.88) yields:

$$\ddot{h} - 8h[(\alpha_0 + d_i f_0)(\beta_0 - d_i g_0) + (d_i^2 + 4d_e^2)fg + \alpha_0\beta_0 - 2d_e^2 f_0 g_0] = 0,$$

which simplifies to

$$\ddot{h} - 2(d_i^2 + 4d_e^2)h^3 + [8d_e^2(h_0^2 - 2f_0 g_0) - a^2]h = 0. \tag{4.89}$$

Note equation (4.89) was erroneously published as (6.19) in Litvinenko and McMahon (2015b) with the term $4d_e^2(h_0^2 - 2f_0 g_0)$ instead of $8d_e^2(h_0^2 - 2f_0 g_0)$. This error was corrected by Janda (2018). This equation generalises the Hall MHD result (4.33). The singularity is driven by the nonlinear term, which is proportional to $d_i^2 + 4d_e^2$. Because $d_e^2/d_i^2 = m_e/m_i \ll 1$, we conclude that electron inertia is unlikely to modify the X-point collapse in a significant manner, unless an initial perturbation is already localised on the electron scale $\sim d_e$.

4.7 Further Research- Exact Solutions

4.7.1 Weierstrass Elliptic Function

We used an asymptotic analysis on equation (4.33) to obtain the approximate solution (4.55) and the singularity time (4.56). However, it is possible to find

an exact solution for (4.33) or the more general (4.89). Hence, Janda (2018) multiplied equation (4.89) by $\dot{h}$ and integrated to obtain

$$\dot{h}^2 - bh^4 + 2ch^2 = 2E_0, \tag{4.90}$$

where

$$a = \sqrt{2[8\alpha_0\beta_0 - 4d_i(\alpha_0 g_0 - \beta_0 f_0) - d_i^2 h_0^2]}, \tag{4.91}$$

$$b = d_i^2 + 4d_e^2, \tag{4.92}$$

$$c = 4d_e^2(h_0^2 - 2f_0 g_0) - \frac{a^2}{2}, \tag{4.93}$$

$$E_0 = 8\left(\alpha_0 g_0 + \beta_0 f_0\right)^2 - \frac{bh_0^4}{2} + ch_0^2. \tag{4.94}$$

Note Janda (2018) originally published equation (4.94) with the a sign error corresponding to

$$E_0 = -8\left(\alpha_0 g_0 + \beta_0 f_0\right)^2 - \frac{bh_0^4}{2} + ch_0^2, \tag{4.95}$$

an error that was noticed by Brizard (2019) and fixed in Janda (2019). In doing so, Brizard (2019) asserts that E_0 is the energy of the system and thus should be conserved. It should be pointed out that E_0 is not a physical energy but an analogue of energy (Janda, 2019). Nevertheless, Janda (2018) introduces the rescaling variable

$$q(t) = \sqrt{d_i^2 + 4d_e^2}\, h(t), \tag{4.96}$$

which transforms (4.90) to

$$\dot{q}^2 - q^4 + 2cq^2 = \left(d_i^2 + 4d_e^2\right) E_0, \tag{4.97}$$

In order to complete the square we let

$$c_0 = \sqrt{c^2 - \left(d_i^2 + 4d_e^2\right) E_0}, \tag{4.98}$$

which works out to be (Janda, 2019)

$$c_0 = 4\sqrt{\left[2\alpha_0\beta_0 - d_i\left(\alpha_0 g_0 - \beta_0 f_0\right) + 2d_e^2 f_0 g_0\right]^2 - \left(d_i^2 + 4d_e^2\right)\left(\alpha_0 g_0 + \beta_0 f_0\right)^2}, \tag{4.99}$$

so that (4.97) becomes

$$\dot{q}^2 - \left(q^2 - c\right)^2 = c_0^2. \tag{4.100}$$

Janda (2018) introduces the variable

$$q(t) = b_1 \left(1 + \frac{b_2}{w(t) + b_3}\right), \tag{4.101}$$

with unknown constants b_1, b_2 and b_3, to reduce (4.97) to

$$b_1^2 b_2^2 \dot{w}^2 - b_1^2 \left[b_1^2 \left(w + b_2 + b_3\right)^2 - c \left(w + b_3\right)^2\right]^2 = c_0^2 \left(w + b_3\right)^4 \tag{4.102}$$

from which we obtain a Weierstrass elliptic equation

$$\dot{w}^2 - 4w^3 + g_2 w + g_3 = 0. \tag{4.103}$$

Matching the w^4, w^3 and w^2 terms in (4.102) and (4.103) requires

$$\begin{aligned} \left(b_1^2 - c\right)^2 =& c_0^2, \\ b_2 b_1^2 \left(b_1^2 - c\right) + b_3 \left(b_1^2 - c\right)^2 =& c_0^2 b_3 + b_1^2 b_2^2, \\ \left[b_2 b_1^2 + b_3 \left(b_1^2 - c\right)\right]^2 =& c_0^2 b_3^2 + \frac{b_1^2 b_2^2 c}{3}, \end{aligned} \tag{4.104}$$

which yields

$$b_1 = \sqrt{c \pm c_0}, \tag{4.105}$$

$$b_2 = \pm\, c_0, \tag{4.106}$$

$$b_3 = \mp\, \frac{c_0}{2} \mp \frac{c}{3}. \tag{4.107}$$

Matching the w^1 and w^0 terms in (4.102) and (4.103) requires

$$\begin{aligned} b_2^3 b_1^4 + 3 b_3 b_2^2 b_1^2 \left(b_1^2 - \frac{c}{3}\right) + 3 b_3^2 b_2 b_1^2 \left(b_1^2 - c\right) + b_3^3 \left(b_1^2 - c\right)^2 = c_0^2 b_3^3 - \frac{g_2 b_1^2 b_2^2}{4}, \\ \left[b_2 b_1^2 \left(b_2 + 2 b_3\right) + b_3^2 \left(b_1^2 - c\right)\right]^2 = c_0^2 b_3^4 - b_1^2 b_2^2 g_3. \end{aligned} \tag{4.108}$$

After some algebra, and employing the identities

$$b_1^2 - c = b_2, \qquad b_1^2 - \frac{c}{3} = -2 b_3, \qquad b_2 + 2 b_3 = -\frac{2c}{3}, \tag{4.109}$$

we obtain

$$g_2 = \frac{4c^2}{3} - c_0^2, \tag{4.110}$$

$$g_3 = \frac{c}{3}\left(c_0^2 - \frac{8}{9}c^2\right). \tag{4.111}$$

Equation (4.103) has the solution

$$w(t) = \wp\left(t - t_0; g_2; g_3\right), \tag{4.112}$$

where

$$\wp(z; g_2; g_3) = z^{-2} + \frac{g_2}{20}z^2 + \frac{g_3}{28}z^4 + \mathcal{O}\left(z^6\right) \tag{4.113}$$

is the Weierstrass elliptic function (Southard, 1972),

$$t_0 = \pm\wp^{-1}\left(\frac{b_1 b_2}{b_0 - b_1} - b_3; g_2; g_3\right) \tag{4.114}$$

is an integration constant and

$$b_0 = h_0\sqrt{d_i^2 + d_e^2}. \tag{4.115}$$

The exact solution for $h(t)$ is obtained by substituting (4.112) into (4.101) to obtain $q(t)$. Scaling up by (4.96) produces $h(t)$. Finally, noticing that the singularity occurs when the denominator of (4.101) vanishes, Janda (2019) obtains the exact singularity time

$$t_s = t_0 + \wp^{-1}\left(-b_3; g_2, g_3\right). \tag{4.116}$$

4.7.2 Jacobi Elliptic Function

Instead of using Weierstrass elliptic functions, we could search for solutions based on the Jacobi elliptic function. Brizard (2019) rearranges (4.100) to

$$\dot{q}^2 = \left(q^2 - c\right)^2 - c_0^2 \tag{4.117}$$

which reduces to

$$\dot{q}^2 = c^2\epsilon\left(1 - \frac{q^2}{c + c_0}\right)\left(1 - \frac{q^2}{c - c_0}\right), \tag{4.118}$$

where

$$\epsilon = 1 - \frac{c_0^2}{c^2}. \tag{4.119}$$

Introducing the variables

$$\bar{q} = \frac{q}{\sqrt{c + c_0}}, \qquad \bar{z} = \sqrt{\frac{c^2\epsilon}{c + c_0}}\, t + \text{const.}, \qquad m = \frac{c + c_0}{c - c_0}, \tag{4.120}$$

reduces (4.118) to the Jacobi elliptic equation

$$\bar{q}'(\bar{z})^2 = \left(1 - \bar{q}(\bar{z})^2\right)\left(1 - m\,\bar{q}(\bar{z})^2\right), \tag{4.121}$$

and thus

$$\bar{q} = \pm \mathrm{sn}(\bar{z}|\bar{m}), \tag{4.122}$$

where

$$\mathrm{sn}(z|m) = \sin\phi, \tag{4.123}$$

is the Jacobi elliptic function, where $\phi(z, m)$ is given by solving

$$z = \int_0^{\phi} \frac{\mathrm{d}t'}{\sqrt{1 - m^2 \sin^2 t'}} \tag{4.124}$$

(Milne-Thompson, 1972). Substituting (4.122) into (4.120) gives an exact $q(t)$ which can be scaled by (4.96) to produce $h(t)$ in terms of the Jacobi elliptic function.

4.8 Discussion

In this chapter we have analysed the dynamics of a weakly collisional plasma and presented a self-similar solution for current sheet formation at a magnetic neutral line in incompressible Hall MHD. This solution generalises previous studies (Litvinenko, 2007, and references therein) by considering a general set of initial conditions. We derived a criterion for finite-time singularity formation, which describes the collapse to a current sheet, and we illustrated both the criterion and predicted collapse time with numerical solutions of the Hall

MHD equations. Finally, we generalised the self-similar solution to incorporate the resistive, viscous and electron inertia terms in Ohm's law and the momentum equation.

The predicted collapse time t_s decreases if the strength of the Hall term, quantified by the ion skin depth d_i, increases. This result is consistent with numerical solutions (e.g., Birn et al., 2001, 2005; Shay et al., 2001; Drake et al., 2008) which show that the Hall effect speeds up the reconnection process. In the limit $d_i \to 0$, the singularity formation time $t_s \to \infty$, corresponding to the well-established lack of a finite-time singularity in standard MHD collapse. An alternative point of view is that the Hall effect suppresses the singularity (Shivamoggi, 2011). We have shown, however, that the singularity is suppressed only for a particular pressure profile in the self-similar solution and only for a particular set of initial conditions.

In the context of a general initial and boundary value problem, our solution can be considered as a low-order Taylor expansion of the flux and stream functions at the origin. This approximation implies that the solution only holds locally and breaks down at some finite time. Another possible limitation, as in the corresponding MHD solutions (Chapman and Kendall, 1966), is that for the solution to be valid in a resistive plasma, a specific varying electric field must be applied, which is proportional to the plasma resistivity. However, the argument made by Chapman and Kendall (1966) essentially assumes the resistive MHD equations have no exact solutions. Uberoi (1966) demonstrates that the electric field is easily worked out from the solution to Ohm's law and therefore applies regardless of whether the resistivity is finite or infinite.

Our solution may be applicable in a weakly collisional plasma of the solar corona, where the reference values of $L = 10^{9.5}\,\mathrm{cm}$, $B_0 = 10^2\,\mathrm{G}$ and $n = 10^9\,\mathrm{cm}^{-3}$ yield the dimensionless ion skin depth $d_i \approx 10^{-6.5}$. Hall reconnection occurs when $d_i \gg \eta^{1/2}$. If the Sweet-Parker length scale $\eta^{1/2}$ is based on the collisional resistivity $\eta \sim T^{-3/2}$ of the corona (Spitzer, 1962), then the coronal temperature $T = 10^6\,\mathrm{K}$ gives $\eta \sim 10^{-14.5}$ and so $d_i \gg \eta^{1/2}$ (e.g., Craig and

Litvinenko, 2008). Cassak et al. (2006) argue that an explosive character of magnetic reconnection in solar flares can be explained by a rapid transition from slow Sweet-Parker reconnection to fast Hall reconnection in an evolving current sheet. The solution presented here models such rapid transition as a singularity formation at time t_s. Assuming $a \sim h_0 \sim 1$, our solution predicts the transition time $t_s \sim 10\, t_A$, where the Alfvèn time $t_A = L/v_A = 10^{0.5}$ s. This estimate is consistent with typical flare onset times and simulation results of Cassak et al. (2006).

Chapter 5

Purely Resistive 2D Linear Reconnection

5.1 Introduction

Due to the complexity of the full non-linear MHD equations, an exact general solution for reconnection is difficult to obtain. A simple, but powerful method of analysing the MHD equations is linearisation. Whereas in usual analytical treatments, assuming incompressibility is a necessary simplification, linearisation allows us to study an arbitrarily compressible plasma. Linearisation had been previously used to investigate the tearing instability (Furth et al., 1963) and wave propagation near MHD null points (Bulanov and Syrovatskii, 1980; Bulanov et al., 1990). However, apart from a few other brief forays in the literature (e.g. Ara et al., 1978; Porcelli, 1987), a full theoretical picture of linear reconnection was not given until the independent studies of Craig and McClymont (1991) and Hassam (1992). The linear model was shown to be able to predict fast reconnection rates proportional to the logarithm of the dimensionless resistivity. Moreover, features of the linear model, namely oscillatory reconnection, have been present in observations (Hong et al., 2019).

The popularity of the linear reconnection model owes to its ability to release magnetic energy at a fast rate, proportional to the logarithm of the dimension-

less resistivity. The model we review is set up by considering an equilibrium magnetic field perturbed by a reconnective magnetic field. The equilibrium field takes the form of a magnetic X-point with separatrices initially at right angles. We then enclose the X-point with a circular conducting boundary through which no magnetic flux is lost. From this boundary, we send a reconnective disturbance towards the origin, upon which it pushes the separatrices closer together and the reconnection process starts. The system pushes the separatrices back apart, using pressure forces, in order to try and re-establish equilibrium. The competition of these effects leads to the oscillatory nature of the linear reconnection model.

In this chapter, we first review the Craig and McClymont (1991) solution which is effectively the simplest possible model. We examine the three phases of linear reconnection- the initial implosion as the disturbance travels out from the boundary, the oscillatory phase, and a non-oscillatory long-time tail that occurs once enough energy has been removed from the system. We then review extensions of the model such as higher-order equilibrium fields (Craig, 1994) and non-azimuthally symmetric perturbations (Craig and McClymont, 1993).

5.1.1 Governing Equations and Setup

Initially, we want to find the simplest possible model for reconnection using the linearised MHD equations. Hence, we neglect Hall, electron inertia, viscous and axial effects. The MHD equations (2.7)-(2.12) in the 2D compressible, purely resistive regime reduce to

$$\mathbf{E} + \mathbf{v} \times \mathbf{B} = \eta \mathbf{J}, \tag{5.1}$$

$$\rho \left(\partial_t \mathbf{v} + (\mathbf{v} \cdot \nabla) \mathbf{v} \right) = -\nabla p + \mathbf{J} \times \mathbf{B}, \tag{5.2}$$

$$\partial_t \rho + \nabla \cdot (\rho \mathbf{v}) = 0 \tag{5.3}$$

$$\nabla \cdot \mathbf{B} = 0, \tag{5.4}$$

$$\mathbf{J} = \nabla \times \mathbf{B}, \tag{5.5}$$

$$\nabla \times \mathbf{E} = -\partial_t \mathbf{B}. \tag{5.6}$$

We use the flux function $\psi(x, y)$ to satisfy equation (5.4):

$$\mathbf{B} = \nabla \times (\psi \hat{\mathbf{z}}), \tag{5.7}$$

Assuming $\mathbf{E}$ only has a $\hat{\mathbf{z}}$ component, the solution to (5.6) is

$$\mathbf{E} = -\partial_t \psi \, \hat{\mathbf{z}}, \tag{5.8}$$

In order to analyse the MHD system, we linearise by

$$\psi = \psi^E + \delta\psi + \ldots, \tag{5.9}$$

$$\mathbf{v} = \mathbf{0} + \delta\mathbf{u} + \ldots, \tag{5.10}$$

$$\rho = \rho^E + \delta\rho + \ldots \tag{5.11}$$

$$p = 0 + \delta p + \ldots \tag{5.12}$$

where $\mathbf{u}$ is the planar plasma velocity. Our equilibrium terms are denoted with an E superscript and are spatially dependent only. Our first order terms, multiplied by the perturbation magnitude $\delta \ll 1$, are spatially and temporally dependent. We normalise the equilibrium density to be uniform in our units. That is

$$\rho^E(x, y) = 1. \tag{5.13}$$

We adopt the polytropic gas pressure

$$p = \bar{\beta}\rho^\gamma, \tag{5.14}$$

which produces the relation

$$\nabla p = \bar{\beta} \nabla \left(\rho^\gamma\right). \tag{5.15}$$

We linearise about $\rho = 1$ to obtain

$$\nabla p \approx \beta \nabla \rho, \tag{5.16}$$

where $\beta = \gamma\bar{\beta}$ is a rescaled plasma beta based on B_0. Our system reduces to

$$-\rho_t = \nabla \cdot \mathbf{v} \tag{5.17}$$

$$\mathbf{u}_t = -\beta \nabla \rho - \nabla^2 \psi \nabla \psi^E \tag{5.18}$$

$$\psi_t = -\mathbf{u} \cdot \nabla \psi^E + \eta \nabla^2 \psi, \tag{5.19}$$

where we use subscript notation for time derivatives.

5.2 Craig-McClymont Solution

Initially, we want to find the simplest possible model for reconnection using the linearised MHD equations (Craig and McClymont, 1991). Hence, we neglect pressure effects, in other words take a cold plasma with $\beta \ll 1$, which reduces (5.18)-(5.19) to

$$\mathbf{u}_t = -\nabla^2\psi\nabla\psi^E, \tag{5.20}$$

$$\psi_t = \eta\nabla^2\psi - \mathbf{u}\cdot\nabla\psi^E. \tag{5.21}$$

The equilibrium flux function must satisfy the zeroth order expansion of (5.20) and (5.21)

$$\psi \to \psi^E + \psi, \qquad \mathbf{u} \to \mathbf{0} + \mathbf{u}, \tag{5.22}$$

which requires a current-free equilibrium

$$\nabla^2\psi^E = 0. \tag{5.23}$$

A simple 2D X-point is described by

$$\psi^E = \frac{1}{2}r^2\sin(2\theta), \tag{5.24}$$

in polar co-ordinates. Note we could also rotate the X-point 90 degrees to

$$\psi^E = \frac{1}{2}r^2\cos(2\theta). \tag{5.25}$$

Since these two solutions are topologically equivalent, we treat them as the same. Furthermore, the shape of our boundary can be chosen to be circular or rectangular. These two boundaries are not topologically distinct and we are looking for solutions that change the topology at the origin. So while cylindrical co-ordinates are easier for analytical work, we switch to rectangular boundaries for numerical simulations. Any important scalings will carry over from cylindrical co-ordinates to Cartesian co-ordinates (Craig and Watson, 1992).

We differentiate equation (5.21) with respect to time and substitute in (5.20) and our equilibrium field (5.24). This yields the equation

$$\psi_{tt} = r^2\nabla^2\psi + \eta\nabla^2\psi_t. \tag{5.26}$$

A quick asymptotic analysis shows that as $r \to 0$

$$\psi_t = \eta\nabla^2\psi. \tag{5.27}$$

In other words, we have resistive (Ohmic) dissipation near the origin. Far from the origin, where $\eta \ll r^2$, we have

$$\psi_{tt} = r^2\nabla^2\psi, \tag{5.28}$$

which describes wave-like behaviour at the boundary. There are three phases to linear reconnection -an initial implosion, the oscillatory eigenmode solution and finally a long-time tail. We outline each of these phases in the next three sections.

5.3 Initial Implosive Phase

We perturb our equilibrium magnetic field by sending a reconnective disturbance from the boundary $r = 1$ towards the origin. For the initial phase, we use the outer boundary approximation (5.28). Introducing the co-ordinate (Craig and Watson, 1992)

$$s = -\ln r, \tag{5.29}$$

yields

$$\psi_{tt} = \psi_{ss}. \tag{5.30}$$

Equation (5.30) has the d'Alembert solution

$$\psi(s,t) = \frac{1}{2}\left[f(s-t) + f(s+t)\right], \tag{5.31}$$

for any arbitrary function $f(s,t)$. To find f we apply the reconnective initial disturbance

$$\psi(0,r) = k(1-r^2), \tag{5.32}$$

where $k \ll 1$ is the magnitude of the initial disturbance. Letting $f = k(1 - 2\ln s)$ in (5.31) produces

$$\psi(r,t) = k\left[1 - r^2\cosh(2t)\right], \tag{5.33}$$

for $t < |\ln r|$. In order to find out how long the solution (5.33) stays significant, we let $\partial_t \sim -1$ in (5.21) and (5.20) then combine to find the length scale

$$l \sim \sqrt{\eta}, \tag{5.34}$$

as in the Sweet-Parker model. Hence the time for a disturbance to travel from the boundary to the diffusion region is

$$T = \int_l^1 \frac{dr}{v}. \tag{5.35}$$

We use the wave speed from equation (5.28) $v = r$. Substituting into (5.35) we find

$$T \sim |\ln(\sqrt{\eta})|. \tag{5.36}$$

Notably, the time for the disturbance to reach the origin blows up as $\eta \to 0$. So, this model predicts that reconnection will not occur in ideal MHD as expected.

5.4 Exact Hypergeometric solution

The wave-like behaviour of the initial phase motivates an eigenmode analysis of (5.26) (Craig and McClymont, 1991).

$$\psi \to \mathrm{e}^{im\theta}\mathrm{e}^{-\lambda t}\psi(r,t). \tag{5.37}$$

We stress here that we have no reason to expect this solution to be complete. In fact, (5.37) turns out to be incomplete in the long-time regime. Nevertheless, substituting into equation (5.26), we find

$$r(r\psi')' = \left[\frac{\lambda^2 r^2}{r^2 - \eta\lambda} + m^2\right]\psi, \tag{5.38}$$

which has a solution in terms of the Bessel function

$$\psi_m = J_m\left(\sqrt{\frac{-\lambda}{\eta}}r\right)\mathrm{e}^{im\theta}. \tag{5.39}$$

Equation (5.39) predicts that there will be no current at the null point unless $m = 0$, which implies that only $m = 0$ modes can cause reconnection. Hassam (1992) found an exact solution to (5.38) by using the change of co-ordinates $z = r^2/(\eta\lambda)$:

$$(z-1)\,(zf')' = \frac{\lambda^2}{4}f + m\frac{z-1}{4z}f, \tag{5.40}$$

where the dash now refers to differentiation with respect to z. Setting $m = 0$ yields

$$(z-1)\,(zf')' = \frac{\lambda^2}{4}f, \tag{5.41}$$

which has the exact solution

$$f(z) = F(b, -b; 1; z), \tag{5.42}$$

where $b = -\lambda/2$. We note that at the boundary $r = 1$, we have

$$z = \frac{1}{\eta\lambda}. \tag{5.43}$$

To approximate $f(z)$ we use a first order series expansion for $1/z \to 0$ (see also Craig, 1994; Ofman et al., 1993):

$$\begin{aligned} F(b, -b; 1; z) =& z^{-b}\left(\frac{(-1)^{-b}\Gamma(-2b)}{\Gamma(1-b)\Gamma(-b)} + \frac{(-1)^{-b}b^2\Gamma(-2b)}{(1+2b)\Gamma(1-b)\Gamma(-b)z} + \dots\right) \\ &+ z^{b}\left(\frac{(-1)^{b}\Gamma(2b)}{\Gamma(b)\Gamma(1+b)} + \frac{(-1)^{b}b^2\Gamma(2b)}{(1-2b)\Gamma(b)\Gamma(1+b)z} + \dots\right). \end{aligned} \tag{5.44}$$

At the boundary $z = 1/\eta\lambda$, the flux is set to zero. Similarly, for small η, the terms proportional to $1/z$ also disappear. This yields

$$z^{-2b} = -\frac{\Gamma(2b)\Gamma^2(-b)}{\Gamma(-2b)\Gamma^2(b)}. \tag{5.45}$$

For sufficiently small b we can make the approximation

$$\Gamma(b) \approx \frac{1}{b}, \tag{5.46}$$

and hence for $z = 1/(\eta\lambda)$ and $b = -\lambda/2$

$$(\eta\lambda)^{\lambda} \approx -1. \tag{5.47}$$

Equation (5.47) has the solution

$$\lambda = \frac{i\pi}{W_0(i\eta\pi)}, \tag{5.48}$$

where $W_0(x)$ is the Lambert-W function. Using the approximation

$$W_0(x) \approx \ln(x), \tag{5.49}$$

the identity

$$\ln(ix) = \ln(x) + \frac{i\pi}{2}, \tag{5.50}$$

and noting that $|\ln\eta| \gg \ln\pi$, we find

$$\lambda \approx 2i\pi \left(\frac{2\ln\eta - i\pi}{4(\ln\eta)^2 + \pi^2} \right). \tag{5.51}$$

Further noting that $|\ln\eta| \gg \pi/4$, we can break λ into its real and imaginary components as

$$\lambda = \alpha - i\omega, \tag{5.52}$$

since we want to write

$$\exp(-\lambda t) = \exp\left[(-\alpha + i\omega)t\right] \tag{5.53}$$

in order to match with the notation used by Craig and McClymont (1991). Hence

$$\omega \approx \frac{\pi}{|\ln\eta|}, \tag{5.54}$$

$$\alpha \approx \frac{\omega^2}{2}. \tag{5.55}$$

5.5 Asymptotic analysis

While Hassam's exact hypergeometric solution works well for the purely resistive case, it is difficult to obtain exact solutions once we generalise our model to add more effects such as viscosity and the Hall effect. Hence, we provide a complimentary method to obtain the scalings (5.54) and (5.55). To do this, we

note that the linear problem lends itself well to a boundary layer analysis since we have clearly defined regions -the inner diffusive area and the outer region near the boundary that contains wave-like behaviour. Hence, we take an inner solution f_I and an outer solution f_O and match the ratio of their derivatives to their solutions f_O and f_I and their derivatives f_I' and f_0' in the intermediate zone (Craig and McClymont, 1993). That is to say

$$\frac{f_I'}{f_I} = \frac{f_O'}{f_O} \tag{5.56}$$

For the inner solution f_I we approximate (Craig and McClymont, 1993; Hassam, 1992)

$$f_I(r) = 1, \tag{5.57}$$

in the right hand side of equation (5.38) (upon letting $m = 0$). Hence

$$(rf_I')' = \frac{\lambda^2 r}{r^2 - \eta\lambda}, \tag{5.58}$$

which has the solution

$$f_I'(r) = \frac{c}{r} + \frac{\lambda^2 \ln(r^2 - \eta\lambda)}{2r}. \tag{5.59}$$

At the origin, the magnetic field vanishes (i.e. $f'(0) = 0$). Near the origin ($r \to 0$) the inner solution $f_I'(r)$ goes to

$$f_I'(r) = \frac{c}{r} + \frac{\lambda^2 \ln(-\eta\lambda)}{2r}. \tag{5.60}$$

In order to attain a non-singular solution, we set the integration constant to

$$c = -\frac{\lambda^2 \ln(-\eta\lambda)}{2}. \tag{5.61}$$

For the outer solution f_O, we let $\eta = 0$ in equation (5.38):

$$r(rf_O')' = \lambda^2 f_O. \tag{5.62}$$

Integration yields

$$f_O(r) = c_1 \cosh\left[\lambda \ln(r)\right] + c_2 \sinh\left[\lambda \ln(r)\right]. \tag{5.63}$$

At the boundary, we set the flux to zero to create a closed boundary to our system (i.e. $f_O(1) = 0$). Hence

$$c_1 = 0. \tag{5.64}$$

Now we match our asymptotic solutions by matching the inner solution in the limit of large r and the outer solution in terms of small r. For large r, the inner magnetic field f_I' goes to

$$f_I'(r) = \frac{\lambda^2}{2r} \ln\left(\frac{r^2}{\eta\lambda}\right). \tag{5.65}$$

Recalling equation (5.56), we have the following functions to match

$$\frac{f_O'}{f_O} = \frac{\lambda}{r} \coth\left(\lambda \ln(r)\right) \tag{5.66}$$

$$\frac{f_I'}{f_I} = \frac{\lambda^2}{2r} \ln\left(\frac{r^2}{\eta\lambda}\right) \tag{5.67}$$

Equating yields

$$\coth\left(\lambda \ln(r)\right) = \frac{\lambda}{2} \ln\left(\frac{r^2}{\eta\lambda}\right). \tag{5.68}$$

which follows to

$$\lambda \ln(r) = \coth^{-1}\left[\lambda \ln(r) - \frac{\lambda \ln(\eta\lambda)}{2}\right]. \tag{5.69}$$

Using the identity (Craig and McClymont, 1993)

$$\coth^{-1} x \approx x + \frac{i\pi}{2}, \tag{5.70}$$

and letting $\lambda \ll 1$ yields

$$\lambda \ln r = \lambda \ln r - \frac{\lambda}{2} \ln \eta\lambda + \frac{i\pi}{2}, \tag{5.71}$$

which reduces to

$$\lambda \ln(\eta\lambda) = i\pi, \tag{5.72}$$

as before.

5.6 Long time solution

Mathematically speaking, the reason for three phases of linear reconnection arises from the non-completeness of the eigenmode solution (5.37). The initial implosive phase is described by equation (5.33) but we have not yet found a solution that is valid at large times. Accordingly, we let the change in time be small, i.e. $\ddot{\psi} = 0$, in equation (5.26). Hence

$$r^2 \nabla^2 \psi = -\eta \partial_t \nabla^2 \psi, \tag{5.73}$$

which produces (Hassam, 1992)

$$J(r,t) = \exp\left(-\frac{r^2}{\eta} t\right), \tag{5.74}$$

where the current

$$J(r,t) = -\nabla^2 \psi, \tag{5.75}$$

has been normalised to be 1 at the origin. Integrating (5.74) yields

$$\psi'(r,t) = \frac{\eta}{2t}\left(\frac{c}{r} - \frac{1}{r}\exp\left(-\frac{r^2}{\eta}t\right)\right). \tag{5.76}$$

Noting that the magnetic field vanishes at the origin ($\psi'(0,t) = 0$), we set the integration constant $c = 1$. Further integration yields

$$\psi(0,t) = \frac{\eta \ln\left(\frac{t}{\eta}\right) - \eta\gamma}{4t} + c, \tag{5.77}$$

where γ is the Euler constant and this c is a new integration constant. For large t we obtain

$$\psi(0,t) = \frac{\eta}{4t} \ln\left(\frac{t}{\eta}\right). \tag{5.78}$$

This equation describes the long time tail. We also note that during the oscillatory phase, the current is described by

$$J = -\frac{\lambda^2}{r^2 - \eta\lambda} f \tag{5.79}$$

which becomes no longer square integrable as r^2 approaches $\eta\lambda$ (McClements et al., 2004). Noting from (5.18) that

$$\mathbf{u}_t = J \nabla \psi^E, \tag{5.80}$$

this implies that the kinetic energy is not square integrable and is thus the bulk of the remaining energy is kinetic rather than magnetic during the long time tail (McClements et al., 2004).

We note here that the long-time solution may seem unimportant since it does not become significant until $t \sim \eta^{-1/2}$ (e.g. Craig et al., 2005). However, in generalised simulations that include terms such as the viscosity (Craig et al., 2005) or a background axial magnetic field (Craig and McClymont, 1993; McClymont and Craig, 1996) the long-time tail can become significant as quickly as one Alfvén time.

Finally, linear reconnection is upset if nonlinear effects are significantly large. By comparing terms in (6.2), we estimate the magnitude of perturbation δ needed for nonlinear terms to invalidate the linear model as $\delta \ll l^2$, which is a very strict condition.

5.7 Generalised Equilibrium Field

In this chapter, so far we have used a simple second order X-point as our equilibrium magnetic field in all of our calculations. This begs the question, what happens if we use a higher order equilibrium field? A zeroth order expansion of equations (5.1)-(5.6) (i.e. $\delta = 0$) requires that the equilibrium field satisfy Laplace's equation:

$$\nabla^2 \psi^E = 0. \tag{5.81}$$

We consider the family of harmonic solutions

$$\psi^E = \frac{r^n}{n} \sin(n\theta), \qquad n \in \mathbb{Z}, \tag{5.82}$$

where setting $n = 2$ returns us to the Craig and McClymont (1991) solution. Hence the solution to the system (5.20)-(5.21) becomes

$$\psi_{tt} = r^{2n-2} \nabla^2 \psi + \eta \nabla^2 \psi_t, \tag{5.83}$$

which implies a wave speed r^{n-1} in the outer region. The time for a disturbance to reach the origin from the boundary (5.36) is modified to (Craig, 1994)

$$\tau = \int_{\sqrt{\eta}}^{1} \frac{\mathrm{d}r}{r^{n-1}}, \tag{5.84}$$

which integrates to

$$\tau = \begin{cases} \frac{1}{2}|\ln \eta|, & n = 2, \\ \frac{\eta^{-1+2/n}}{n-2}, & n > 2. \end{cases} \tag{5.85}$$

Hence the initial signal propagation time will only be "fast" (that is- logarithmic) if $n = 2$. Accordingly, the bounce time and thus the oscillation frequency will only be "fast" if $n = 2$. Thus, for the rest of this thesis we only consider the potentially fast case of $n = 2$.

5.8 Azimuthal Modes

For the eigenmode solution (5.38) to describe reconnection requires $\partial_\theta \psi = m = 0$. This essentially forces any reconnective disturbances to oscillate directly back and forth between the origin and the outer boundary. However, we could also include non-reconnective disturbances bouncing around our X-point at various azimuthal angles in addition to the reconnective perturbations. To compare these azimuthal modes to the non-azimuthal ($m = 0$) modes we follow Craig and McClymont (1993); Craig (1994) and let $\mu = \lambda^2 + m^2$. Then (5.38) becomes

$$r(rf')' = \left(\frac{\mu^2 r^2 - m^2 \eta \lambda}{r^2 - \eta \lambda} \right) f. \tag{5.86}$$

Letting

$$z = \frac{r^2}{\eta \lambda}, \tag{5.87}$$

equation (5.86) is transformed to

$$4z(zf')' = \frac{\mu^2 z - m^2}{z - 1} f, \tag{5.88}$$

which has the solution

$$f(z) = c_1 z^{-m/2} F\left(\frac{-\mu-m}{2}, \frac{\mu-m}{2}; 1-m; z\right) + c_2 z^{m/2} F\left(\frac{-\mu-m}{2}, \frac{\mu-m}{2}; 1-m; z\right). \tag{5.89}$$

Setting the flux to zero at the boundary $f(r=1)=0$ yields

$$F\left(\frac{-\mu-m}{2}, \frac{\mu-m}{2}; 1-m; \frac{1}{\eta\lambda}\right) = 0. \tag{5.90}$$

In the limit $\eta\lambda \to 0$ we approximate (5.90) by

$$\frac{(\mu-m)\Gamma(-\mu)\Gamma^2\left(\frac{\mu-m}{2}\right)}{(\mu+m)\Gamma(\mu)\Gamma^2\left(\frac{-\mu-m}{2}\right)} \approx \left(-\frac{1}{\eta\lambda}\right)^{\mu}. \tag{5.91}$$

From here, Craig (1994); Craig and McClymont (1993) took logs of both sides and matched real and imaginary parts to derive the decay rate

$$\alpha \sim |\ln \eta|^{-3}. \tag{5.92}$$

In other words the non-reconnective disturbances decay even faster than the reconnective disturbances.

5.9 Gas Pressure Effects

We denote the gas pressure gradient force as

$$\mathbf{F_G} = -\beta \nabla \rho \tag{5.93}$$

and aim to find out when the gas pressure has a significant effect of magnetic reconnection. Noting that

$$\dot{\rho} = -\nabla \cdot \mathbf{v}, \tag{5.94}$$

and defining the planar magnetic force as being proportional to the planar acceleration

$$\mathbf{F_P} = \dot{\mathbf{v}}, \tag{5.95}$$

in the linearised system (5.17)-(5.19), we obtain (Craig and McClymont, 1993)

$$\ddot{\mathbf{F}}_\mathbf{G} = \beta \nabla \left(\nabla \cdot \mathbf{F_P}\right). \tag{5.96}$$

Using the approximate scaling from (5.37)

$$\partial_t \sim -\lambda, \tag{5.97}$$

and then natural scaling that emerges from (5.38)

$$r^2 \sim \eta\lambda, \tag{5.98}$$

yields

$$\mathbf{F_G} \sim \frac{\beta}{\eta\lambda^3}\mathbf{F_P}. \tag{5.99}$$

Noting that (5.54) and (5.55) tell us that the oscillation rate is much faster than the decay rate, and due to its logarithmic dependence on η we can approximate

$$|\lambda| \sim |\omega| \sim 1. \tag{5.100}$$

Hence we conclude that back pressures will become significant when $\beta \sim \eta$, which is a severe restriction.

5.10 Numerical Results

In order to verify our analytical predictions we turn to numerical methods. In this section we neglect pressure, that is we let $\beta \to 0$. We consider pressure effects in numerical simulations in the next chapter. Since, as $\beta \to 0$, the density ρ becomes arbitrary, we set $\rho = 1$ for our simulations. We adopt a basic differencing method as described by Craig and McClymont (1991, 1993) over the grid

$$0 \leq x \leq 1, \tag{5.101}$$

$$0 \leq y \leq 1, \tag{5.102}$$

and then mirrored over the x and y axes. The flux is tied to the boundary, that is to say at $x = \pm 1$ and at $y = \pm 1$

$$\psi = 0. \tag{5.103}$$

Similarly, no plasma is allowed to flow in and out of our system so at the boundary

$$\mathbf{u} = \mathbf{0}. \tag{5.104}$$

Using the length scale $l \sim \sqrt{\eta}$, we set the number of points N on the grid to be

$$N = \frac{3.6}{\sqrt{\eta}}. \tag{5.105}$$

Here, the proportionality constant 3.6 gives us the smallest number of grid points that retain sufficient resolution and arises from performing the simulations. The grid spacing $\Delta = \Delta x = \Delta y$ is set to be

$$\Delta = \frac{1}{N} \tag{5.106}$$

Satisfying the Courant-Friedrichs-Lewy condition (Potter, 1973) for numerical stability requires that the lattice speed $\Delta/\Delta t$ be faster than any physical speeds in our system. This requires

$$\Delta t \leq \frac{\Delta}{u + \sqrt{v_s^2 + v_A^2}}. \tag{5.107}$$

Here u is the wave speed $u \sim \sqrt{\eta}$. Also, $v_s = \gamma p/\rho$ is the sound speed and $v_A \sim 1$ in our units. Substituting and rearranging yields the time step

$$\Delta t = 0.025\,\Delta^2 \frac{1}{\eta + 10^{-3}}. \tag{5.108}$$

From here, we difference the induction equation (5.21) and the momentum equation (5.20) by the first-order forward-time central space differencing scheme with the initial perturbation

$$\psi = 0.1(1 - x^2)(1 - y^2), \tag{5.109}$$

$$\mathbf{u} = \mathbf{0}. \tag{5.110}$$

Note, we also introduce a small viscosity

$$\nu = 10^{-4}\eta, \tag{5.111}$$

to damp the system and smooth potential shocks arising from the resistive dissipation being too small (see e.g. Richtmyer and Morton, 1967). By convention, we are only interested in the maximum reconnection rate, which we describe by

$$\psi_t(0,t) = \eta J_z(0,t), \tag{5.112}$$

or in other words the reconnection rate is proportional to the maximum axial current through the origin. As we see in Fig. 5.2, the maximum axial current is inversely proportional to the resistivity. Hence the maximum reconnection rate is independent of resistivity:

$$\psi_t(0,t) \sim \eta^0. \tag{5.113}$$

We display the evolution of the X-point over five Alfvén times in Fig 5.3 and observe reconnection at the origin.

Finally, we show the temporal evolution of the current and magnetic and kinetic energy of the system with the viscosity reduced to zero. Here, the magnetic energy is given as

$$\mathcal{E}_M = \frac{1}{2}\int_0^1 B^2 \,\mathrm{d}A, \tag{5.114}$$

and the kinetic energy as

$$\mathcal{E}_K = \frac{1}{2}\int_0^1 v^2 \,\mathrm{d}A. \tag{5.115}$$

The energy for $\eta = 10^{-1}$ through to $\eta = 10^{-4}$ is plotted in Fig. 5.4 and the current is plotted in Fig. 5.1.

5.11 Summary

Linear methods provide a strong tool for analysing arbitrarily compressible MHD reconnection and predict a fast rate of energy release. Linear reconnection consists of three distinct phases - an initial implosive phase that occurs on a timescale $\sim |\ln \eta|$, an oscillatory reconnective phase $\sim |\ln \eta|^2$, that removes

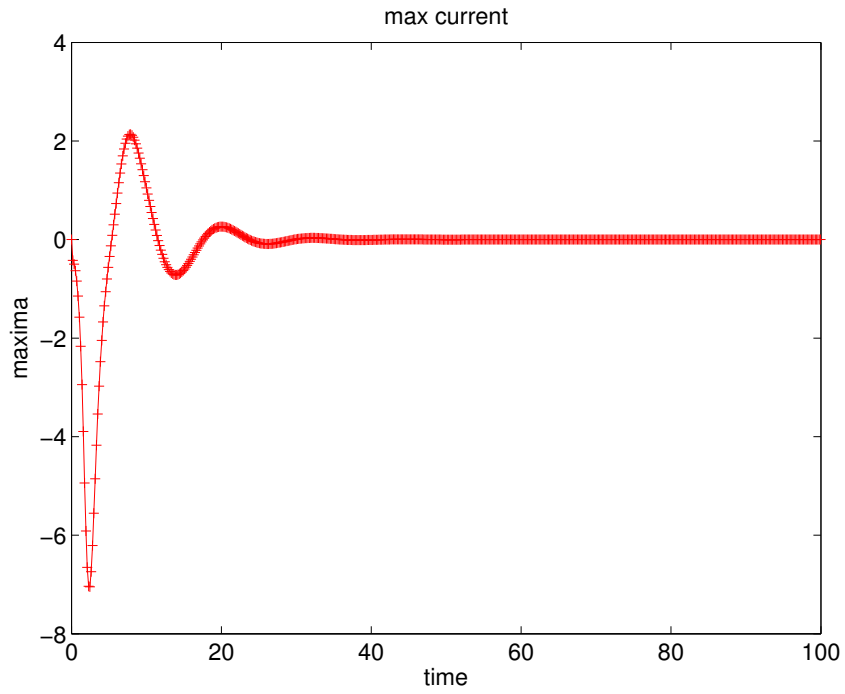

Figure 5.1: Maximum current over time. Parameters are $\eta = 10^{-2}$ and $\nu = 0$. We observe several oscillations before the long-time phase kicks in.

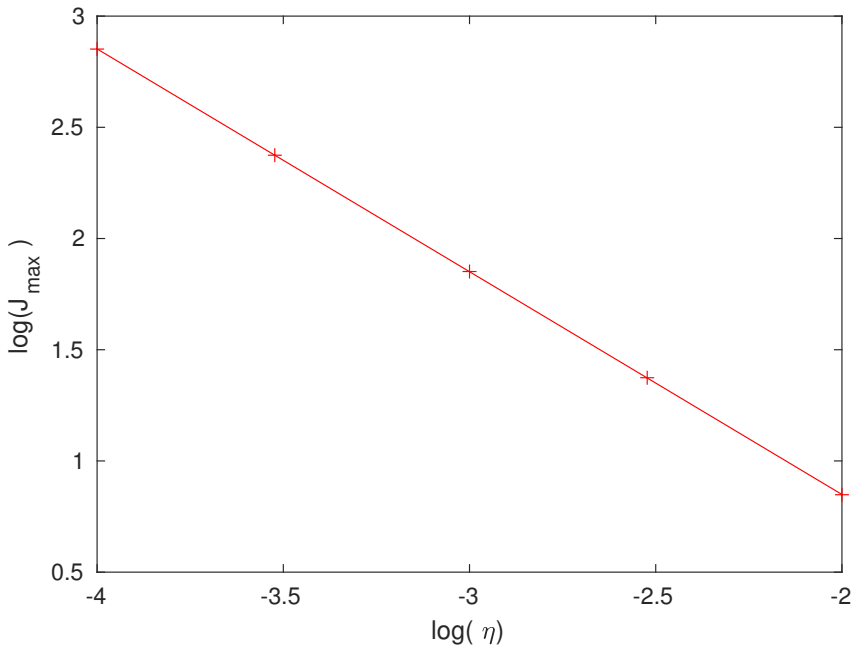

Figure 5.2: Resistivity vs Max Current plotted for varying resistivity (plusses) with $\nu = 10^{-4} \times \eta$. A basic linear fit (solid line) gives the gradient as -1.0016. Hence we expect the maximum reconnection rate $\psi_t(0,0) = \eta J_z(0,0)$ to be independent of η.

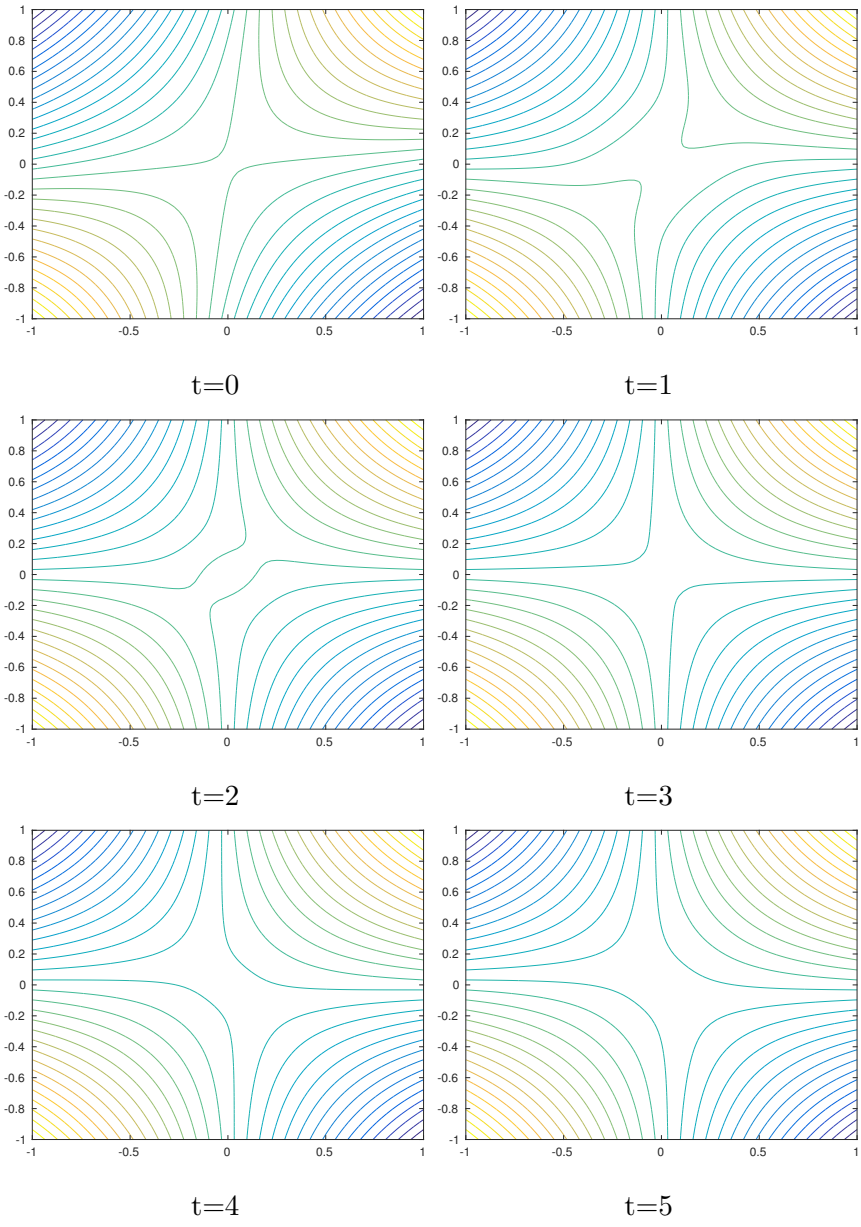

Figure 5.3: Plot of the magnetic field lines over time. Resistivity is set to $\eta = 0.01$ and viscosity to 10^{-4}. We can see the magnetic field lines approach the centre then reconnect.

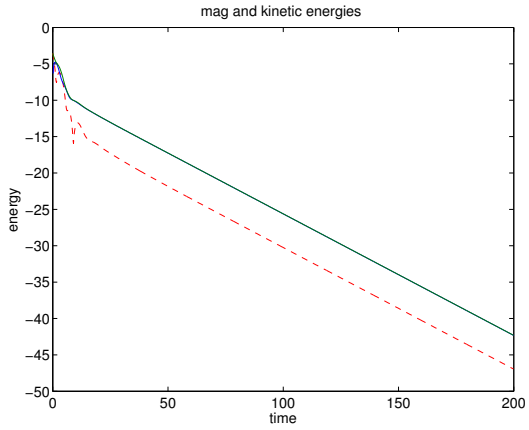

$\eta = 10^{-1}$.

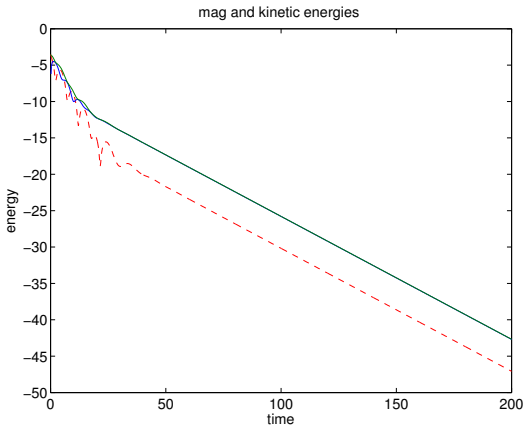

$\eta = 3 \times 10^{-2}$

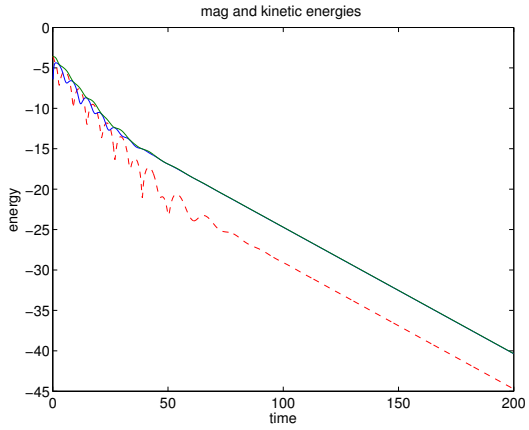

$\eta = 10^{-2}$.

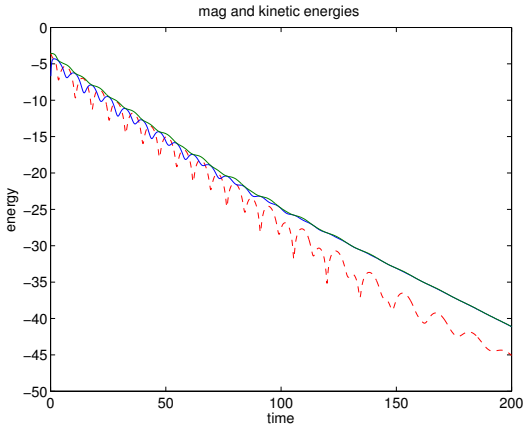

$\eta = 3 \times 10^{-3}$.

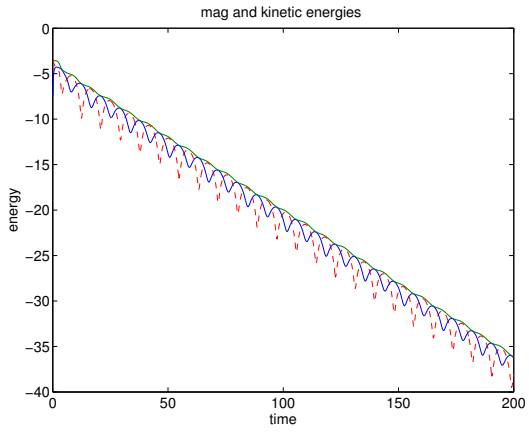

$\eta = 10^{-3}$.

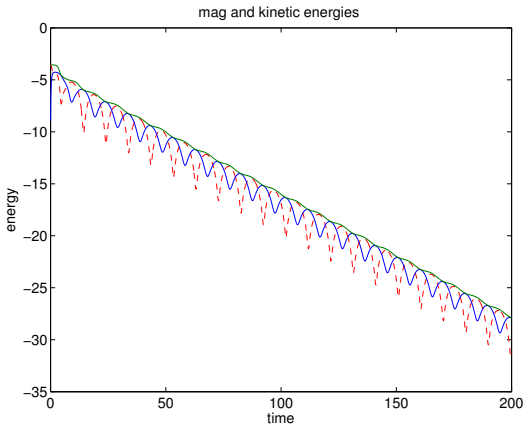

$\eta = 3 \times 10^{-4}$.

Figure 5.4: Energy plotted against time. Magnetic energy is red, kinetic energy is blue and total energy is green. We observe that as resistivity is increased the duration of oscillations decreases and the long-time phase begins earlier.

most of the energy out of the system until we are left with a slow energy decay on a timescale $\sim \eta$.

We find here, following Craig and McClymont (1993) that azimuthal modes do not contribute to reconnection and in fact are faster that non-azimuthal reconnective modes. However, Vekstein and Bian (2005) argue that $m \neq 0$ modes will contribute to reconnection. This warrants further research.

We are severely restricted by the many simplifications we have made. For instance, gas pressure pushes back against reconnective perturbations and has the potential to stall reconnection even for small back pressures (Craig and McClymont, 1993). Yet we assume that the plasma beta is negligible, even though, out of necessity, we include the much smaller resistive term. Therefore, even before we start looking at generalisations of the linear reconnection model in the next chapter, we are already seeing some significant obstacles to attaining fast reconnection.

In the next chapter we turn our attention to generalisations of the purely resistive linear reconnection model, namely viscous, axial and pressure effects, and collisionless effects.

Chapter 6

Generalisations of the Linear Reconnection Model

6.1 Introduction

In the previous chapter, we gave a complete description of 2D purely resistive linear reconnection, which describes fast reconnection. This chapter focuses upon the conditions in which linear reconnection can remain fast. Hence, we turn our attention to generalisations of the linear reconnection model. Namely, viscous, axial and pressure effects; and Hall and electron inertial effects.

We classify non-ideal effects into three categories: dissipative effects, namely resistivity and viscosity (Craig et al., 2005; Tavabi and Koutchmy, 2014); pressure and axial effects (Craig and Litvinenko, 2005; Craig and McClymont, 1993); and collisionless effects, for example the Hall (Senanayake and Craig, 2006b; Craig and Litvinenko, 2008) or electron inertia terms (McClements et al., 2004; Senanayake, 2007; McClements and Thyagaraja, 2004). Viscous effects, though they stall the reconnective process, provide an additional avenue for dissipative energy release. In other words, there is a possibility for the fast energy release rate during a solar flare to occur despite a formally slow reconnection rate as a consequence of a viscous mechanism (Craig et al., 2005; Armstrong et al., 2011).

Additionally, we extend the theory of linear reconnection to 2.5D by testing two different sites for reconnection. In two dimensions, magnetic reconnection can only occur at a magnetic null point. However, in three dimensions, a possible new site for magnetic reconnection emerges called a quasi-separatrix layer (QSL) (Priest and Démoulin, 1995). Craig and Effenberger (Craig and Effenberger, 2014; Effenberger and Craig, 2016) argued that a null point is required for fast reconnection and that QSL reconnection will be slow. Using a linear model, we investigate whether fast oscillatory reconnection is attainable in 2.5D at two different sites- one being a 2.5D null line and the other with a constant background axial field that mimics a QSL. Note, in a fully 3D system, our sites would correspond to a 3D null line and a QSL with an infinite squashing factor $Q_\perp \to \infty$ (Craig and Pontin, 2014) respectively. However, since these sites are as close to representing QSLs and 3D null points as possible in 2.5D, we will refer to our sites as 'QSL-type' and '3D null-type' here. We find evidence that fast reconnection is only possible at 3D null-type site.

6.2 Governing Equations and Length Scales

For the sake of convenience, we start by restating the dimensionless, compressible MHD equations (2.7)-(2.12):

$$\mathbf{E} + \mathbf{v} \times \mathbf{B} = \eta \mathbf{J} + d_i(\mathbf{J} \times \mathbf{B} - \nabla p_e) + d_e^2[\partial_t \mathbf{J} + (\mathbf{v} \cdot \nabla)\mathbf{J} + (\mathbf{J} \cdot \nabla)\mathbf{v}], \tag{6.1}$$

$$\rho\left[\partial_t \mathbf{v} + (\mathbf{v} \cdot \nabla)\mathbf{v}\right] = -\nabla p + \mathbf{J} \times \mathbf{B} + \nu \nabla^2 \mathbf{v}, \tag{6.2}$$

$$\frac{\partial \rho}{\partial t} + \nabla \cdot (\rho \mathbf{v}) = 0, \tag{6.3}$$

$$\nabla \cdot \mathbf{B} = 0, \tag{6.4}$$

$$\mathbf{J} = \nabla \times \mathbf{B}, \tag{6.5}$$

$$\nabla \times \mathbf{E} = -\partial_t \mathbf{B}. \tag{6.6}$$

We use a scalar viscosity, though the full Braginskii viscosity case has been previously considered by Craig (2008) (see also Craig and Litvinenko, 2007;

Minoshima et al., 2016; MacTaggart et al., 2017).

In 2.5D we consider three dimensions but let $\partial_z = 0$ and represent the velocity $\mathbf{v}$ by its planar component $\mathbf{u}$ and its axial component W:

$$\mathbf{v} = (\mathbf{u}, W). \tag{6.7}$$

To represent the magnetic field, we use the flux function $\psi(x, y)$ with an axial component Z to satisfy equation (6.4) in 2.5D:

$$\mathbf{B} = \nabla \times (\psi \hat{\mathbf{z}}) + Z\hat{\mathbf{z}}. \tag{6.8}$$

We again adopt the polytropic gas pressure (5.14) and linearise about $\rho = 1$ to obtain

$$\nabla p \approx \beta \nabla \rho, \tag{6.9}$$

where $\beta = \gamma\bar{\beta}$ is again a rescaled plasma beta based on B_0. Our system linearises to

$$-\rho_t = \nabla \cdot \mathbf{u}, \tag{6.10}$$

$$\begin{aligned}\mathbf{u}_t + \nabla(Z^E Z) =& -\beta\nabla\rho - \nabla^2\psi\nabla\psi^E - \nabla^2\psi^E\nabla\psi \\ &+ \nu(\nabla^2\mathbf{u} + \tfrac{1}{3}\nabla(\nabla\cdot\mathbf{u})),\end{aligned} \tag{6.11}$$

$$\psi_t + \mathbf{u}\cdot\nabla\psi^E = \eta\nabla^2\psi + d_e^2\nabla^2\psi_t + d_i[\psi^E, Z] + d_i[\psi, Z^E], \tag{6.12}$$

$$\begin{aligned}Z_t + \nabla\cdot(Z^E\mathbf{u}) =& \eta\nabla^2 Z + [W, \psi^E] + d_e^2\nabla^2 Z_t \\ &+ d_i[\nabla^2\psi, \psi^E] + d_i[\nabla^2\psi^E, \psi],\end{aligned} \tag{6.13}$$

$$W_t = [Z^E, \psi] + [Z, \psi^E] + \nu\nabla^2 W, \tag{6.14}$$

where a superscript E denotes an equilibrium quantity, t subscripts denote time derivatives, and Poisson bracket notation is typified by

$$[\psi, Z] = (\partial_x\psi)\,\partial_y Z - (\partial_y\psi)\,\partial_x Z. \tag{6.15}$$

While the linearised MHD system appears complicated, it contains a fast reconnection solution in the purely resistive regime. So the linearised system allows us to investigate the way viscous, pressure, axial or collisionless effects perturb fast reconnection in an analytically convenient manner.

6.2.1 Equilibrium Fields

We obtain an equilibrium solution by letting $\rho \to 1$, $p \to \beta$, $\mathbf{v} \to \mathbf{0}$ and $\mathbf{B} \to \mathbf{B}^E$ in equation (6.2). Hence, we require a force free equilibrium

$$\mathbf{J}^E \times \mathbf{B}^E = \mathbf{0}. \tag{6.16}$$

Employing (6.16) yields

$$\nabla^2\psi^E \nabla\psi^E = - Z^E \nabla Z^E, \tag{6.17}$$

$$[Z^E, \psi^E] = 0. \tag{6.18}$$

In order to satisfy equation (6.18) we take

$$Z^E = Z^E(\psi^E), \tag{6.19}$$

and substitute back into equation (6.17). Now, Z^E satisfies the Grad-Shafranov equation

$$\nabla^2\psi^E = -Z^E \left(\frac{\mathrm{d}Z^E}{\mathrm{d}\psi^E}\right). \tag{6.20}$$

If $Z^E = 0$, the right hand side vanishes and thus the equilibrium flux function satisfies Laplace's equation (Craig, 1994)

$$\nabla^2\psi^E = 0, \tag{6.21}$$

which has the solution

$$\psi^E = \psi^E(z), \tag{6.22}$$

where $z = x + iy$. We expand ψ^E as a function of powers z^n, for which Craig (1994) showed only terms of the order $n = 2$ can accommodate fast dissipation. Therefore, we set

$$\psi^E = \mathrm{Im}\left[\frac{1}{2}(x+iy)^2\right] = xy. \tag{6.23}$$

A simple extension of (6.23) into 2.5D, which preserves (6.21), is

$$\psi^E = xy, \qquad\qquad Z^E = z_0 = \text{const.}, \tag{6.24}$$

which mimics a QSL. We note that a true QSL is bounded on the z axis, what we describe here is a 2.5D analogue of a QSL, with squashing factor $Q_\perp \to \infty$. Here, the squashing factor between the planes $z = \pm z_m$ is defined (Titov, 2007) as

$$Q_\perp = 2\cosh\left(\frac{4z_m}{B_z}\right). \tag{6.25}$$

Hence, we refer to (6.24) as a 'QSL-type' magnetic field.

More generally, we solve (6.20) by assuming

$$\nabla^2\psi^E = f\left(\psi^E\right). \tag{6.26}$$

A mathematically convenient solution to (6.26) is to set $f \sim \psi^E$, which yields

$$\psi^E = \frac{1}{\mu^2}\sin(\mu x)\sin(\mu y), \qquad Z^E = \sqrt{2}\mu\psi^E, \tag{6.27}$$

which describes a 3D null line. However, since (6.27) is a 2.5D analogue of a 3D null point, we refer to (6.27) as a '3D null-type' magnetic field.

The parameter μ describes the magnitude of the axial field and letting $\mu \to 0$ recovers the planar X-point equilibrium (6.23). We note that other functions f also generate solutions, for example $f \sim \exp\left(\psi^E\right)$. However, we restrict ourselves to the case (6.27) for the sake of simplicity. The equilibrium fields in (6.24) and (6.27) are particular cases of

$$\psi^E = \frac{1}{\mu^2}\sin(\mu x)\sin(\mu y),\ Z^E = \sqrt{2\mu^2(\psi^E)^2 + z_0^2}, \tag{6.28}$$

where we have chosen the axial field to be positive.

6.2.2 Length Scales

In this subsection, we determine estimates for a length scale that incorporates viscous, pressure and axial effects; and a length scale that includes the Hall effect and electron inertia. Considering equations (6.10)-(6.14) with $d_i = d_e =$

0 and $Z^E = z_0$ yields the system

$$-\rho_t = \nabla \cdot \mathbf{u} \tag{6.29}$$

$$\mathbf{u}_t = -z_0 \nabla Z - \beta \nabla \rho - \nabla^2 \psi \nabla \psi^E + \nu(\nabla^2 \mathbf{u} + \tfrac{1}{3} \nabla (\nabla \cdot \mathbf{u})), \tag{6.30}$$

$$\psi_t = -\mathbf{u} \cdot \nabla \psi^E + \eta \nabla^2 \psi \tag{6.31}$$

$$Z_t = -z_0 \nabla \cdot \mathbf{u} + \eta \nabla^2 Z + \left(\mathbf{B}^E \cdot \nabla\right) W \tag{6.32}$$

$$W_t = \left(\mathbf{B}^E \cdot \nabla\right) Z + \nu \nabla^2 W. \tag{6.33}$$

We use these equations to infer a characteristic length scale of magnetic reconnection. Dimensionally, we take

$$\nabla \to 1/r, \quad \partial_t \to -\lambda, \quad \psi^E \to r^2, \quad |\mathbf{u}| \to u, \tag{6.34}$$

to obtain

$$\lambda \rho \sim \frac{u}{r}, \tag{6.35}$$

$$-\lambda u \sim -\frac{z_0 Z}{r} - \frac{\beta \rho}{r} - \frac{\psi}{r} + \frac{\nu u}{r^2}, \tag{6.36}$$

$$-\lambda \psi \sim -ur + \frac{\eta \psi}{r^2}, \tag{6.37}$$

$$-\lambda Z \sim -\frac{z_0 u}{r} + \frac{\eta Z}{r^2} + W, \tag{6.38}$$

$$-\lambda W \sim Z + \frac{\nu W}{r^2}. \tag{6.39}$$

We want to understand how viscous and axial effects modify the length scale. While it is possible to solve equations (6.35)-(6.39) for r, the solution is too complicated to allow any simple understanding to be extracted. Instead, we insist that the axial field Z affects the velocity $\mathbf{u}$ solely as a back pressure (Craig and McClymont, 1993). That is to say, we expect the pressure, dissipation and shearing terms on the right hand side of (6.32) to have comparable magnitudes:

$$-z_0 \nabla \cdot \mathbf{u} \sim \eta \nabla^2 Z \sim \left(\mathbf{B}^E \cdot \nabla\right) W, \tag{6.40}$$

since

$$\eta \lambda \nabla^2 Z \sim Z \sim \lambda W, \tag{6.41}$$

by (6.33) and

$$\frac{|W|}{|\mathbf{u}|} \sim \frac{z_0}{|\mathbf{B}^E|}. \tag{6.42}$$

Hence, we reduce equation (6.32) to its dynamic and back pressure terms and let

$$\nabla Z \sim -\frac{z_0}{\lambda}\nabla\left(\nabla \cdot \mathbf{u}\right) \tag{6.43}$$

in (6.30). Now applying (6.34) to (6.30), taking into account (6.43), and rearranging yields

$$\lambda^2 r^2 u \sim \left(z_0^2 + \beta - \nu\lambda\right) u + \lambda r \psi. \tag{6.44}$$

The length scale of the diffusion region is the distance from the origin to the point where the diffusion speed matches the advection speed. The advective and diffusive terms in (6.31) will balance when

$$ru \sim \frac{\eta\psi}{r^2}, \tag{6.45}$$

at the point $r = r_s$. Substituting (6.45) into (6.44) and rearranging yields

$$r_s^4 \sim r_s^2\eta\lambda - \frac{\eta}{\lambda}\left(\beta + z_0^2 - \nu\lambda\right). \tag{6.46}$$

Solving for r_s^2, we obtain

$$r_s^2 \sim \frac{\eta\lambda \pm \eta\lambda\left(1 + \frac{\nu\lambda-\beta-z_0^2}{\eta\lambda^3}\right)^{1/2}}{2}, \tag{6.47}$$

which, since $\eta\lambda \lesssim \eta\lambda\left(1 + \frac{\nu\lambda-\beta-z_0^2}{\eta\lambda^3}\right)^{1/2}$, implies the length scale

$$r_s^2 \sim \eta\lambda\left(1 + \frac{\nu\lambda - \beta - z_0^2}{\eta\lambda^3}\right)^{1/2}. \tag{6.48}$$

Note that if we set $\nu = \beta = z_0 = 0$, we recover the Sweet-Parker length scale $r_s = \eta^{1/2}$. Furthermore, we recover the visco-resistive length scale $r_s = (\eta\nu)^{1/4}$ if we set $\beta = z_0 = 0$ and $\nu \gg \eta$ (Park et al., 1984). In order to find the collisionless length scale we consider equations (6.11)-(6.14) with $\nu = Z^E =$

$\beta = 0$:

$$\mathbf{u}_t = -\nabla^2\psi\nabla\psi^E \tag{6.49}$$

$$\psi_t = -\mathbf{u}\cdot\nabla\psi^E + \eta\nabla^2\psi + d_e^2\nabla^2\psi_t + d_i[\psi^E, Z], \tag{6.50}$$

$$Z_t = \eta\nabla^2 Z + [W, \psi^E] + d_e^2\nabla^2 Z_t + d_i[\nabla^2\psi, \psi^E], \tag{6.51}$$

$$W_t = [Z, \psi^E]. \tag{6.52}$$

Comparing terms in (6.51)

$$\eta\nabla^2 Z \sim d_i[\nabla^2\psi, \psi^E]. \tag{6.53}$$

Taking $\partial_r \sim 1/r$, $\psi^E \sim r$, $\partial_t \sim -\lambda$ and $r^2 \sim \eta\lambda$, we estimate that

$$Z \sim d_i\lambda\nabla^2\psi. \tag{6.54}$$

Substituting (6.49) and (6.54) into (6.50), we obtain the collisionless length scale

$$r_s^2 \approx \eta\lambda\left(1 - \frac{(d_i^2 + d_e^2)\,\lambda}{\eta}\right). \tag{6.55}$$

Setting $d_i = d_e = 0$ recovers the Sweet-Parker scale $r_s = \sqrt{\eta}$ as expected. Equations (6.48) and (6.55) show that viscous and resistive effects increase the area of the diffusion region, while pressure, axial and collisionless effects decrease the size of the diffusion region. We note that our length scale only applies under the condition that the magnitude of axial dissipation or shearing are less than or comparable to the magnitude of axial back pressure in (6.32).

6.3 Oscillatory Reconnection

6.3.1 Introduction

The Craig and McClymont (1991) model describes an equilibrium magnetic field $\psi^E = xy$ disturbed by a reconnective perturbation field. The equilibrium field takes the form of a magnetic X-point with separatrices initially at right angles. We then enclose the X-point with a circular conducting boundary through which no magnetic flux is lost. From this boundary, we send a

reconnective disturbance towards the origin. The disturbance gets advected into the diffusion region, then diffuses through the origin and gets advected out towards the opposite boundary.

Far from the origin, where $\eta, \nu, z_0, \beta \rightarrow 0$, equations (6.30) and (6.31) reduce to the wave equation

$$\psi_{tt} = r^2 \nabla^2 \psi, \tag{6.56}$$

with wave speed r (Craig and McClymont, 1991). Consequently, the wave slows down and builds up as it approaches the origin. Furthermore, the wave would take an infinite time $t \sim 1/r$ to reach the null in the absence of resistive or other diffusive effects. More generally, in a non-radial context, the wave focuses towards the null point due to a refraction effect (McLaughlin and Hood, 2004; McLaughlin et al., 2011).

In this section, we neglect collisionless effects and set $d_i = d_e = 0$. Furthermore, we consider a QSL-type axial equilibrium field that is much smaller than the magnitude of the planar magnetic field $Z^E = z_0 \ll 1$.

There are three stages of energy release as seen in Figs. 6.1-6.3. First, there is an initial implosive phase that begins when we send a disturbance from the boundary of our system towards the origin (Craig and Watson, 1992). We call the duration of the initial phase the bounce time:

$$t_b = \int_l^1 \frac{\mathrm{d}r}{v} = |\ln r_s|, \tag{6.57}$$

where r_s is the length scale of the diffusion region given by equation (6.48). Once the disturbance reaches the diffusion region, a second oscillatory stage of energy release commences. As shown in previous studies oscillations are only possible if viscous, pressure or collisionless effects are sufficiently small (e.g. Craig et al., 2005; McClements et al., 2004; McClymont and Craig, 1996). We consider larger pressure, axial and viscous effects in the next section. We also note that there is a final slow stage of energy release after which the bulk of the energy has been lost (e.g. Hassam, 1992). However, we do not consider the effect of viscous, collisionless or axial effects on the long-time phase.

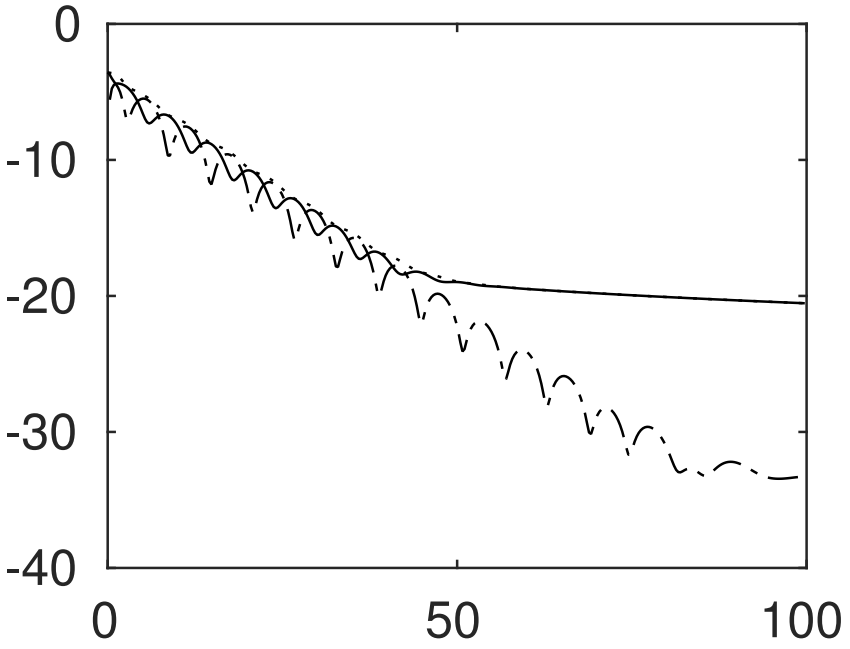

Figure 6.1: Magnetic energy (dot-dashed), kinetic energy (solid) and total energy (dotted) plotted against time where $\eta = 10^{-2}$, $\nu = 0.01\eta$ and $\beta = z_0 = 0$.

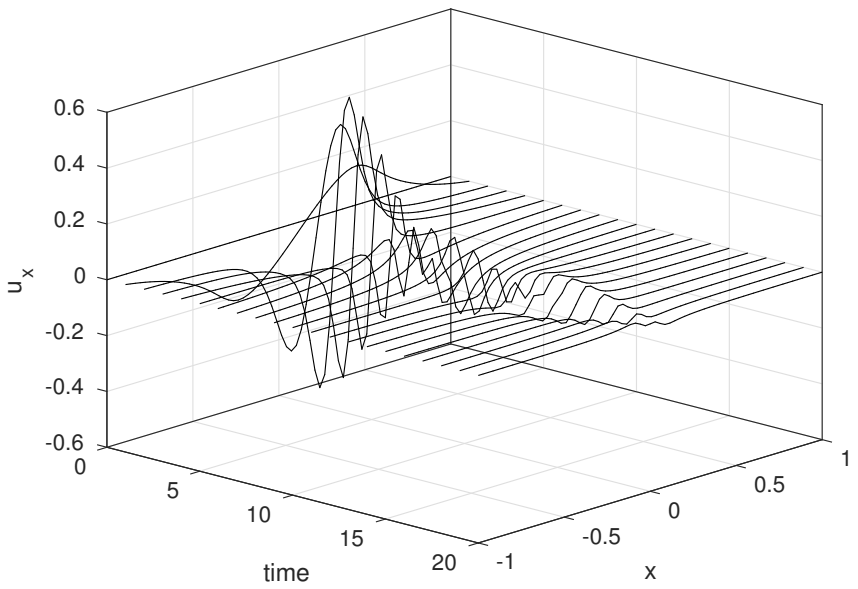

Figure 6.2: Velocity field $\mathbf{u}_x$ plotted against x over time where $\eta = 10^{-2}$, $\nu = 0.01\eta$ and $\beta = z_0 = 0$.

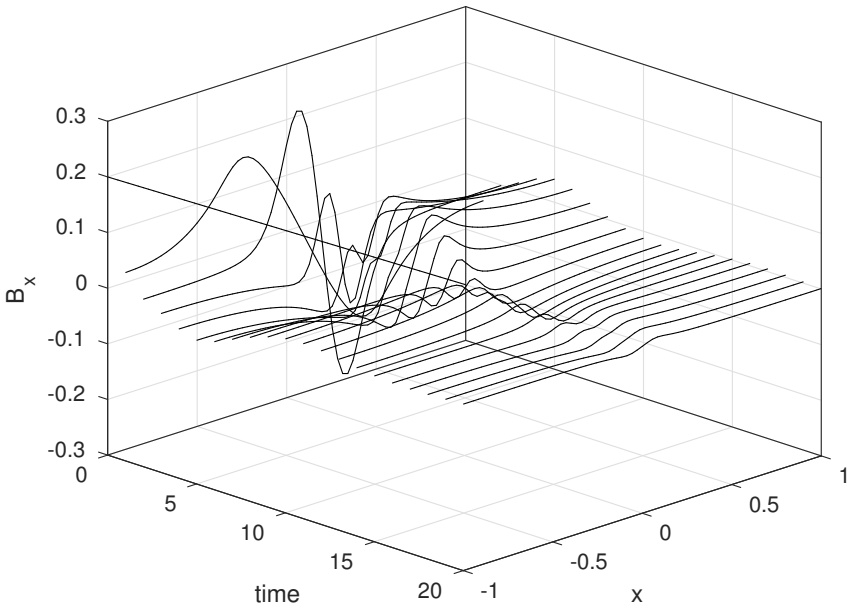

Figure 6.3: Magnetic field $\mathbf{B}_x$ plotted against x over time where $\eta = 10^{-2}$, $\nu = 0.01\eta$ and $\beta = z_0 = 0$.

The decay and oscillation rates are important quantifiers of oscillatory reconnection, particularly in comparing our model to observations (Thurgood et al., 2019). Craig and McClymont (1991) quantified the oscillatory phase by considering an eigenmode solution to (6.10)-(6.14). In other words they let

$$\psi(r, \theta, t) = \mathrm{e}^{-\lambda t + im\theta} f(r), \tag{6.58}$$

where the eigenvalue $\lambda = \alpha - i\omega$ consists of the decay rate α and the oscillation frequency ω. Our purpose here is to extend the Craig and McClymont (1991) scalings

$$\alpha_0 = \frac{\omega_0^2}{2}, \qquad \omega_0 = \frac{\pi}{|\ln \eta|}, \tag{6.59}$$

to incorporate pressure, viscous and axial effects. We detail a generalisation of Craig and McClymont (1991) and Hassam's (1992) asymptotic method for calculating λ and Hassam's (1992) Hypergeometric method in the next two sections. However, for estimating λ a simpler energetic scaling argument gives us insight into the modifications of viscous, pressure or axial terms on energy release.

We derive a generalisation by perturbing the Craig and McClymont (1991) solution. Hence, the condition required for topological change at the origin $m = 0$, inferred by equation (5.39), remains approximately true.

6.3.2 Asymptotic Solution

We construct an asymptotic solution to equations (6.10)-(6.14) by considering an inner solution and an outer solution (e.g. Hassam, 1992; Craig and McClymont, 1993). In the purely resistive case, after employing (6.58) with $m = 0$, equations (6.11) and (6.12) combine to

$$\lambda^2 f = \left(r^2 - \eta\lambda\right) \nabla^2 f, \tag{6.60}$$

which we generalise to

$$\lambda^2 f = \left(r^2 - r_s^2\right) \nabla^2 f, \tag{6.61}$$

where r_s is given by equations (6.48) or (6.55). The inner solution f_I is approximately unity near the origin, so we solve

$$\frac{1}{r}\left(r f_I'\right)' = \frac{\lambda^2}{r^2 - r_s^2}. \tag{6.62}$$

Integrating and requiring that f_I' remains finite as $r \to 0$ to solve for the integration constant yields

$$f_I' = \frac{\lambda^2}{2r} \ln\left(1 - \frac{r^2}{r_s^2}\right). \tag{6.63}$$

On the other hand, we solve the outer solution f_O of (6.61) by letting $r^2/r_s^2 \gg 1$. Accordingly,

$$r^2 \nabla^2 f_O = \lambda^2 f_O, \tag{6.64}$$

which has the solution

$$f_O = k \sinh\left(\lambda \ln r\right), \tag{6.65}$$

for the boundary condition $f_O(1) = 0$, and some arbitrary constant k. We match the asymptotic solutions by applying the matching condition (Craig

and McClymont, 1993)

$$\left.\frac{f_I'}{f_I}\right|_{r\to\infty} = \left.\frac{f_O'}{f_O}\right|_{r\to 0}. \tag{6.66}$$

Hence

$$\frac{\lambda^2}{2r}\ln\left(\frac{r^2}{r_s^2}\right) = \frac{\lambda}{r}\coth\left(\lambda\ln r\right). \tag{6.67}$$

For small λ, we use the identity $\coth^{-1}(x) \approx x + i\pi/2$. Thus, we reach the equation

$$\lambda\ln\left(r_s^2\right) = i\pi, \tag{6.68}$$

which Craig and McClymont (1991) separated into real and imaginary parts, for $r_s^2 = \eta\lambda$, to obtain the scalings (6.59). More generally, considering viscous, axial and pressure effects, we substitute equation (6.48) into (6.68):

$$\lambda\ln\left[\eta\lambda\left(1+\frac{\nu}{\eta\lambda^2}-\frac{z_0^2+\beta}{\eta\lambda^3}\right)^{1/2}\right] = i\pi, \tag{6.69}$$

In the collisionless case, we substitute (6.55) into (6.68):

$$\lambda\ln\left[\eta\lambda - \left(d_i^2+d_e^2\right)\lambda^2\right] = i\pi. \tag{6.70}$$

The more general equations (6.69) and (6.70) are too complex to solve analytically. Hence, we end up turning to a scaling argument. Alternatively, equations (6.69) and (6.70) can be derived using Hypergeometric functions (e.g. Hassam, 1992), which we demonstrate for completeness in the next subsection

6.3.3 Hypergeometric Solution

We search for an exact solution to (6.61) in terms of the Hypergeometric function by employing the change of co-ordinates $z = r^2/r_s^2$:

$$(z-1)\left(zf'\right)' = \frac{\lambda^2}{4}f + m\frac{z-1}{4z}f, \tag{6.71}$$

where the dash now refers to differentiation with respect to z. Setting $m = 0$ yields

$$(z-1)\left(zf'\right)' = \frac{\lambda^2}{4}f, \tag{6.72}$$

which has the exact solution

$$f(z) = F(b, -b; 1; z), \tag{6.73}$$

where $b = -\lambda/2$. We note that at the boundary $r = 1$, we have

$$z = \frac{1}{r_s^2}. \tag{6.74}$$

To approximate $f(z)$ we use a first order series expansion for $1/z \to 0$ (see also Craig, 1994; Ofman et al., 1993):

$$\begin{aligned} F(b, -b; 1; z) =& z^{-b}\left(\frac{(-1)^{-b}\Gamma(-2b)}{\Gamma(1-b)\Gamma(-b)} + \frac{(-1)^{-b}b^2\Gamma(-2b)}{(1+2b)\Gamma(1-b)\Gamma(-b)z} + \dots\right) \\ &+ z^{b}\left(\frac{(-1)^{b}\Gamma(2b)}{\Gamma(b)\Gamma(1+b)} + \frac{(-1)^{b}b^2\Gamma(2b)}{(1-2b)\Gamma(b)\Gamma(1+b)z} + \dots\right). \end{aligned} \tag{6.75}$$

At the boundary $z = 1/r_s^2$, the flux is set to zero. Similarly, for small η, the terms proportional to $1/z$ also disappear. This yields

$$z^{-2b} = -\frac{\Gamma(2b)\Gamma^2(-b)}{\Gamma(-2b)\Gamma^2(b)}. \tag{6.76}$$

For sufficiently small b we can make the approximation

$$\Gamma(b) \approx \frac{1}{b}, \tag{6.77}$$

and hence for $z = 1/r_s^2$ and $b = -\lambda/2$

$$(r_s)^{2\lambda} \approx -1, \tag{6.78}$$

which matches equation (6.68).

6.3.4 Scaling Argument

In order to calculate the oscillation frequency, we estimate that the time for a disturbance to travel to and from the diffusion region $t_b \sim |\ln r_s|$ is much greater than the diffusion time $t_d \sim 1$. Furthermore, a full oscillation must last for four bounce times, so the period is $T = 4t_b$ (Thurgood et al., 2019) and the oscillation frequency is

$$\omega \sim \frac{2\pi}{T} \sim \frac{\pi}{|\ln(r_s^2)|}. \tag{6.79}$$

Expanding the logarithm yields

$$\omega \sim \frac{\pi}{\left|\ln\eta + \frac{1}{2}\ln\left(1+\frac{\nu-\beta-z_0^2}{\eta}\right)\right|}. \tag{6.80}$$

For sufficiently small axial and viscous terms

$$\frac{\nu-\beta-z_0^2}{\eta} \ll 1, \tag{6.81}$$

we take

$$\ln\left(1+\frac{\nu-\beta-z_0^2}{\eta}\right) \approx \frac{\nu-\beta-z_0^2}{\eta}, \tag{6.82}$$

and hence

$$\omega \sim \frac{\pi}{|\ln\eta|}\left(1-\frac{\nu-\beta-z_0^2}{2\eta|\ln\eta|}\right)^{-1}. \tag{6.83}$$

Finally, we assume $\eta|\ln\eta| \sim \eta$ since $|\ln\eta|$ is near unity when compared to the very small η, to obtain

$$\omega \sim \frac{\pi}{|\ln(\eta)|}\left(1+\frac{\nu-\beta-z_0^2}{\eta}\right). \tag{6.84}$$

The oscillation frequency (6.84) reduces to the purely resistive frequency (6.59) upon setting $\nu = \beta = z_0 = 0$. In order to estimate the energy decay rate, we calculate the perturbation energy of the system

$$\mathcal{E} = \mathcal{E}_{\text{total}} - \mathcal{E}_{\text{equilibrium}}, \tag{6.85}$$

by adding the kinetic and magnetic energies per unit length in the z direction. We describe the total density by adding the equilibrium density $\rho^E = 1$ and the perturbation density ρ. Since the equilibrium kinetic energy is zero, the perturbation kinetic energy is the same as the total kinetic energy:

$$\mathcal{E}_K = \frac{1}{2}\iint_A (1+\rho)\,u^2\,r\mathrm{d}r\,\mathrm{d}\theta, \tag{6.86}$$

where $u^2 = \mathbf{u}\cdot\mathbf{u}$. The perturbation magnetic energy is

$$\mathcal{E}_M = \frac{1}{2}\iint_A \left(B^2 + 2\mathbf{B}\cdot\mathbf{B}^E\right) r\mathrm{d}r\,\mathrm{d}\theta, \tag{6.87}$$

where the equilibrium magnetic field in polar co-ordinates is given by

$$\mathbf{B}^E = (r\cos(2\theta), -r\sin(2\theta), z_0)\,. \tag{6.88}$$

Integrating over θ, the planar components of $\mathbf{B}^E$ will vanish. Similarly, the terms $z_0 Z$ and ρu^2 will be sinusoidal, and thus vanish, since we expect, based on equation (6.30), that Z and ρ will take a similar form to ψ^E. Therefore, we obtain the perturbation energy

$$\mathcal{E} = \frac{1}{2}\int_0^{2\pi}\int_0^1 \left[\left(\frac{\partial\psi}{\partial r}\right)^2 + u^2 + Z^2 + W^2\right] r\,\mathrm{d}r\,\mathrm{d}\theta. \tag{6.89}$$

We assume that $u^2 \sim B^2$, in other words that the magnitudes of kinetic energy and magnetic energy at the onset of the oscillatory phase are roughly equal, as observed in Fig. 6.1 (see also e.g. Craig et al., 2005; McClements et al., 2004). Hence, we estimate the total energy in the plane to be

$$\mathcal{E} \sim 2\pi q|\psi|^2, \tag{6.90}$$

where the factor

$$q = 1 + \frac{|Z|^2}{|\mathbf{B}_p|^2}, \tag{6.91}$$

reduces to unity in the 2D case. In order to explore how the kinetic energy changes over time, we again assume (6.43)- that the axial field Z primarily affects the velocity $\mathbf{u}$ as a back pressure. We now differentiate the total energy (6.89) with respect to time and substitute equations (6.30)-(6.33) with (6.43). Furthermore, integrating by parts, we obtain

$$\begin{aligned}\frac{\mathrm{d}\mathcal{E}}{\mathrm{d}t} = -\int_0^{2\pi}\int_0^1 \Bigg[&\nu\left(\partial_r W\right)^2 + \left(\eta - \frac{\beta + z_0^2}{\lambda}\right)\left(\partial_r Z\right)^2 \\ &+\eta J^2 + \left(\frac{4\nu}{3} - \frac{\beta + z_0^2}{\lambda}\right)\left|\nabla\cdot\mathbf{u}\right|^2 + \nu\left|\nabla\times\mathbf{u}\right|^2\Bigg] r\mathrm{d}r\mathrm{d}\theta.\end{aligned} \tag{6.92}$$

Comparing terms from (6.30) dimensionally,

$$\lambda|u| \sim rJ, \tag{6.93}$$

and taking $\partial_r \sim 1/r$, we approximate

$$|\nabla \cdot \mathbf{u}| \sim |\nabla \times \mathbf{u}| \sim \frac{J}{\lambda}. \tag{6.94}$$

It follows that equation (6.92) reduces to

$$\frac{\mathrm{d}\mathcal{E}}{\mathrm{d}t} = -2\pi q \left(\eta + \frac{\nu\lambda - \beta - z_0^2}{\lambda^3}\right) \int_0^1 J^2 \, r\mathrm{d}r. \tag{6.95}$$

We assume all of the Ohmic heating occurs within the resistive diffusion region and thus integrate (6.95) between $0 < r < r_s$. Roughly, following (Craig and McClymont, 1993) and (Hassam, 1992), we assume that the flux is relatively constant, or in other words $\psi \approx \psi(0,t)$ within the diffusion region. Near the origin, the plasma velocity $u \to 0$ so we approximate (6.31) by

$$\psi_t \approx \eta J. \tag{6.96}$$

We let $|\partial_t| \sim |\lambda| = (\alpha^2 + \omega^2)^{1/2}$ and approximate $\omega^2 \gg \alpha^2$, which is true for small η, to obtain the magnitude of diffused current as

$$J \sim \frac{\omega}{\eta}\psi. \tag{6.97}$$

Substituting (6.97) into (6.95) and integrating for an approximately constant current J yields

$$\left|\frac{\mathrm{d}\mathcal{E}}{\mathrm{d}t}\right| = \frac{\pi q r_s^2 \omega^2}{\eta}\left(1 + \frac{\nu\lambda - \beta - z_0^2}{\eta\lambda^3}\right). \tag{6.98}$$

The decay rate α is defined as

$$\alpha = \left|\frac{\mathrm{d}\mathcal{E}}{\mathrm{d}t}\right| / \mathcal{E}. \tag{6.99}$$

Hence, we divide (6.98) by the total energy (6.90) and take

$$\eta\lambda \sim \eta, \tag{6.100}$$

since we expect λ to be logarithmic and thus near unity in comparison to the very small η, to obtain

$$\alpha \approx \frac{\omega^2}{2}\left(1 + \frac{\nu - \beta - z_0^2}{\eta}\right)^{3/2}. \tag{6.101}$$

Equations (6.101) and (6.84) generalise the Craig and McClymont (1991) decay and oscillation rates (6.59) for the cases $\nu, \beta, z_0 \neq 0$.

6.3.5 Gas Pressure Effects

The previous subsection begs the question- under what circumstances will oscillatory reconnection persist? Fast, oscillatory reconnection can be undone by a sufficiently large pressure gradient that blocks the entry of fresh magnetic flux to the diffusion region (Craig and McClymont, 1993). For gas pressure effects we denote the gas pressure force as

$$\mathbf{F_G} = -\beta\nabla\rho \tag{6.102}$$

and aim to find out when the gas pressure has a significant effect of magnetic reconnection. Noting that

$$\dot{\rho} = -\nabla\cdot\mathbf{v}, \tag{6.103}$$

and defining the planar magnetic force as being proportional to the planar acceleration

$$\mathbf{F_P} = \dot{\mathbf{v}}, \tag{6.104}$$

we obtain

$$\ddot{\mathbf{F}}_\mathbf{G} = \beta\nabla\left(\nabla\cdot\mathbf{F_P}\right). \tag{6.105}$$

Letting $\nabla \sim 1/r_s$ and $\partial_t \sim -\lambda$,

$$\mathbf{F_G} \sim \frac{\beta}{\lambda^2 r_s^2}\mathbf{F_P}. \tag{6.106}$$

Hence, Craig and McClymont (1993) showed gas pressure will stall resistive dissipation, where $r_s^2 \sim \eta\lambda$, if

$$\beta \gtrsim \eta\lambda^3 \tag{6.107}$$

However, consider the magnitude of viscous forces

$$\mathbf{F}_\nu = \nu\nabla^2\mathbf{v}. \tag{6.108}$$

Comparing to (6.105), we observe

$$\mathbf{F_G} \sim \frac{\beta}{\nu\lambda}\mathbf{F}_\nu. \tag{6.109}$$

Hence, we conclude that gas pressure stalls viscous dissipation if

$$\beta \gtrsim \nu\lambda. \tag{6.110}$$

Significantly, the stalling caused by pressure forces can be counter-balanced by viscous effects. Gas pressure can only stall energy release if the conditions (6.107) or (6.110) are met. In the solar corona, the dimensionless viscosity $\nu \sim 10^{-4.5}$ (e.g. Spitzer, 1962; Craig et al., 2005) and the plasma beta $\beta \sim 10^{-2} - 10^{-4}$ (e.g. Gary, 2001) are roughly equivalent but β is many orders of magnitude larger than the dimensionless resistivity η. Hence plasma pressure forces will significantly oppose resistive dissipation but not viscous dissipation.

6.3.6 Axial Magnetic Effects

The axial magnetic field acts as a back pressure (Craig and McClymont, 1993) that opposes energy dissipation. Hence, a similar analysis to the previous subsection can be performed to compare whether a QSL-type site or a 3D null-type site would better accommodate fast energy dissipation. We define the axial force

$$\mathbf{F_A} = \nabla \left(Z^E Z \right). \tag{6.111}$$

For a QSL-type axial magnetic field, we let $Z^E = z_0$ and differentiate (6.43) with respect to time to obtain

$$\dot{\mathbf{F}}_\mathbf{A} \sim \frac{z_0}{\lambda} \nabla \left(\nabla \cdot \mathbf{F_P} \right) \tag{6.112}$$

Letting $\nabla \sim 1/r_s$, $\partial_t \sim -\lambda$, we obtain

$$\mathbf{F_A} \sim \frac{z_0^2}{\lambda^2 r_s^2} \mathbf{F_P}. \tag{6.113}$$

Hence, axial magnetic pressure will stall resistive dissipation, where $r_s^2 = \eta\lambda$, if

$$z_0^2 \gtrsim \eta\lambda^3. \tag{6.114}$$

On the other hand, if we have an initial 3D null -type geometry $Z^E = \mu\psi^E$, where ψ^E is bounded by $r^2/2$, then we estimate

$$|Z^E| \sim \mu r^2 \sim \mu\eta\lambda. \tag{6.115}$$

Replacing z_0 with $\mu\eta$ in (6.114) implies

$$\mu \gtrsim \left(\frac{\lambda}{\eta}\right)^{1/2}, \tag{6.116}$$

as the condition for axial effects to stall resistive energy dissipation. Considering that η is a very small quantity in the corona, we would require an axial magnetic field many orders of magnitude larger than the planar magnetic field to stall reconnection in the 3D null-type case. We might expect the axial magnetic field to have, at most, a similar magnitude to the planar magnetic field.

The key result of this section is that we do not expect a QSL-type site to support fast reconnection, however a 3D null-type site has the potential to accommodate fast reconnection.

6.4 Numerical Results

In order to verify our analytical predictions we turn to numerical methods. We adopt a basic differencing method as described by Craig and McClymont (1991, 1993) over the grid

$$0 \leq x \leq 1, \qquad 0 \leq y \leq 1, \tag{6.117}$$

and then mirrored over the x and y axes. The flux is tied to the boundary and no plasma is allowed to flow in or out of our system, that is to say that

$$\psi = 0, \qquad \mathbf{u} = \mathbf{0}, \tag{6.118}$$

$$\nabla Z = \mathbf{0}, \qquad W = 0, \tag{6.119}$$

at

$$(x, y) = (\pm 1, \pm 1). \tag{6.120}$$

The number of points in our grid is inversely proportional to the Sweet-Parker scale $\sqrt{\eta}$. We difference equations (6.10)-(6.14) by the forward time central differencing scheme with the initial perturbation

$$\psi = 0.1(1-x^2)(1-y^2), \tag{6.121}$$

$$\mathbf{u} = \mathbf{0}, \tag{6.122}$$

(see e.g. Richtmyer and Morton, 1967). We want to verify the decay and oscillation rates of the magnetic and kinetic energy of the system and so we follow the method of Craig and Litvinenko (2008). We measure the normalised change in decay rate

$$\alpha_1 = \frac{\alpha - \alpha_0}{\alpha_0}, \tag{6.123}$$

and normalised change in oscillation rate

$$\omega_1 = \frac{\omega - \omega_0}{\omega_0} \tag{6.124}$$

by considering the difference between the second and fourth minima in the magnetic energy (for viscous and axial effects) or kinetic energy (for pressure effects). From equations (6.84) and (6.101), we predict that

$$\alpha_1 \sim \frac{\nu - \beta - z_0^2}{\eta}, \qquad \omega_1 \sim \frac{\nu - \beta - z_0^2}{\eta}. \tag{6.125}$$

Note that while in this case α_1 and ω_1 happen to be comparable, this is not always true. Collisionless effects, such as the Hall effect or electron inertia, decrease the length scale and thus decrease the oscillation frequency. However, decreasing the length scale increases the current at the origin and increases the decay rate. Numerical simulations investigating the oscillation and decay rates of collisionless regimes have been carried out elsewhere in the literature (Senanayake and Craig, 2006b; Craig and Litvinenko, 2008; McClements et al., 2004; Senanayake, 2007).

For viscous effects, we expect an increased oscillation frequency $\omega_1 \sim \nu/\eta$ which we verify numerically in Figs. 6.4-6.5. Similarly, equation (6.125) predicts an increased decay rate $\alpha_1 \sim \nu/\eta$ which we verify in Figs. 6.6-6.7. While

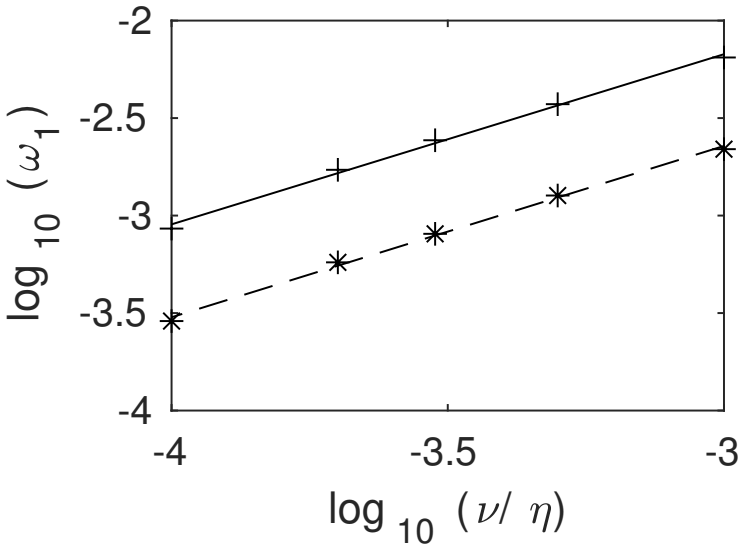

Figure 6.4: Change in oscillation rate plotted against the log of ν/η for fixed η and varied ν. Runs are performed for $\eta = 10^{-2}$ (pluses) and $\eta = 10^{-3}$ (stars). A linear fit describes the lines as $\omega_1 = 2.7884\,(\nu/\eta)^{0.87260}$ (solid line) and $\omega_1 = 0.98307\,(\nu/\eta)^{0.87851}$ (dashed line) respectively, which compare favourably to the predicted (6.125).

the oscillation frequency and decay rate match up well to our predictions for small $\nu/\eta \lesssim 10^{-4}$, as we increase the viscosity we see the onset of the high-frequency long-time phase as $\nu/\eta \to 1$ (see Craig et al., 2005).

Pressure effects reduce the decay and oscillation rates by a factor of β/η, as shown in Figs. 6.8- 6.9 and 6.10-6.11 respectively. These runs require additional dissipation to prevent the system from blowing up, and thus we consider a viscosity $\nu = 0.01\eta$. For large pressure $\beta/\eta \to 1$, oscillations are suppressed. Interestingly, for lower β/η than displayed in Fig. 6.9, the oscillation frequency actually increases.

Finally, axial effects reduce the decay and oscillation rates by a factor of z_0^2/η as depicted in Figs. 6.12-6.13 and 6.14-6.15 respectively. The axial field strength has to be relatively large $z_0/\sqrt{\eta} \gtrsim 10^{-2}$ in order for the difference in oscillation frequencies to become noticeable. The difference in decay rate matches well to our prediction for small $z_0/\sqrt{\eta}$ and starts to decay as $z_0/\sqrt{\eta} \to 1$.

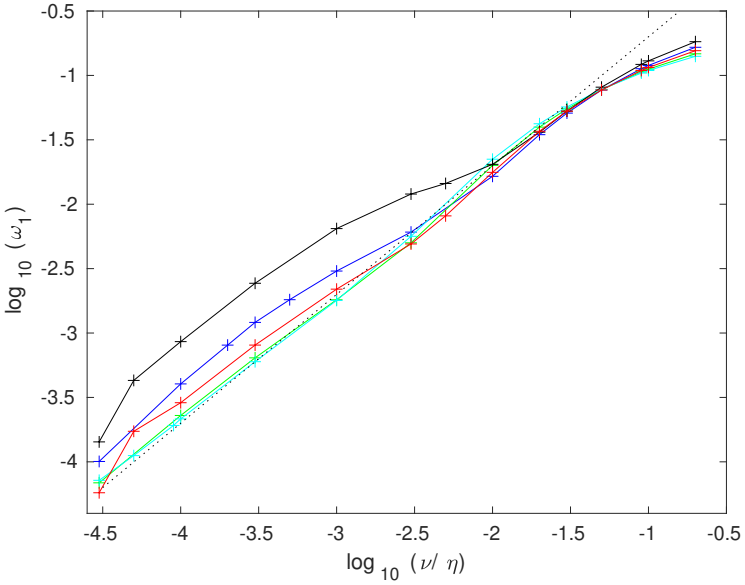

Figure 6.5: Change in oscillation rate plotted against the log of ν/η for fixed η and varied ν. Runs are performed for $\eta = 10^{-2}$ (black), $\eta = 3 \times 10^{-3}$ (blue), $\eta = 10^{-3}$ (red), $\eta = 3 \times 10^{-4}$ (green) and $\eta = 10^{-4}$ (cyan). The dotted line corresponds to an increase in decay rate $\omega_1 \sim \nu/\eta$ as predicted by equation (6.125).

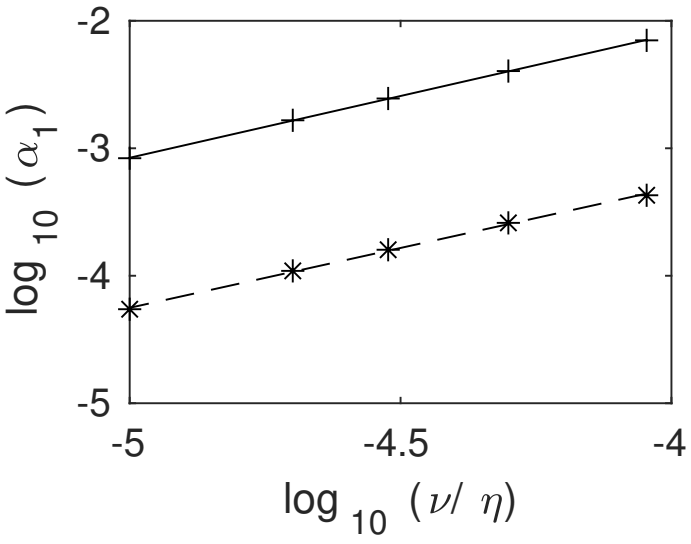

Figure 6.6: Normalised change in decay rate plotted against the log of ν/η for fixed η and varied ν. Runs are performed for $\eta = 10^{-2}$ (pluses) and $\eta = 10^{-3}$ (stars). A linear fit describes the lines as $\alpha_1 = 59.129\,(\nu/\eta)^{0.96927}$ (solid line) and $\alpha_1 = 2.7736\,(\nu/\eta)^{0.93889}$ (dashed line) respectively, which compare favourably to the predicted (6.125).

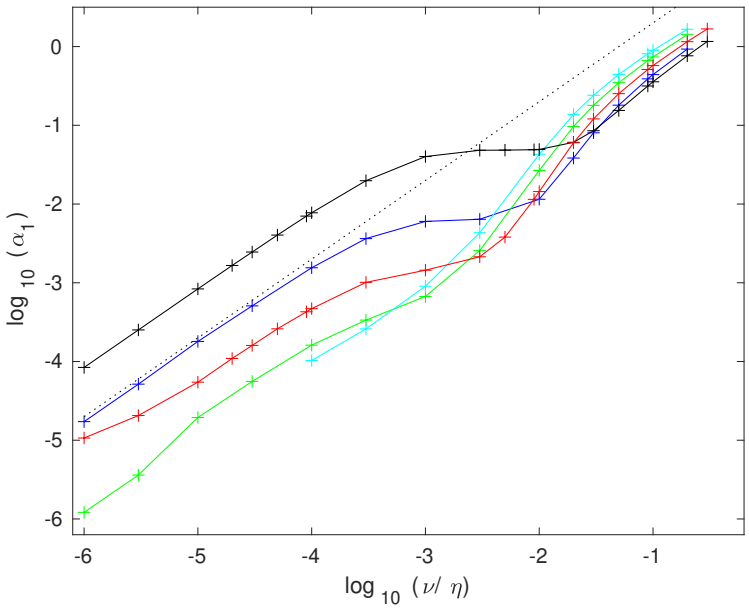

Figure 6.7: Normalised change in decay rate plotted against the log of ν/η for fixed η and varied ν. Runs are performed for $\eta = 10^{-2}$ (black), $\eta = 3 \times 10^{-3}$ (blue), $\eta = 10^{-3}$ (red), $\eta = 3 \times 10^{-4}$ (green) and $\eta = 10^{-4}$ (cyan). The dotted line corresponds to an increase in decay rate $\alpha_1 \sim \nu/\eta$ as predicted by equation (6.125).

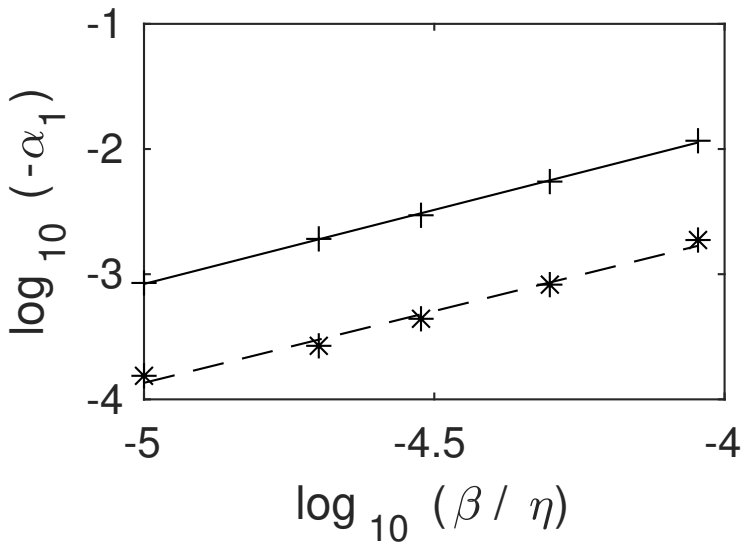

Figure 6.8: Change in decay rate plotted against the log of β/η with $\nu = 0.01\eta$ for fixed η and varied β. Runs are performed for $\eta = 10^{-2}$ (pluses) and $\eta = 3 \times 10^{-3}$ (stars). A linear fit describes the lines as $\alpha_1 = -696.95\,(\beta/\eta)^{1.1843}$ (solid line) and $\alpha_1 = -74.080\,(\beta/\eta)^{1.1476}$ (dashed line) respectively, which compare favourably to the predicted (6.125).

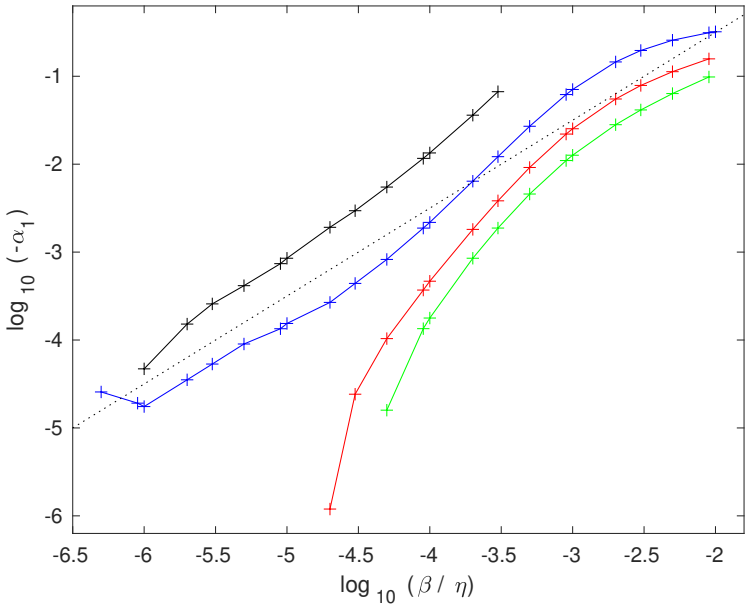

Figure 6.9: Change in decay rate plotted against the log of β/η with $\nu = 0.01\eta$ for fixed η and varied β. Runs are performed for $\eta = 10^{-2}$ (black), $\eta = 3\times10^{-3}$ (blue), $\eta = 10^{-3}$ (red) and $\eta = 3 \times 10^{-4}$ (green). The dotted line corresponds to a decrease in decay rate $\alpha_1 \sim -\beta/\eta$ as predicted by equation (6.125).

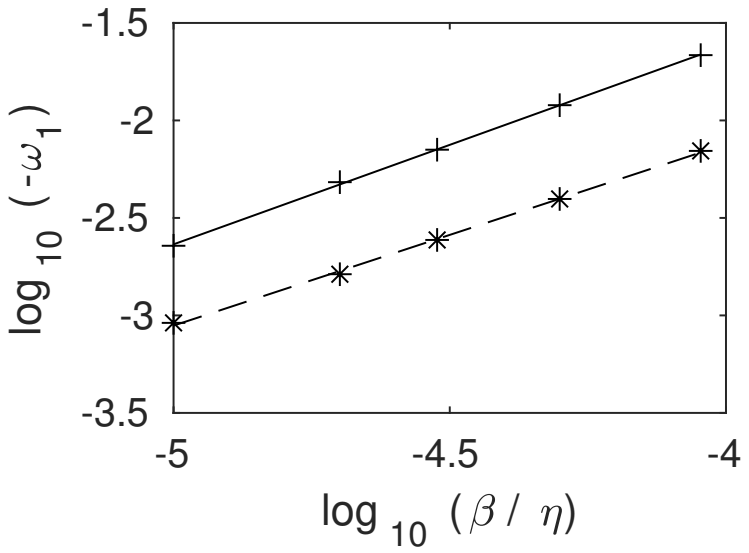

Figure 6.10: Change in oscillation rate plotted against the log of β/η with $\nu = 0.01\eta$ for fixed η and varied β. Runs are performed for $\eta = 10^{-2}$ (pluses) and $\eta = 3\times10^{-3}$ (stars). A linear fit describes the lines as $\omega_1 = -292.48\,(\beta/\eta)^{1.0203}$ (solid line) and $\omega_1 = -39.728\,(\beta/\eta)^{0.93026}$ (dashed line) respectively, which compare favourably to the predicted (6.125).

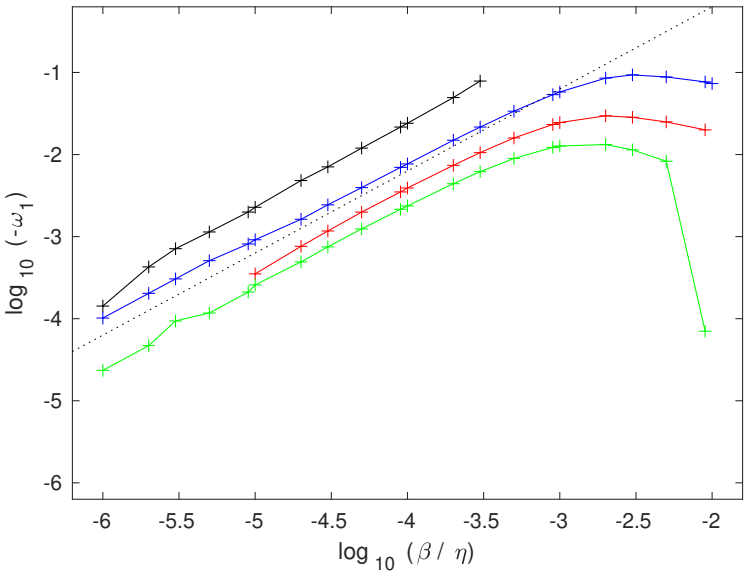

Figure 6.11: Change in oscillation rate plotted against the log of β/η with $\nu = 0.01\eta$ for fixed η and varied β. Runs are performed for $\eta = 10^{-2}$ (black), $\eta = 3 \times 10^{-3}$ (blue), $\eta = 10^{-3}$ (red) and $\eta = 3 \times 10^{-4}$ (green). The dotted line corresponds to a decrease in oscillation rate $\omega_1 \sim -\beta/\eta$ as predicted by equation (6.125).

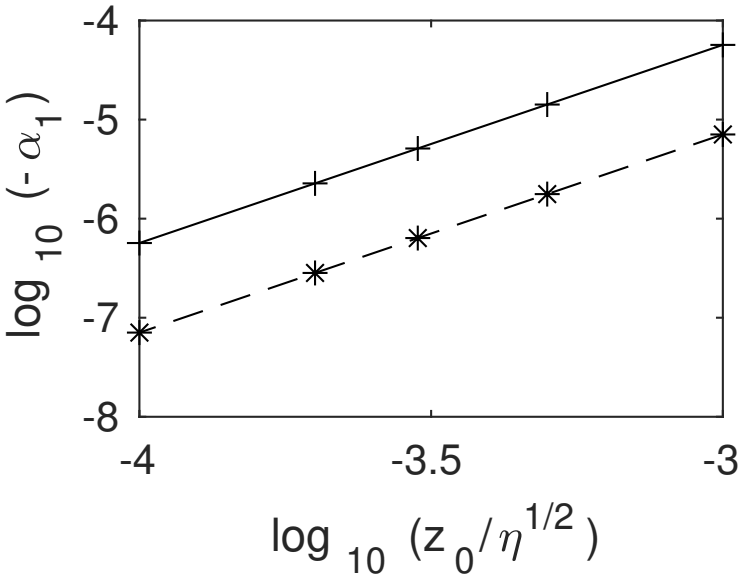

Figure 6.12: Change in decay rate plotted against the log of $z_0/\sqrt{\eta}$ for fixed η and varied z_0. Runs are performed for $\eta = 10^{-2}$ (pluses) and $\eta = 10^{-3}$ (stars), where $\nu = 0$. A linear fit describes the lines as $\alpha_1 = -56.728\left(z_0/\sqrt{\eta}\right)^{2.0000}$ (solid line) and $\alpha_1 = -7.0778\left(z_0/\sqrt{\eta}\right)^{2.0000}$ (dashed line) respectively, which compare favourably to the predicted (6.125).

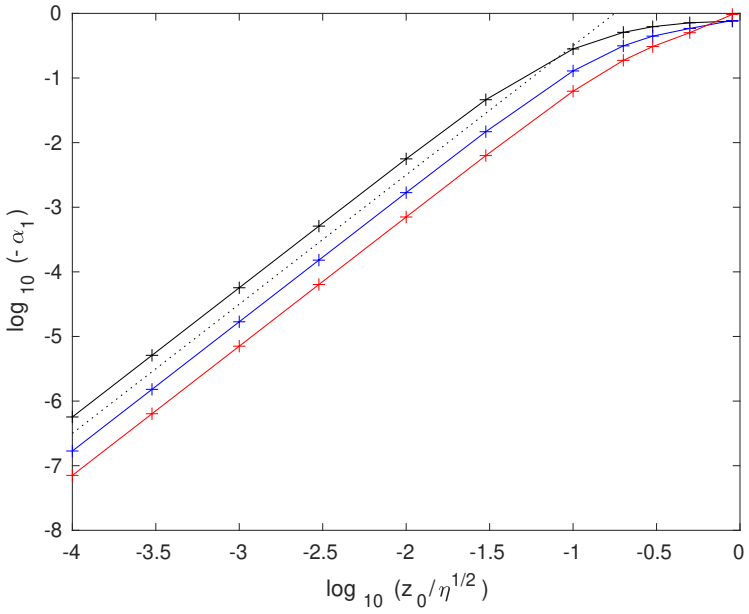

Figure 6.13: Change in decay rate plotted against the log of $z_0/\sqrt{\eta}$ for fixed η and varied z_0. Runs are performed for $\eta = 10^{-2}$ (black), $\eta = 3 \times 10^{-3}$ (blue) and $\eta = 10^{-3}$ (red), where $\nu = 0$. The dotted line corresponds to a decrease in decay rate $\alpha_1 \sim -z_0^2/\eta$ as predicted by equation (6.125).

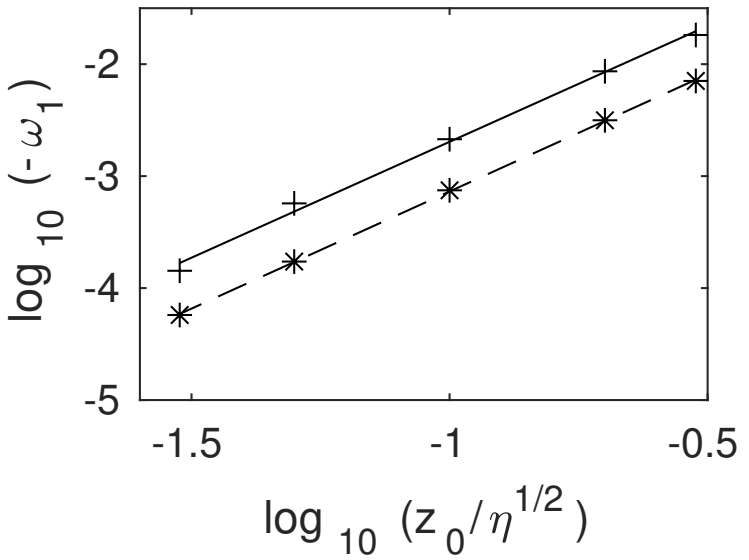

Figure 6.14: Change in oscillation rate plotted against the log of $z_0/\sqrt{\eta}$ for fixed η and varied z_0. Runs are performed for $\eta = 10^{-2}$ (pluses) and $\eta = 10^{-3}$ (stars), where $\nu = 0$. A linear fit describes the lines as $\omega_1 = -0.23830\left(z_0/\sqrt{\eta}\right)^{2.0705}$ (solid line) and $\omega_1 = -0.090282\left(z_0/\sqrt{\eta}\right)^{2.0926}$ (dashed line) respectively, which compare favourably to the predicted (6.125).

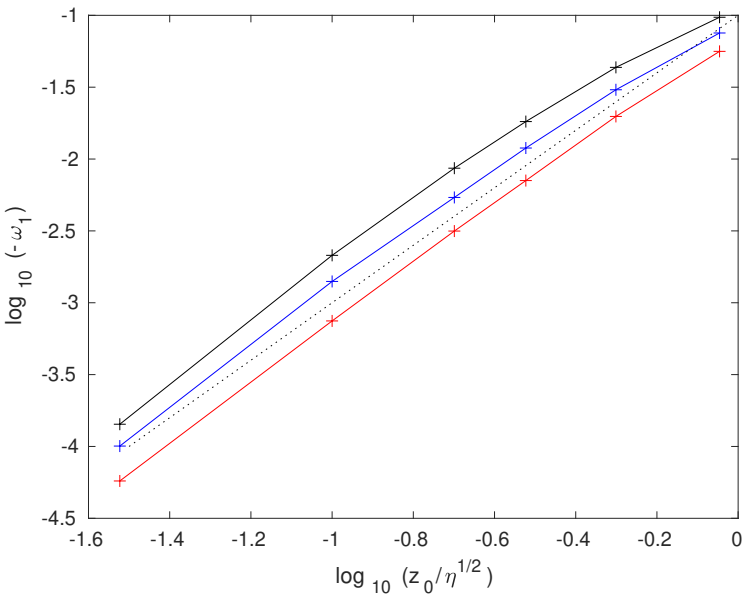

Figure 6.15: Change in oscillation rate plotted against the log of $z_0/\sqrt{\eta}$ for fixed η and varied z_0. Runs are performed for $\eta = 10^{-2}$ (black), $\eta = 3 \times 10^{-3}$ (blue) and $\eta = 10^{-3}$ (red), where $\nu = 0$. The dotted line corresponds to a decrease in decay rate $\omega_1 \sim -z_0^2/\eta$ as predicted by equation (6.125).

We note, however, that we have not accounted for the lower change in decay rates found for lower resistivity.

For large axial, pressure or viscous effects the oscillatory modes are suppressed and for that reason we turn our focus to the maximum reconnection rate. We describe the maximum reconnection rate in 2.5D by

$$\psi_t(0,t) = \eta J_z(0,t), \tag{6.126}$$

or in other words the reconnection rate is proportional to the maximum axial current through the origin (e.g. Effenberger and Craig, 2016). Note, in 3D the reconnection rate with our set up is usually quantified by $\int E_z(0,0,z)\,\mathrm{d}z$ (Schindler et al., 1988; Thurgood et al., 2018).

We depict the maximum reconnection rate against resistivity for the cases $\nu = 0.01$ and $\nu = 0.01\eta$ in Fig. 6.16 and we observe that viscous effects reduce the maximum reconnection rate.

We analytically predicted that a QSL-type axial field would stall reconnection, while a 3D null-type field would not be able to, which we test using

numerical methods. However, our linearised system cannot handle high pressure or axial terms numerically. Accordingly, we use a full nonlinear code, which McClymont and Craig (1996) previously used to show that a constant axial magnetic field and/or pressure effects act to stall fast reconnection. Since those authors have already shown numerically that pressure stalls reconnection, we do not investigate large pressure effects numerically here. We instead focus on axial effects and compare a QSL-type configuration to a 3D null-type configuration.

We use a Crank-Nicolson finite difference method (Potter, 1973) with the initial conditions

$$\psi(0) = \frac{1}{\mu^2}\sin(\mu x)\sin(\mu y) + 0.03\left(1-x^2\right)\left(1-y^2\right), \tag{6.127}$$

$$Z(0) = \sqrt{\frac{2}{\mu^2}\sin^2(\mu x)\sin^2(\mu y) + z_0^2}, \tag{6.128}$$

$$\mathbf{v}(0) = \mathbf{0}, \tag{6.129}$$

to replicate the equilibrium magnetic field profiles (6.28). As Figure 6.17 indicates, as we increase z_0 the reconnection rate is increasingly stalled (as previously shown by McClymont and Craig (1996)), however when we increase the axial field strength μ, the reconnection rate does not significantly stall and is only marginally decreased, as depicted in Figure 6.18.

We conclude that we have provided significant analytical and numerical evidence to suggest that fast reconnection will not occur if we use an initial QSL geometry. However, fast magnetic reconnection will persist if we use a 3D null point initial geometry, at least for a purely resistive plasma.

6.5 Conclusions

Our presentation has shown how the original linear reconnection model (Craig and McClymont, 1991; Hassam, 1992) has been generalised to incorporate viscous, axial, pressure and collisionless effects. Viscosity, analogously to resistivity, acts as a diffusive term increasing the energy release rate. Viscous

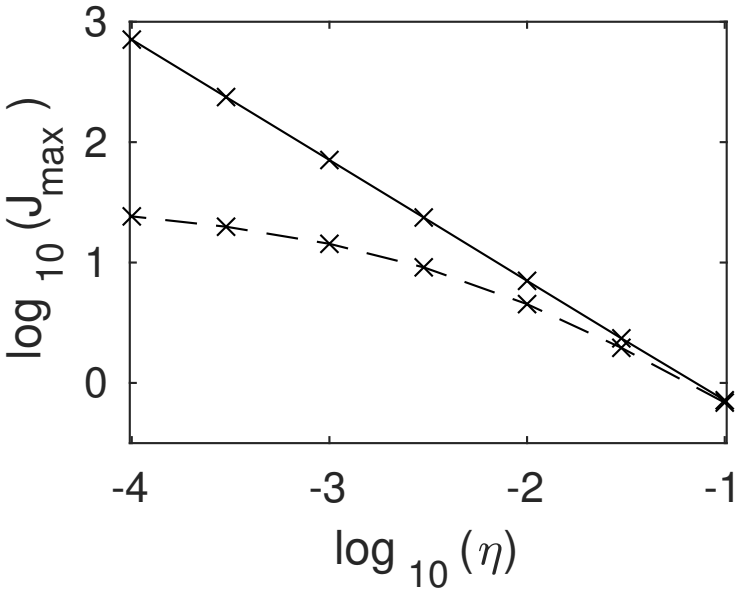

Figure 6.16: Maximum current at the origin vs. resistivity. The solid line is $\nu = 0.0001\eta$ and the dashed line is $\nu = 0.01$. We observe an increased reduction of the reconnection rate $\eta J|_{(0,0)}$ as viscous effects increasingly dominate resistive effects.

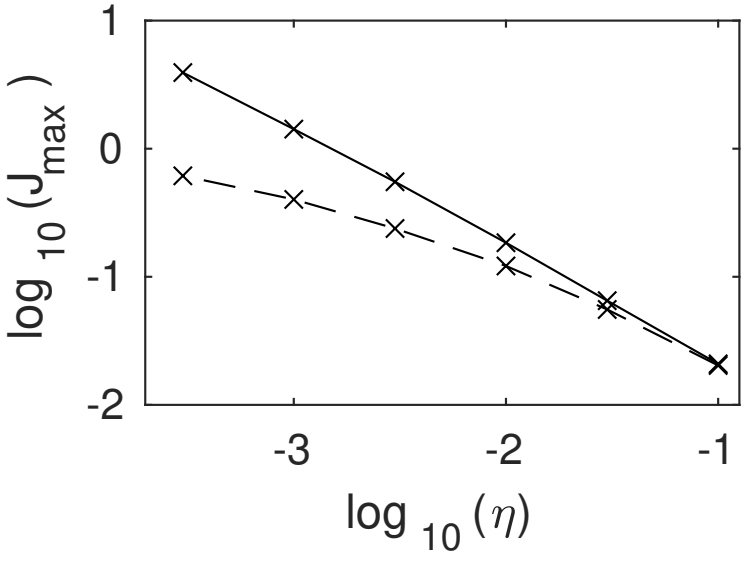

Figure 6.17: Maximum current vs. resistivity for $z_0 = 0$ (solid) and $z_0 = 0.3$ (dashed), where $\mu = 0$. We observe an increased reduction of the reconnection rate $\eta J|_{(0,0)}$ as the strength of the QSL-type axial field increases.

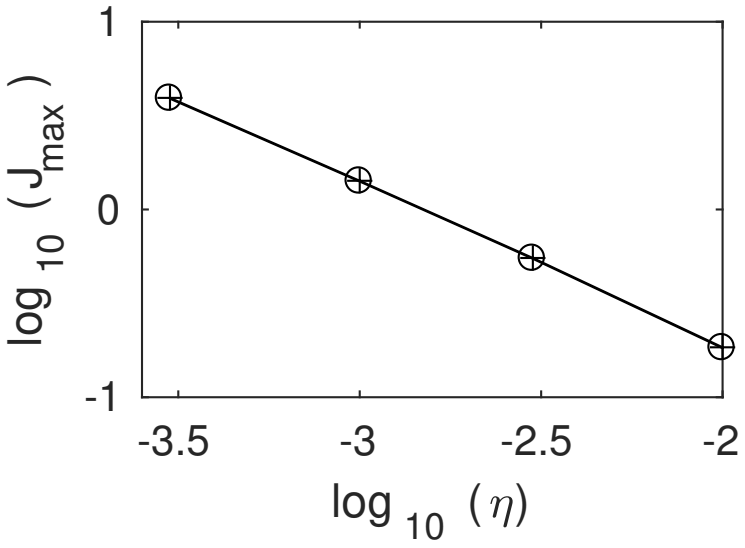

Figure 6.18: Maximum current vs. resistivity for $\mu = 0$ (crosses) and $\mu = 0.3$ (circles) where $z_0 = 0$. We do not observe any significant reduction of the reconnection rate $\eta J|_{(0,0)}$ as the strength of the 3D null-type axial field increases.

effects increase the length scale and thus increase the oscillation frequency. Gas pressure opposes resistive and viscous dissipation. While gas pressure can overwhelm resistive dissipation in the solar corona, gas pressure will not be able to significantly stall viscous dissipation.

Collisionless effects, such as the Hall effect or electron inertia, reduce the length scale and thus the oscillation frequency. Since collisionless effects are not diffusive, they only influence the amount of Ohmic heating, which will increase due to the increased current. Therefore, the Hall and electron inertia terms will increase the decay rate. These effects have been demonstrated elsewhere in the literature (Craig and Litvinenko, 2008; Senanayake and Craig, 2006b; Senanayake, 2007; McClements et al., 2004; McClements and Thyagaraja, 2004).

For large viscous contributions, we have shown that increasing viscosity stalls reconnection. Since the dimensionless viscosity is much larger than the dimensionless resistivity in the solar corona, the rate of viscous dissipation can be considered fast. Furthermore, Craig et al. (2005) demonstrated the fast

viscous dissipation would last for roughly one Alfvén time.

We have provided evidence that fast reconnection is only possible in the presence of a null point. Axial terms oppose dissipation and will overwhelm fast energy release if the dimensionless conditions (6.114) or (6.116) are met. Consequently, for a QSL geometry, axial magnetic fields of even moderate size stall resistive dissipation and reconnection. However for axial effects to stall reconnection with a 3D null point requires a very large axial magnetic field $B_z \sim \eta^{-1/2}$. Null points have been well established as an attractor for MHD waves (see McLaughlin et al., 2011, for a review). Without a null point in the QSL-type domain, the flux gets reconnected at a slow rate.

In addition to the modifications we have considered there are more avenues for generalisations of linear reconnection. We note that there are many more solutions to the Grad-Shafranov equation than those we have considered here, and thus many more possible 2.5D geometries for reconnection. However, we expect that the key reconnection scalings are controlled by the local structure of the velocity and magnetic fields in the vicinity of the reconnection site. Hence, we expect our results to remain valid for other global reconnection solutions.

Finally, our linear system breaks down for larger scale energy perturbations, in which a nonlinear model is needed (e.g. Ofman et al., 1993; McClymont and Craig, 1996; McLaughlin et al., 2009). Thurgood et al. (2019) found that in the nonlinear case, the oscillation period was very weakly dependent on resistivity but strongly dependent on the amount of free energy in the system, a factor that does not control the linear decay or oscillations at all. Furthermore, in extending linear reconnection to 3D, axial magnetic pressure gradients become the dominant stalling mechanism (Thurgood et al., 2018). We expect, based on the results presented here, that viscosity could significantly limit this stalling effect. Incorporating viscous, pressure and 3D effects into a full nonlinear simulation is an avenue for further research.

Chapter 7

Conclusion

7.1 Summary

Purely resistive magnetic reconnection explains how vast magnitudes of magnetic energy are released in the solar corona, but predicts energy release rates that are too slow to match observations of solar flares. This discrepancy is the unresolved problem that has motivated this thesis.

The underlying problem that motivated this thesis is that purely resistive magnetic reconnection predicts energy release rates too slow to match observations of solar flares. To this end, we have analysed some of the ways that non-ideal effects, namely viscosity and the Hall effect, modify reconnection models.

We began by reviewing the basic idea of magnetic reconnection and the solar flare problem. We described the Magnetohydrodynamic (MHD) equations and the requirements for breaking the flux frozen-in condition. We introduced the Sweet-Parker current sheet, the Imshennik and Syrovatskiĭ (1967) solution for current sheet formation (in a compressible plasma) and the Forbes (1982) one-dimensional nonlinear model for unsteady reconnection.

In Chapter 3, we searched for the length scale of a steadily reconnecting visco-resistive current sheet. We investigated two approaches: magnetic annihilation and a quasi-one-dimensional series expansion of a current sheet.

Hence, we reviewed earlier flux pile-up models, namely the purely resistive Sonnerup and Priest (1975) solution, Gratton et al. (1990) and Besser et al. (1990)'s visco-resistive annihilation solutions, and the Craig and Henton (1995) reconnective annihilation solution. We considered why the visco-resistive length scale appeared in some of these solutions, yet not in others. In other words, we wanted to determine whether a single visco-resistive current layer was formed or whether there were separate viscous and resistive layers. We showed, using a dimensional analysis of the Priest et al. (2000) magnetic annihilation solution, that the emergence of a visco-resistive is entirely dependent on the choice of inflow velocity profile.

Furthermore, we considered a series expansion method (Priest and Cowley, 1975) that employs a quasi-one-dimensional Harris current sheet (Biskamp, 1986; Jamitzky and Scholer, 1995). Litvinenko (2009) extended this expansion to include the Hall effect. We employed the series expansion to find an exact visco-resistive length scale, using not only a Harris sheet, but also a Gaussian profile and a Dawson profile.

We concluded that the presence of a VR length scale in reconnection is determined by the form of the inflow velocity $v_x(x, 0)$. If nonlinear terms are present in the inflow velocity profile a VR length scale will be present regardless of how small these nonlinear terms are. Thus we postulated that the Park et al. (1984) scale is a fundamental length scale that is only invalid for a limited range of particular inflow velocity profiles.

In Chapter 4, we presented a self-similar solution for current sheet formation at a magnetic neutral line in incompressible Hall MHD. This solution generalises the Litvinenko (2007) solution by considering a general set of initial conditions. We used a mechanical analogue to generate a criterion for which initial conditions will lead to collapse. We then used an asymptotic analysis to determine an approximate solution, which we employed to find the singularity time. We verified our analytical prediction with a numerical run. Finally, we generalised the self-similar solution to incorporate resistive, viscous and elec-

tron inertia terms. Later researchers (Janda, 2018; Brizard, 2019) would build on our asymptotic solution to find an exact solution and an exact singularity time using the Jacobi and Weierstrass elliptic functions.

In Chapter 5, we examined the linear, oscillatory Craig and McClymont (1991) reconnection solution. In this model, we considered a static X-point with a small perturbation. Craig and McClymont (1991) showed this linear solution could be fast, with a reconnection rate $\sim |\ln \eta|^{-1}$ in the purely resistive regime. We reviewed the three phases of linear reconnection: an initial implosion (Craig and Watson, 1992), the oscillatory phase, and the long-time tail (Hassam, 1992). The oscillatory phase is where the bulk of the energy is lost. We considered azimuthal modes (Craig and McClymont, 1993), which can make reconnection even faster, and higher order X-points (Craig, 1994) which lead to slow reconnection. While linear reconnection initially appeared promising as a means of fast reconnection, it is easily stalled by gas pressure, axial effects (Craig and McClymont, 1993) or viscosity (Craig et al., 2005).

In Chapter 6, we considered a more general model of linear reconnection that included viscous, pressure and axial effects, the Hall effect and electron inertia. We attempted to quantify the role of each effect using a dimensional argument backed up by numerical simulation results. Promisingly, we found, in accordance with previous studies (Armstrong et al., 2011), that viscosity slows reconnection yet increases the amount of energy release through dissipation. Pressure and axial effects act to oppose both reconnection and dissipation. Gas pressure can easily overwhelm reconnection and resistive dissipation, but not viscous dissipation. We considered two axial fields in 2.5D: one that emulated a Quasi-Separatrix Layer (QSL) and the other emulating a 3D null point. We found that the field emulating a QSL could easily stall reconnection even for a small axial field, but the axial field emulating a 3D null point would have to be very large $\sim \eta^{-1/2}$ in order to stall reconnection.

7.2 Suggestions for Future Work

The work in our thesis could be extended in several ways. Firstly, our visco-resistive series solution of Chapter 3 could be extended to include the Hall effect (e.g. Litvinenko, 2009). Furthermore, it is not entirely clear why our length scale initially decreases, and thus our reconnection rate increases, when we increase viscosity in Fig. 3.6.

Our work in Chapter 4 has already been built upon. Janda (2018) and Brizard (2019) have found exact solutions for equation (4.89) in terms of elliptic functions. By extension the self-similar system (4.80)-(4.84) can be solved for a general inflow planar velocity $\gamma(t)$. This work could be further expanded by including, for example, compressible or 3D effects.

The most logical extension of the linear reconnection model, described in Chapter 6, is to create a full analytical 3D model. The development of a full analytical 3D model would allow us to compare a QSL with a 3D null point site. This would mean that we could verify whether a null point is indeed required for fast reconnection. Furthermore, we could incorporate viscous, pressure and axial effects into a non-linear simulation of a perturbed X-point, such as the McClymont and Craig (1996) simulation.

Another possible avenue of research is to incorporate the effects of secondary islands, which have been shown to speed up Sweet-Parker reconnection (Cassak et al., 2009). Secondary islands are a promising area of active research, however it is nontrivial to expand our work to incorporate these effects.

References

Ara, G., B. Basu, B. Coppi, G. Laval, M. N. Rosenbluth, and B. V. Waddell (1978), Magnetic reconnection and m = 1 oscillations in current carrying plasmas, *Annals of Physics*, **112**, 443–476.

Armstrong, C. K., I. J. D. Craig, and Y. E. Litvinenko (2011), Viscous effects in time-dependent planar reconnection, *Astron. & Astrophys.*, **534**, A25.

Aschwanden, M. (2006), *Physics of the solar corona: an introduction with problems and solutions*, Springer, New York, NY.

Besser, B. P., H. K. Biernat, and R. P. Rijnbeek (1990), Planar MHD stagnation-point flows with velocity shear, *Planet. Space Sci.*, **38**, 411–418.

Bhattacharjee, A. (2004), Impulsive magnetic reconnection in the Earth's magnetotail and the solar corona, *Annu. Rev. Astron. Astrophys.*, **42**, 365–384.

Birn, J., et al. (2001), Geospace environmental modeling (GEM) magnetic reconnection challenge, *J. Geophys. Res.*, **106**, 3715–3720.

Birn, J., et al. (2005), Forced magnetic reconnection, *Geophys. Res. Lett.*, **32**, 6105.

Biskamp, D. (1986), Magnetic reconnection via current sheets, *Phys. Fluids*, **29**, 1520–1531.

Biskamp, D. (1993), *Nonlinear magnetohydrodynamics*, Cambridge University Press.

Biskamp, D. (2000), *Magnetic Reconnection in Plasmas*, Cambridge University Press, Cambridge.

Brizard, A. J. (2019), Comment on "Exact solutions and singularities of an X-point collapse in Hall magnetohydrodynamics" [J. Math. Phys. 59, 061509 (2018)], *J. Math. Phys.*, **60**, 024,101.

Bulanov, S. V., and S. I. Syrovatskii (1980), MHD oscillations and waves near a magnetic null line, *Sov. J. Plasma Phys.*, **6**, 1205–1218.

Bulanov, S. V., S. G. Shasharina, and F. Pegoraro (1990), MHD modes near the X-line of a magnetic configuration, *Plasma Phys. & Controlled Fusion*, **32**, 377.

Carrington, R. C. (1859), Description of a singular appearance seen in the Sun on September 1, 1859, *Monthly Notices of the Royal Astronomical Society*, **20**, 13–15.

Case, N. A., A. Grocott, S. Milan, T. Nagai, and J. Reistad (2017), An analysis of magnetic reconnection events and their associated auroral enhancements, *J. Geophys. Res. Space Physics*, **122**, 2922–2935.

Cassak, P., M. Shay, and J. Drake (2009), Scaling of Sweet-Parker reconnection with secondary islands, *Phys. Plasmas*, **16**, 120,702.

Cassak, P. A., J. F. Drake, and M. A. Shay (2006), A model for spontaneous onset of fast magnetic reconnection, *Astrophys. J.*, **644**, L145.

Chapman, S., and P. C. Kendall (1963), Liquid instability and energy transformation near a magnetic neutral line: A soluble non-linear hydromagnetic problem, *Proc. R. Soc. London, Ser. A*, **271**, 435–448.

Chapman, S., and P. C. Kendall (1966), Comment on "Some exact solutions of magnetohydrodynamics", *Phys. Fluids*, **9**, 2306–2307.

Comisso, L., and A. Bhattacharjee (2016), On the value of the reconnection rate, *J. Plasma Phys.*, **82**, 595820,601.

Cowley, S. W. H. (1975), Magnetic field-line reconnection in a highly-conducting incompressible fluid - Properties of the diffusion region, *J. Plasma Phys.*, **14**, 475–490.

Craig, I. J. D. (1994), Current sheet formation and dissipation in general X-point topologies, *Astron. & Astrophys.*, **283**, 331–338.

Craig, I. J. D. (2008), Anisotropic viscous dissipation in compressible magnetic X-points, *Astron. & Astrophys.*, **487**, 1155–1161.

Craig, I. J. D., and F. Effenberger (2014), Current Singularities at Quasi-separatrix Layers and Three-dimensional Magnetic Nulls, *Astrophys. J.*, **795**, 129.

Craig, I. J. D., and R. B. Fabling (1996), Exact Solutions for Steady State, Spine, and Fan Magnetic Reconnection, *Astrophys. J.*, **462**, 969.

Craig, I. J. D., and S. M. Henton (1995), Exact Solutions for Steady State Incompressible Magnetic Reconnection, *Astrophys. J.*, **450**, 280.

Craig, I. J. D., and Y. E. Litvinenko (2005), Current singularities in planar magnetic x points of finite compressibility, *Phys. Plasmas*, **12**, 032,301.

Craig, I. J. D., and Y. E. Litvinenko (2007), Wave Energy Dissipation by Anisotropic Viscosity in Magnetic X-Points, *Astrophys. J.*, **667**, 1235–1242.

Craig, I. J. D., and Y. E. Litvinenko (2008), Influence of the Hall effect on the reconnection rate at line-tied magnetic X-points, *Astron. & Astrophys.*, **484**, 847–850.

Craig, I. J. D., and Y. E. Litvinenko (2012), Inflow Reconnection Solutions in Incompressible Visco-resistive Plasmas, *Astrophys. J.*, **747**, 16.

Craig, I. J. D., and A. N. McClymont (1991), Dynamic magnetic reconnection at an X-type neutral point, *Astrophys. J. Lett.*, **371**, L41–L44.

Craig, I. J. D., and A. N. McClymont (1993), Linear theory of fast reconnection at an X-type neutral point, *Astrophys. J.*, **405**, 207–215.

Craig, I. J. D., and D. I. Pontin (2014), Current singularities in line-tied three-dimensional magnetic fields, *Astrophys. J.*, **788**, 177.

Craig, I. J. D., and P. G. Watson (1992), Fast dynamic reconnection at X-type neutral points, *Astrophys. J.*, **393**, 385–395.

Craig, I. J. D., and P. G. Watson (2005), Exact models for Hall current reconnection with axial guide fields, *Phys. Plasmas*, **12**, 012,306.

Craig, I. J. D., Y. E. Litvinenko, and T. Senanayake (2005), Viscous effects in planar magnetic X-point reconnection, *Astron. & Astrophys.*, **433**, 1139–1143.

Drake, J. F., M. A. Shay, and M. Swisdak (2008), The Hall fields and fast magnetic reconnection, *Phys. Plasmas*, **15**, 042,306.

Dungey, J. W. (1953), Conditions for the occurence of electrical discharges in astrophysical systems, *Philos. Mag.*, **44**, 725–738.

Effenberger, F., and I. J. D. Craig (2016), Simulations of 3D Magnetic Merging: Resistive Scalings for Null Point and QSL Reconnection, *Solar Phys.*, **291**, 143–153.

Fabling, R. B. (1997), The infuence of hall currents, plasma viscosity and electron inertia on magnetic reconnection solutions, PhD thesis, The University of Waikato.

Fabling, R. B., and I. J. D. Craig (1996), Exact solutions for steady-state, planar, magnetic reconnection in an incompressible viscous plasma, *Phys. Plasmas*, **3**, 2243–2247.

Forbes, T. G. (1982), Implosion of a uniform current sheet in a low-beta plasma, *J. Plasma Phys.*, **27**, 491–505.

Forbes, T. G., and T. W. Speiser (1979), Temporal evolution of magnetic reconnection in the vicinity of a magnetic neutral line, *J. Plasma Phys.*, **21**, 107–126.

Furth, H. P., J. Killeen, and M. N. Rosenbluth (1963), Finite-resistivity instabilities of a sheet pinch, *Phys. Fluids*, **6**, 459–484.

Gary, G. A. (2001), Plasma Beta above a Solar Active Region: Rethinking the Paradigm, *Solar Phys.*, **203**, 71–86.

Gratton, F. T., M. F. Heyn, H. K. Biernat, R. P. Rijnbeek, and G. Gnavi (1988), MHD stagnation point flows in the presence of resistivity and viscosity, *J. Geophys. Res.*, **93**, 7318–7324.

Gratton, F. T., G. Gnavi, M. F. Heyn, H. K. Biernat, and R. P. Rijnbeek (1990), Pressure drive and viscous dragging: A reply, *J. Geophys. Res.*, **95**, 261–263.

Grauer, R., and C. Marliani (1998), Geometry of singular structures in magnetohydrodynamic flows, *Phys. Plasmas*, **5**, 2544.

Hassam, A. B. (1992), Reconnection of stressed magnetic fields, *Astrophys. J.*, **399**, 159–163.

Hassam, A. B., and R. P. Lambert (1996), Shear Alfvenic Disturbances in the Vicinity of Magnetic Null X-Points, *Astrophys. J.*, **472**, 832.

Heerikhuisen, J., I. J. D. Craig, and P. G. Watson (2000), Time-dependent magnetic reconnection in two-dimensional periodic geometry, *Geophys. Astrophys. Fluid Dyn.*, **93**, 115–142.

Heyn, M. F., and V. S. Semenov (1996), Rapid reconnection in compressible plasma, *Phys. Plasmas*, **3**, 2725–2741.

Hodgson, R. (1859), On a curious appearance seen in the sun, *Monthly Notices of the Royal Astronomical Society*, **20**, 15–16.

Hollweg, J. V. (1985), Viscosity in a magnetized plasma - Physical interpretation, *J. Geophys. Res.*, **90**, 7620–7622.

Hong, J., J. Yang, H. Chen, Y. Bi, B. Yang, and H. Chen (2019), Observation of a reversal of breakout reconnection preceding a jet: Evidence of oscillatory magnetic reconnection?, *Astrophys. J.*, **874**, 146.

Imshennik, V. S., and S. I. Syrovatskiĭ (1967), Two-dimensional flow of an ideally conducting gas in the vicinity of the zero line of a magnetic field, *Sov. Phys.–JETP*, **25**, 656.

Jamitzky, F., and M. Scholer (1995), Steady state magnetic reconnection at high magnetic reynolds number: A boundary layer analysis, *J. Geophys. Res.*, **100**, 19,277–19.

Janda, A. Z. (2018), Exact solutions and singularities of an X-point collapse in Hall magnetohydrodynamics, *J. Math. Phys.*, **59**, 061,509.

Janda, A. Z. (2019), Response to Comment on Exact solutions and singularities of an X-point collapse in Hall magnetohydrodynamics [J. Math. Phys. 60, 024101 (2019)], *Journal of Mathematical Physics*, **60**, 024,102.

Jardine, M., H. R. Allen, R. E. Grundy, and E. R. Priest (1992), A family of two-dimensional nonlinear solutions for magnetic field annihilation, *J. Geophys. Res.*, **97**, 4199–4207.

Klapper, I. (1998), Constraints on finite-time current sheet formation at null points in two-dimensional ideal incompressible magnetohydrodynamics, *Phys. Plasmas*, **5**, 910–914.

Lau, Y.-T., and J. M. Finn (1990), Three-dimensional kinematic reconnection in the presence of field nulls and closed field lines, *Astrophys. J.*, **350**, 672–691.

Litvinenko, Y. E. (2006), Shear-driven magnetic reconnection in viscous resistive incompressible plasmas, *Phys. Plasmas*, **13**, 092,305.

Litvinenko, Y. E. (2007), Current sheet formation at a magnetic neutral line in Hall magnetohydrodynamics, *Phys. Plasmas*, **14**, 112,303.

Litvinenko, Y. E. (2009), Analytical description of steady magnetic reconnection in Hall magnetohydrodynamics, *Astrophys. J.*, **694**, 1464.

Litvinenko, Y. E., and L. C. McMahon (2015a), Finite-time singularity formation at a magnetic neutral line in Hall magnetohydrodynamics, *Applied Mathematics Letters*, **45**, 76–80.

Litvinenko, Y. E., and L. C. McMahon (2015b), Hall MHD and electron inertia effects in current sheet formation at a magnetic neutral line, *East Asian J. Appl. Math*, **5**, 109–125.

MacTaggart, D., L. Vergori, and J. Quinn (2017), Braginskii magnetohydrodynamics for arbitrary magnetic topologies: coronal applications, *J. Fluid Mech*, **826**, 615–635.

Malyshkin, L. M. (2008), Model of Hall reconnection, *Phys. Rev. Lett.*, **101**, 225,001.

McClements, K. G., and A. Thyagaraja (2004), Electron inertial effects on the resistive magnetohydrodynamic spectrum of a magnetic X-point, *Plasma Phys. & Controlled Fusion*, **46**, 39–60.

McClements, K. G., A. Thyagaraja, N. Ben Ayed, and L. Fletcher (2004), Electron Inertial Effects on Rapid Energy Redistribution at Magnetic X-Points, *Astrophys. J.*, **609**, 423–438.

McClymont, A. N., and I. J. D. Craig (1996), Dynamical Finite-Amplitude Magnetic Reconnection at an X-Type Neutral Point, *Astrophys. J.*, **466**, 487.

McLaughlin, J. A., and A. W. Hood (2004), Mhd wave propagation in the neighbourhood of a two-dimensional null point, *Astron. & Astrophys.*, **420**, 1129–1140.

McLaughlin, J. A., I. De Moortel, A. W. Hood, and C. S. Brady (2009), Nonlinear fast magnetoacoustic wave propagation in the neighbourhood of a 2D magnetic X-point: oscillatory reconnection, *Astron. & Astrophys.*, **493**, 227–240.

McLaughlin, J. A., A. W. Hood, and I. De Moortel (2011), Review Article: MHD Wave Propagation Near Coronal Null Points of Magnetic Fields, *Space Sci. Rev.*, **158**, 205–236.

McMahon, L. C. (2017), Visco-resistive length scale in flux pile-up and series solutions for magnetic reconnection, *Phys. Plasmas*, **24**, 052,304.

McMahon, L. C. (2019), Oscillatory regimes of compressible 2.5 d viscous linear magnetic reconnection, *Phys. Plasmas*, **26**, 112,110.

Milne-Thompson, L. M. (1972), Jacobian elliptic functions and theta functions, in *Handbook of mathematical functions: with formulas, graphs, and mathematical tables, 10th Printing*, edited by M. Abramowitz and I. A. Stegun, chap. 10, pp. 567–586, Dover, New York, NY.

Minoshima, T., T. Miyoshi, and S. Imada (2016), Boosting magnetic reconnection by viscosity and thermal conduction, *Phys. Plasmas*, **23**, 072122.

Núñez, M., J. Álvarez, and J. Rojo (2008), Blowup of certain analytic solutions of the Hall magnetohydrodynamic equations, *Phys. Plasmas*, **15**, 062,104.

Ofman, L., P. J. Morrison, and R. S. Steinolfson (1993), Magnetic Reconnection at Stressed X-Type Neutral Points, *Astrophys. J.*, **417**, 748.

Park, W., D. A. Monticello, and R. B. White (1984), Reconnection rates of magnetic fields including the effects of viscosity, *Phys. Fluids*, **27**, 137–149.

Parker, E. N. (1957), Sweet's mechanism for merging magnetic fields in conducting fluids, *J. Geophys. Res.*, **62**, 509–520.

Petschek, H. E. (1964), Magnetic field annihilation, in *Physics of Solar Flares*, edited by W. N. Hess, pp. 425–439, NASA SP-50, Washington, D.C.

Phan, T. D., and B. U. O. Sonnerup (1990), MHD stagnation-point flows at a current sheet including viscous and resistive effects - General two-dimensional solutions, *J. Plasma Phys.*, **44**, 525–546.

Pontin, D. (2011), Three-dimensional magnetic reconnection regimes: A review, *Advances in Space Research*, **47**, 1508–1522.

Porcelli, F. (1987), Viscous resistive magnetic reconnection, *Phys. Fluids*, **30**, 1734–1742.

Potter, D. (1973), *Computational physics*, Wiley, New York.

Priest, E. R., and S. W. H. Cowley (1975), Some comments on magnetic field reconnection, *J. Plasma Phys.*, **14**, 271–282.

Priest, E. R., and P. Démoulin (1995), Three-dimensional magnetic reconnection without null points. 1. Basic theory of magnetic flipping, *J. Geophys. Res.*, **100**, 23,443–23,464.

Priest, E. R., and T. G. Forbes (1986), New models for fast steady state reconnection, *J. Geophys. Res.*, **91**.

Priest, E. R., and T. G. Forbes (2000), *Magnetic Reconnection*, Cambridge University Press, Cambridge,UK.

Priest, E. R., V. S. Titov, R. E. Grundy, and A. W. Hood (2000), Exact solutions for reconnective magnetic annihilation, *Proc. R. Soc. A*, **456**, 1821.

Richtmyer, R. D., and K. W. Morton (1967), *Difference methods for initial-value problems*, Interscience, New York.

Rossi, B., and S. Olbert (1970), *Introduction to the Physics of Space*, McGraw-Hill, New York.

Schindler, K., M. Hesse, and J. Birn (1988), General magnetic reconnection, parallel electric fields, and helicity, *J. Geophys. Res.*, **93**, 5547–5557.

Senanayake, T. (2007), The infuence of hall currents, plasma viscosity and electron inertia on magnetic reconnection solutions, PhD thesis, The University of Waikato.

Senanayake, T., and I. J. D. Craig (2006a), Hall effects on dynamic magnetic reconnection at an X-type neutral point, **451**, 1117–1124.

Senanayake, T., and I. J. D. Craig (2006b), Hall effects on dynamic magnetic reconnection at an X-type neutral point, *Astron. & Astrophys.*, **451**, 1117–1124.

Shay, M. A., J. F. Drake, B. N. Rogers, and R. E. Denton (1999), The scaling of collisionless, magnetic reconnection for large systems, *Geophys. Res. Lett.*, **26**, 2163–2166.

Shay, M. A., J. F. Drake, B. N. Rogers, and R. E. Denton (2001), Alfvénic collisionless magnetic reconnection and the Hall term, *J. Geophys. Res.*, **106**, 3759–3772.

Shibata, K., and T. Magara (2011), Solar flares: Magnetohydrodynamic processes, *Living Reviews in Solar Physics*, **8**, 6.

Shivamoggi, B. K. (1986), Evolution of current sheets near a hyperbolic magnetic neutral point, *Phys. Fluids*, **29**, 769–772.

Shivamoggi, B. K. (2009), Hall magnetohydrodynamics near an X-type magnetic neutral line, *Europhys. Lett.*, **85**, 25,001.

Shivamoggi, B. K. (2011), Steady and unsteady Hall magnetohydrodynamics near an X-type magnetic neutral line, *Phys. Plasmas*, **18**, 052,304.

Simakov, A. N., and L. Chacón (2009), Quantitative analytical model for magnetic reconnection in Hall magnetohydrodynamics, *Phys. Plasmas*, **16**, 055,701.

Simakov, A. N., L. Chacón, and A. Zocco (2010), Fundamental role of ion viscosity on fast magnetic reconnection in large-guide-field regimes, *Phys. Plasmas*, **17**, 060,701.

Sonnerup, B. U. Ö. (1979), Magnetic field reconnection, in *Solar System Plasma Physics*, vol. 3, edited by L. J. Lanzerotti, C. F. Kennel, and E. N. Parker, pp. 45–108, North-Holland Pub. Co., Amsterdam.

Sonnerup, B. U. Ö. (1988), On the theory of steady state reconnection, *Computer Phys. Commun.*, **49**, 143–159.

Sonnerup, B. U. O., and T. D. Phan (1990), Comment on 'MHD stagnation point flows in the presence of resistivity and viscosity' by F. T. Gratton, M. F. Heyn, H. K. Biernat, R. P. Rijnbeek, and G. Gnavi, *J. Geophys. Res.*, **95**, 259.

Sonnerup, B. U. O., and E. R. Priest (1975), Resistive MHD stagnation-point flows at a current sheet, *J. Plasma Phys.*, **14**, 283–294.

Southard, T. H. (1972), Weierstrass elliptic and related functions, in *Handbook of mathematical functions: with formulas, graphs, and mathematical tables, 10th Printing*, edited by M. Abramowitz and I. A. Stegun, chap. 18, pp. 627–684, Dover, New York, NY.

Spitzer, L. (1962), *Physics of Fully Ionized Gases*, 2 ed., Interscience, New York.

Sulem, P. L., U. Frisch, A. Pouquet, and M. Meneguzzi (1985), On the exponential flattening of current sheets near neutral X-points in two-dimensional ideal MHD flow, *J. Plasma Phys.*, **33**, 191–198.

Sweet, P. A. (1958), The neutral point theory of solar flares, in *Electromagnetic Phenomena in Cosmical Physics*, *IAU Symp.*, vol. 6, edited by B. Lehnert, pp. 123–134, Cambridge University Press, London.

Syrovatskiĭ, S. I. (1971), Formation of Current Sheets in a Plasma with a Frozen-in Strong Magnetic Field, *Sov. Phys.–JETP*, **33**, 933.

Tavabi, E., and S. Koutchmy (2014), Oscillations in solar jets observed with the SOT of Hinode: viscous effects during reconnection, *Astrophys. Space Sci.*, **352**, 7–15.

Thurgood, J. O., D. I. Pontin, and J. A. McLaughlin (2018), Implosive collapse about magnetic null points: A quantitative comparison between 2d and 3d nulls, *Astrophys. J.*, **855**, 50.

Thurgood, J. O., D. I. Pontin, and J. A. McLaughlin (2019), On the periodicity of linear and nonlinear oscillatory reconnection, *Astron. & Astrophys.*, **621**, A106.

Titov, V. (2007), Generalized squashing factors for covariant description of magnetic connectivity in the solar corona, *Astrophys. J.*, **660**, 863.

Titov, V. S., and E. R. Priest (1997), Visco-resistive magnetic reconnection due to steady inertialess flows. Part 1. Exact analytical solutions, *J. Fluid Mech*, **348**, 327–347.

Uberoi, M. S. (1963), Some exact solutions of magnetohydrodynamics, *Phys. Fluids*, **6**, 1379–1381.

Uberoi, M. S. (1966), Reply to comments by S. Chapman and P. C. Kendall, *Phys. Fluids*, **9**, 2307.

Uzdensky, D. A. (2009), On the physical interpretation of Malyshkin's (2008) model of resistive Hall magnetohydrodynamic reconnection, *Phys. Plasmas*, **16**, 040,702.

Uzdensky, D. A., and R. M. Kulsrud (1998), On the viscous boundary layer near the center of the resistive reconnection region, *Phys. Plasmas*, **5**, 3249–3256.

Vekstein, G., and N. Bian (2005), Forced Magnetic Reconnection at a Neutral X-Point, **632**, L151–L154.

Wang, X., A. Bhattacharjee, and Z. W. Ma (2000), Collisionless reconnection: Effects of Hall current and electron pressure gradient, *J. Geophys. Res.*, **105**, 27,633–27,648.

Zweibel, E. G., and M. Yamada (2009), Magnetic reconnection in astrophysical and laboratory plasmas, *Annu. Rev. Astron. Astrophys.*, **47**, 291–332.